

**Dissertation zur Erlangung des Doktorgrades
der Fakultät für Chemie und Pharmazie
der Ludwig-Maximilians-Universität München**

**Functional characterization of
intracellular ion channels with the endolysosomal
patch-clamp technique**

Yu-Kai Chao

aus

Kaohsiung, Taiwan

2019

Erklärung

Diese Dissertation wurde im Sinne von § 7 der Promotionsordnung vom 28. November 2011 von Herrn Prof. Dr. Dr. Christian Grimm betreut.

Eidesstattliche Versicherung

Diese Dissertation wurde eigenständig und ohne unerlaubte Hilfe erarbeitet.

München, 22.05.2019

.....

(Yu-Kai Chao)

Dissertation eingereicht am 23.05.2019

1. Gutachter: Prof. Dr. Dr. Christian Grimm
2. Gutachter: Prof. Dr. Martin Biel

Mündliche Prüfung am 24.06.2019

Table of content

<u>TABLE OF CONTENT</u>	<u>3</u>
<u>LIST OF MANUSCRIPTS</u>	<u>4</u>
<u>INTRODUCTION</u>	<u>5</u>
ENDOLYSOSOMAL SYSTEM	5
ENDOLYSOSOMAL ION CHANNELS	7
ENDOLYSOSOMAL PATCH CLAMP	14
<u>AIMS OF THE THESIS</u>	<u>17</u>
<u>SHORT SUMMARY OF MANUSCRIPTS</u>	<u>18</u>
<u>REFERENCES</u>	<u>23</u>
<u>CURRICULUM VITAE</u>	<u>35</u>
<u>COMPLETE LIST OF ORIGINAL PUBLICATIONS</u>	<u>36</u>
<u>ACKNOWLEDGEMENT</u>	<u>37</u>
<u>APPENDIX</u>	<u>38</u>

List of manuscripts

This thesis is based on the following publications, which are referred to in the text by their numerals. (1-4):

1. Patch-clamp technique to characterize ion channels in enlarged individual endolysosomes

Cheng-Chang Chen*, Chunlei Cang*, Stefanie Fenske, Elisabeth Butz, **Yu-Kai Chao**, Martin Biel, Dejian Ren, Christian Wahl-Schott & Christian Grimm
Nat Protocol. 2017 Aug;12(8):1639-1658. * equal contribution

2. Small Molecules for Early Endosome-Specific Patch Clamping

Cheng-Chang Chen*, Elisabeth S. Butz*, **Yu-Kai Chao**, Yulia Grishchuk, Lars Becker, Stefan Heller, Susan A. Slaugenhaupt, Martin Biel, Christian Wahl-Schott*, and Christian Grimm*
Cell Chemical Biology. 2017 Jul 20;24(7):907-916. * equal contribution

3. Two-Pore Channel Function Is Crucial for the Migration of Invasive Cancer Cells

Ong Nam Phuong Nguyen*, Christian Grimm*, Lina S. Schneider, **Yu-Kai Chao**, Carina Atzberger, Karin Bartel, Anna Watermann, Melanie Ulrich, Doris Mayr, Christian Wahl-Schott, Martin Biel, and Angelika M. Vollmar
Cancer Research. 2017 Mar 15;77(6):1427-1438. * equal contribution

4. TPC2 polymorphisms associated with a hair pigmentation phenotype in humans result in gain of channel function by independent mechanisms

Yu-Kai Chao*, Verena Schludi*, Cheng-Chang Chen, Elisabeth Butz, O. N. Phuong Nguyen, Martin Müller, Jens Krüger, Claudia Kammerbauer, Manu Ben-Johny, Angelika M. Vollmar, Carola Berking, Martin Biel, Christian A. Wahl-Schotta, and Christian Grimm
PNAS. 2017 Oct 10;114(41):E8595-E8602. * equal contribution

Introduction

Endolysosomal system

The endolysosomal system is the transportation system inside eukaryotic cells, which comprises early endosomes, late endosomes, lysosomes, recycling endosomes, autophagosomes, and lysosome related organelles. [1-3] These intracellular vesicles communicate by vesicular carriers that are generated on one organelle, detach, migrate, and fuse with another organelle. This vesicle-mediated transport is required to deliver specific proteins and lipids to an acceptor organelle. [4, 5] For instance, receptors from cell surface can be endocytosed through clathrin-dependent and clathrin-independent mechanisms, as well as through phagocytosis and pinocytosis into early endosomes [6, 7], and then be targeted for degradation after reaching lysosomes via late endosomes. Alternatively, receptors can also be recycled back to the cell surface either directly from early endosomes or by trafficking through recycling endosomes. Macromolecules can be degraded by fusion of autophagosomes or phagosomes with lysosomes, which contain acidic hydrolases required for degradation. Late endosomes and lysosomes receive newly synthesized hydrolytic enzymes from the trans-Golgi network (TGN), and can fuse with the plasma membrane to mediate plasma membrane repair and secretion of lysosomal content by lysosomal exocytosis (Fig. 1). Finally, lysosome-related organelles (LROs) are a heterogeneous set of organelles derived from the endolysosomal system and usually contain lysosomal proteins. They exist in different specialized cells such as dense granules in platelets, lytic granules in cytotoxic T lymphocytes, lamellar bodies in lung epithelial type II cells, and melanosomes in melanocytes [8-10].

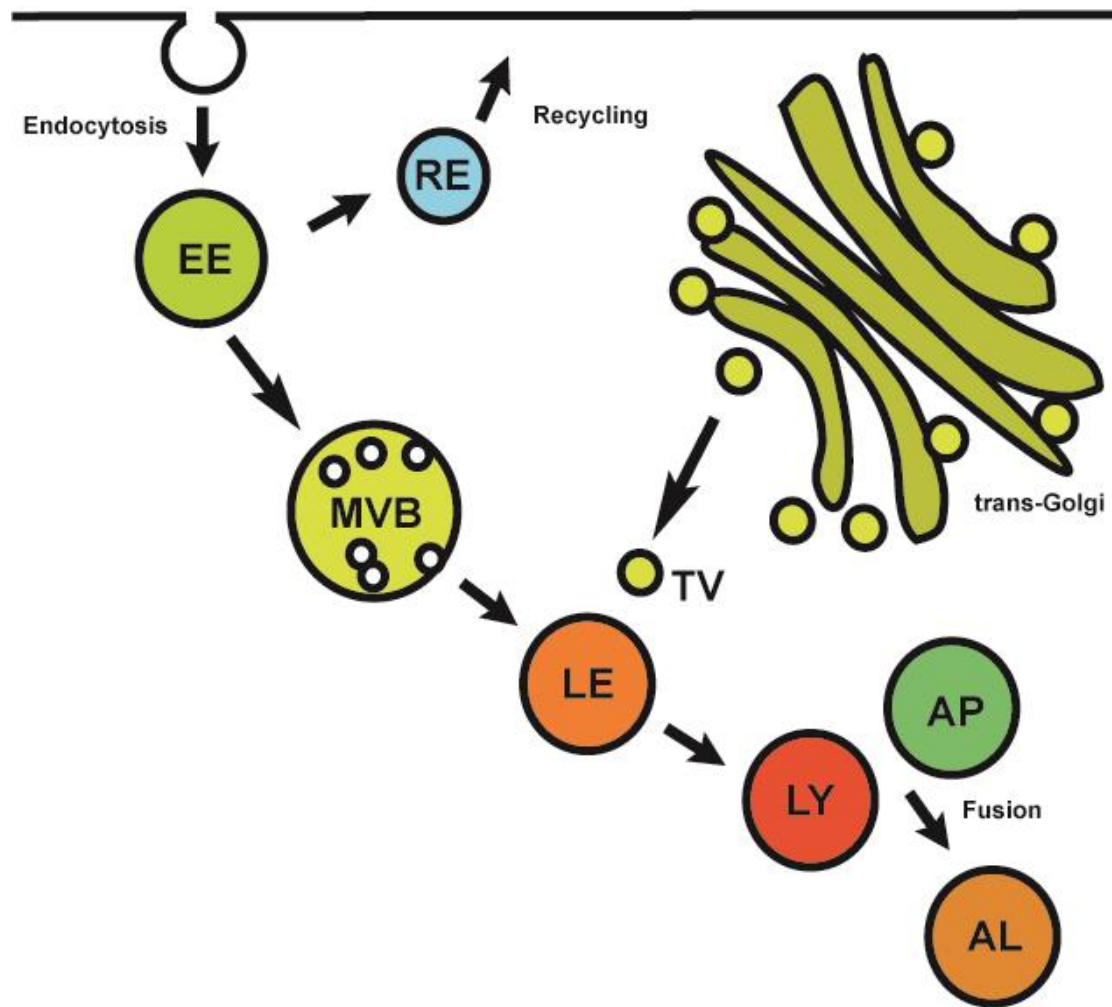


Figure 1. A schematic view of the endosomal trafficking network. During endocytosis, a piece of the plasma membrane is excised and enters the cytosol and recruits early endosomal proteins to become early endosomes (EE). Membrane receptors are sorted and recycled back to the plasma membrane through recycling endosomes (RE). Material destined for degradation is passed on to multi-vesicular bodies (MVB). Multi-vesicular bodies further mature into late endosomes (LE) and hydrolytic enzymes are transported to late endosomes through transport vesicles (TV) from the trans-Golgi network. Late endosomes then mature into lysosomes (LY) either through further acidification, or through fusion with existing lysosomes. During starvation or when organelles are damaged, lysosomes also accept cargo from autophagosomes (AP) carrying damaged organelles or cytosolic material for degradation, resulting in autophagic lysosomes (AL).

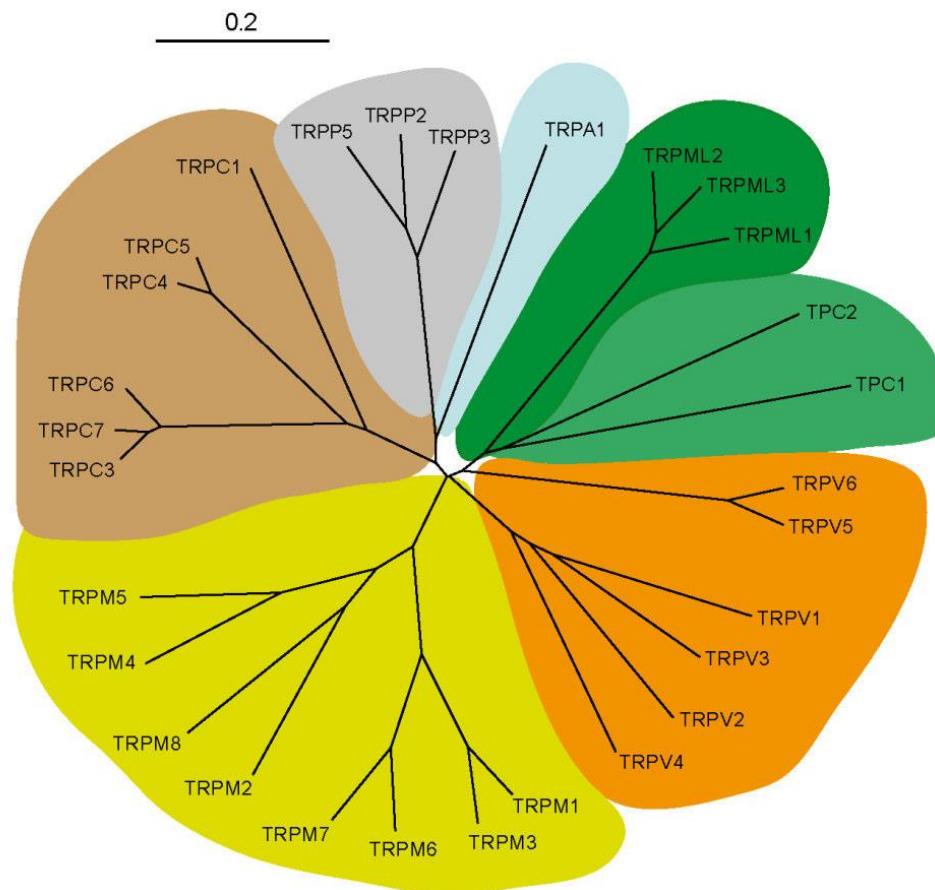
Endolysosomal ion channels

The membranes of intracellular organelles make up the majority of the total cell membrane and harbor a large number of transmembrane proteins, including many ion channels. Ion channels are classically understood to mediate the flux of ions across the plasma membrane in response to cellular stimulation. However, they also reside on intracellular membranes to regulate various organellar and cellular functions as well [11, 12]. Numerous ion channels have been identified in the endosomal-lysosomal compartment such as chloride channels (CIC), potassium channels (BK and TMEM175), and transient receptor potential channels (TRP) [13-19], which allow anions and cations to cross endolysosomal membranes; however, their physiological roles still need to be further evaluated. The resting membrane potential of these endolysosomal vesicles is around +10 to +40 mV because the charge inside the organelle lumen is more positive than in the cytosol [20, 21]. This positive resting membrane potential is generally considered to be highly favorable for cation release.

The transient receptor potential ion channels were first identified as receptor-operated sensory cation channels required for sustained light responses in *Drosophila* [22-24]. Subsequent homology cloning led to the discovery of a 28-member superfamily of cation channels in mammals [14, 25-28]. Most of TRP channels are non-selectively cation permeable and gated by a diverse range of chemical signals, such as environmental sensory signals, extracellular neurotransmitters, or intracellular messengers [28, 29]. Therefore TRP channels belong to the ligand-gated cation channel superfamily, however some TRPs can also be gated by physical signals like temperature, mechanical force, and voltage [30]. There are 27 members of the TRP family in the human genome (Fig. 2A; TRPC2 is a pseudogene in humans but is functional, e.g. in mouse), which are expressed in many different tissues and cell types [31, 32]. A common feature of TRP channels is the homotetrameric assembly of subunits containing six transmembrane segments (S1–S6), with N- and C-terminal domains facing the cytosol, S1–S4 form a voltage-sensor-like domain (VSLD) and S5–S6 domain forms the cationic selectivity filter and channel activation gate [33-38] (Fig. 2B). Tetrameric assembly of either homomeric or heteromeric TRP polypeptides forms TRP channels [39]. The TRP family contains seven subfamilies that are classified

according to sequence and topological homology [15, 40-42]. TRPC1-7 (C for canonical), TRPV1-6 (V for vanilloid), TRPM1-8 (M for melastatin), TRPA1 (A for Ankyrin), TRPML1-3 (ML for mucolipin), TRPP1-3 (P for polycystin). The endolysosomal two pore channels (TPC1 and TPC2) do not belong to the TRP superfamily but are most closely related to the TRPML channels. Most organellar TRPs have a role in either biosynthetic or secretory pathways involving ER and Golgi, or in the endocytic pathway involving endosomes and lysosomes [43]. TRPV1 and TRPP1 are known to be localized on the ER membranes; TRPC3-5, TRPV5-6, TRPM2, TRPM8, TRPA1, TPC1-2, and TRPML1-3 are present in secretory vesicles, early and recycling endosomes, late endosomes, and lysosomes. Those organelles are intracellular Ca^{2+} stores. Ca^{2+} release by organellar TRP channels can increase juxtaorganellar Ca^{2+} levels, specifically affecting the dynamics and function of the organelles [43]. Furthermore, changes in membrane potential across organellar membranes may also affect organellar functions [44]. The transient receptor potential channel mucolipins (TRPMLs) and the two-pore channels (TPCs) are the main focus of this thesis and will be discussed in more detail in the following section.

(A)



(B)

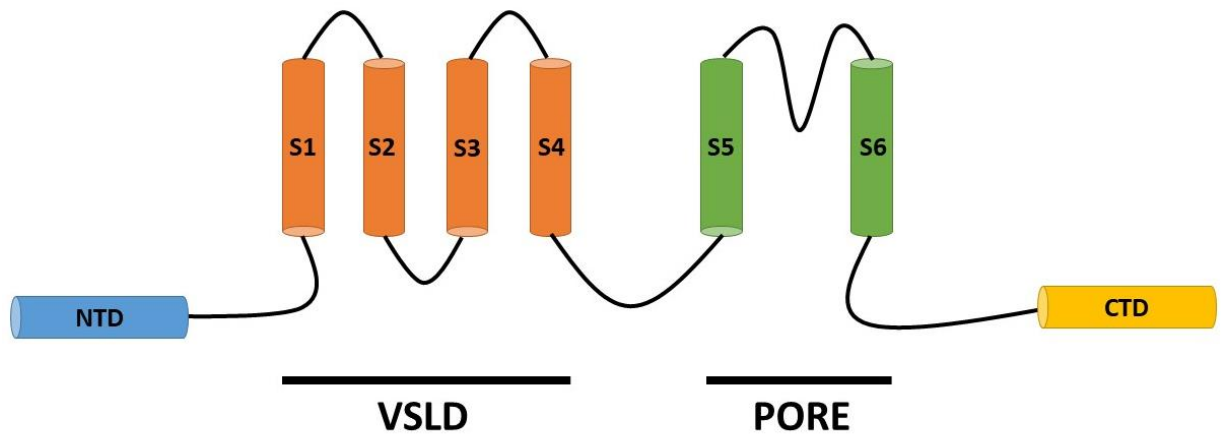


Figure 2. (A) Shown is a phylogenetic analysis of human TRPs and the two-pore channels (TPCs) based on the amino acid sequences in the pore region (S5 – S6). The corresponding alignment was generated using DNAMAN software, the phylogenetic tree was generated using NJPlot software [45]. (B) TRPs are cation channels with six transmembrane segments (S1–S6) and N- and C-terminal domains facing the cytosol.

Two-pore channels (TPCs) are cation channels localized on endosomes and lysosomes as well as plant vacuoles. Di-leucine motifs in their N-termini target them to endolysosomes [44, 46-51]. In contrast to TPC1 and TPC2, a third isoform, TPC3, is absent from the genomes of several species including human, mouse, rat, and fly [44, 52-55]. TPC1 tends to distribute to less acidic early-endosomal sections, while TPC2 is predominately found in late-endosomes and lysosomes [20, 54, 56]. TPCs contain two repeats of a 6 transmembrane pore-forming domain [54, 56] and are closely related to the voltage-gated cation channels (VGCCs) on the one hand and TRPML channels on the other hand. TPCs assemble as dimers through interactions between transmembrane domains and hold a key position in the evolution of voltage-gated ion channels due to their dimeric nature and the duplicated domain structure of each subunit [57-62]. This structural organization places TPCs between tetrameric one-domain (6 TM) channels, such as CatSper channels and voltage-gated K⁺ channels (Kv), and monomeric four-domain (4 × 6 TM) channels, such as Cav and Nav channels [63]. Pore loop I and II from TPCs contain glycosylated residues to provide protection from the acidic luminal environment [61, 64, 65].

Several studies have suggested different roles for TPCs in endolysosomal trafficking, especially endolysosomal fusion [64, 66-69]. Additional roles for TPCs

have been identified, such as trafficking of bacterial cholera toxin B [64], cholera toxin (CT), *Pasteurella multocida* toxin (PMT), diphtheria toxin (DT), and Lethal Factor of anthrax toxin (LF) [69, 70], EGF/EGFR and LDL-cholesterol trafficking [66] as well as platelet-derived growth factor receptor β (PDGFR β) trafficking [69], regulation of autophagy [71, 72], nutrient sensing modulated by intracellular ATP through mTORC1 kinase [73], exocytosis [74, 75], angiogenesis [76, 77], fertilization and embryogenesis [78], and cytokinesis [79]. Besides, TPCs are also involved in disease progression including Parkinson's disease [67], fatty liver disease [66], and MERS-CoV and Ebola infection [80, 81]. Although these diseases have distinct pathologies, there is a mechanistic convergence most probably due to defective trafficking events within the endolysosomal system. Moreover, three independent interactome screens revealed putative interaction partners for TPC2 that are involved in intracellular vesicle trafficking and fusion processes, such as Rab- and soluble N-ethylmaleimide-sensitive factor attachment receptor (SNARE-) proteins [66, 68, 70]. Furthermore, human TPC2 polymorphisms have been postulated to play a role in hair pigmentation, which implies a potential role of TPCs in melanosomes which are lysosome-related organelles in melanocytes (LROs) [82]. Recently, a direct role for TPC2 in melanosomal pH regulation and melanin production in melanocytes has been demonstrated. Thus, TPC2-deficient melanosomes, the melanin producing organelles in melanocytes, showed an increase in pH and size, resulting in an enhanced tyrosinase activity and increased melanin production. TPC2 activation or overexpression had the opposite effect, reducing the melanin production [83, 84].

TPCs were originally functionally characterized as the targets for the Ca^{2+} mobilizing messenger NAADP. Several studies suggested that manipulation of TPC2 expression affects NAADP-induced Ca^{2+} release from lysosomal stores [46-48, 64, 71, 74, 85-89]; further investigations strongly demonstrated TPC2 being the NAADP receptor due to the high affinity NAADP binding proteins complexing with TPC2 [46, 64, 90], its sensitivity to the NAADP antagonist Ned-19 [51, 91], and the bell-shaped NAADP concentration-response curve [46, 48, 91]. However, subsequent studies have identified a pronounced Na^{+} -selective current activated by the endolysosomal phosphoinositide $\text{PI}(3,5)\text{P}_2$ (phosphatidylinositol-3, 5-bisphosphate) [92, 93]. Due to the controversy raised by above studies, several follow-up works have been performed to resolve the permeability and ligand activation of TPCs. In lysosomal patch-clamp experiments it has been confirmed

that TPC2 is activated by PI(3,5)P₂, is Na⁺-permeable, and is regulated by ATP [93], nevertheless, endogenous TPC2-like Ca²⁺ currents were likewise recorded in response to PI(3,5)P₂ and NAADP, and these currents were substantially reduced in embryonic fibroblasts derived from a TPC2-knockout mouse [66]. Calculation of the Na⁺/Ca²⁺ permeability ratio for endogenous TPC2 indicated that TPC2 is not exclusively Na⁺-selective [66, 94]. Consistent with this finding is the presence of conserved asparagine residues in the putative selectivity filter of TPCs similar to NMDA (N-methyl-D-aspartate) receptors of the glutamate receptor family, which are Ca²⁺ and Na⁺ permeable [95]. Structure-guided mutational analyses have identified the determinants in the pore loop that are responsible for Ca²⁺ versus Na⁺ selectivity [96], and high-resolution structural studies have demonstrated that PI(3,5)P₂ opens the channel gate by binding to positively charged amino acid residues in the S4–S5 link and S6 [97]. In summary, although the bulk of evidence suggests that TPCs are indeed NAADP targets, their mode of activation and permeability is more complex than initially envisaged and is perhaps exquisitely sensitive to experimental configuration. Therefore, the controversies of ligand-gating and ion permeability of TPC channels need to be further investigated. Besides, specific, lipophilic small molecule TPC agonists are highly desired as pharmacological tools for future TPC studies.

The mucolipin subfamily of transient receptor potential channels (TRPMLs) is the other cation channel group which can be activated by late endosome and lysosome (LEL) specific phosphoinositide PI(3,5)P₂ in the endolysosomal system [98]. TRPML1–3 are tetrameric six-transmembrane (TM) channels that are mainly localized on endosomes and lysosomes [99]. While TRPML1 is ubiquitously expressed, expression of TRPML2 and TRPML3 is more restricted to certain tissues and cell types [44, 99, 100]. Whole-endolysosome patch-clamp studies revealed that mammalian TRPML1–3 channels are permeable to both Ca²⁺ and Na⁺, as well as to K⁺ (TRPML1) and heavy metal ions such as Fe²⁺ (TRPML1^{Va} and TRPML2^{Va}) and Zn²⁺, the latter one specifically demonstrated for TRPML1 [101–103]. Recent high-resolution structural studies have confirmed that the cationic selectivity is determined by negatively charged amino acid residues in the pore loop, and the activation gate is made of the segment S6 TM helices [36, 104]. TRPML1 contains two di-leucine sorting motifs at the intracellular N- and C-termini which are responsible for the localization of the protein to membranes of

late endosomes and lysosomes [99, 105-108]. PI(3,5)P₂ binds to positively charged residues in the N-terminal region of TRPML1, resulting in opening of the S6 gate through the S2–S3 linker as modeled in high-resolution structures [36]. Mutations in the PI(3,5)P₂ binding sites of TRPML1 affect PI(3,5)P₂-dependent lysosomal functions [109]. Whole-endolysosome patch-clamp studies had demonstrated that TRPML1 might conduct Ca²⁺, Fe²⁺, Zn²⁺, Na⁺, and K⁺ across lysosomal membranes [98, 101]. In addition to PI (3,5)P₂, TRPML1 is also directly activated by reactive oxygen species (ROS), which are released from mitochondria under stress conditions to activate autophagosome and lysosome biogenesis as a negative feedback mechanism to maintain cellular health [110]. Activation of TRPML1 triggers the Ca²⁺-sensor calcineurin, which then promotes the nuclear translocation of transcription factor EB (TFEB), a master transcriptional regulator of autophagosome and lysosome biogenesis [111]. TFEB activation is sufficient to promote mitophagy, removing damaged mitochondria to reduce excessive ROS in the cell. There are several endogenous factors that reportedly inhibit TRPML1 such as phosphatidylinositol 4,5-bisphosphate [PI(4,5)P₂], sphingomyelin, luminal pH, and mTOR. PI(4,5)P₂ and sphingomyelin were proposed to prevent TRPML1 from being active in non-lysosomal compartments [112, 113]; lysosomal PI(4,5)P₂ and sphingomyelin levels are aberrantly elevated in some LSDs, therefore, pathogenic TRPML1 inhibition may underlie the trafficking defects in many LSDs [112, 114]. Luminal pH regulates the channel activities of TRPML1, hence, cellular cues affecting lysosome acidification may regulate lysosome functions via TRPML-dependent mechanisms [115]. mTOR was also shown to inhibit TRPML1 by direct phosphorylation [116-118]. During starvation, TRPML1 is activated due to mTORC1 dissociating from the lysosomal surface and inhibiting its activity. At the same time, calcineurin activity is locally induced near the lysosome by lysosomal calcium release through TRPML1. This leads to a decreased rate of TFEB phosphorylation through mTORC1 inhibition, and an induction of TFEB dephosphorylation through calcineurin induction. Dephosphorylated TFEB will translocate from the cytoplasm to the nucleus and induce expression of lysosomal and autophagic genes [119], it is possible that starvation-induced mTOR inhibition serves as a nutrient-derived signal to modulate TRPML1-mediated Ca²⁺ release. On the other hand, it has been reported that upregulating TRPML1 promotes lysosomal mTORC1 recruitment and mTORC1 activity during starvation through calmodulin (CALM) [118]. Future

studies are needed to elucidate how these pathways between mTORC1 and TRPML1 work cooperatively to maintain cellular homeostasis in response to nutrient starvation and other types of cellular stresses. Mutations in the human TRPML1 gene cause mucopolipidosis type IV disease (MLIV), a devastating pediatric neurodegenerative disease with motor impairment, mental retardation, and iron deficiency anemia [101, 120, 121]. Besides neurodegenerative diseases, TRPML1 also plays a role in immune cell migration [122], cancer cell development [123, 124], and release of exosomes [125, 126].

TRPML2 was discovered through database searches. Investigation in drosophila S2 cells revealed that the TRPML2 channel displays nonselective cation permeability, which is Ca^{2+} permeable and inhibited by low extracytosolic pH [127]. Several groups have demonstrated expression of TRPML2 in different immune cells and tissues and TRPML2 has been shown to be expressed primarily on RE and LE/LY by immunocytochemistry experiments using overexpression conditions [128-133]. In macrophages, LPS (lipopolysaccharide) exposure leads to a strong upregulation of TRPML2 expression, resulting in an increased release of the chemokine CCL2 from LPS-stimulated WT macrophages via the early/recycling endosomal pathway, while TRPML2^{-/-} macrophages show much reduced release, suggesting that TRPML2 channel activity is directly linked to CCL2 trafficking and secretion [134]. Similar to TPCs, TRPML2 is also involved in the trafficking of endocytosed viruses [135].

TRPML3 channel function was first demonstrated in mice with the varitint-waddler (Va) phenotype [127, 136-144]. The gain-of-function mutant isoforms Va (A419P) and Va^l (A419P + I362T) cause severe auditory, vestibular, coat color dilution, deafness and circling behavior. The A419P mutation renders the channel constitutively active leading to large inward fluxes of calcium and sodium [127, 136-143]. TRPML3 is expressed in multiple intracellular compartments. When overexpressed TRPML3 is found to a high extent also in the plasma membrane, endogenous plasma membrane expression, however, is uncertain [145]. Measurement of reversal potentials with the different external cations and intracellular K^+ indicated monovalent cation selectivity of $\text{Na}^+ > \text{K}^+ > \text{Cs}^+$ [146]. TRPML3 is also regulated by luminal pH, besides high sodium. Low pH blocks TRPML3 activity, for example in uroepithelial cells. Here, pathogen invasion induces lysosome alkalization to trigger TRPML3 activity and Ca^{2+} -dependent exosome release [115]. And TRPML3 KO mice, however, breed normally and have

no acutely visible defects, showed no circling behavior, head bobbing, waddling, or imbalance when walking [147, 148]. However, recent works indicated that co-deficiency of TRPML3 and TRPML1 lead to a phenotype of neonatal failure-to-thrive with intestinal pathology in TRPML3^{-/-}; TRPML1^{-/-} mice because of pathological vacuolation of enterocytes [149]. The mice also suffered from accelerated age-related hearing loss (ARHL) due to auditory outer hair cell (OHC) degeneration resulting from enlargement and permeabilization of lysosomes inside the cells [150].

Further studies regarding TRPML3 could focus on a more detailed and in-depth analysis of TRPML3 KO mice and the cellular signals that activate TRPML3 in early-endosomes.

Endolysosomal patch clamp

Patch-clamping is one of the most powerful techniques used in the study of ion channels, which allows high-resolution, low noise measurement of the ionic currents flowing through the cell membrane [151]. And it has been widely applied to investigate different electrical properties such as ion selectivity, channel kinetics, and gating. Electrical activity of channels can be recorded from a section of the cell membrane or the whole cell by different configurations [152]. There are four different kinds of approach to perform patch clamp recordings: cell-attached mode, whole-cell mode, inside-out mode, and outside-out mode. In cell-attached mode, a glass micropipette with an opening of few micrometers in diameter is used as an electrode which is placed on the surface of the plasma membrane of an intact cell, followed by application of air suction an omega shaped piece of plasma membrane is generated and subsequently the patched membrane adheres tightly to the pipette to reach “giga seal” formation (seal resistance > 10⁹ Ω), which maintains the intact membrane and intracellular environment to avoid leakage current and allow for high-resolution measurements. The whole-cell mode is achieved by rupturing the patch formed in the cell-attached mode through applying a pulse of voltage or a quick suction, which allows recording of the whole-cell current at certain voltage (voltage clamp) or the changes in the membrane potential with the fixed current (current clamp). Inside-out mode is achieved by pulling the pipette from the cell-attached mode therefore the cytosolic side of the membrane is exposed to the bath solution. Outside-out mode is established by

pulling out the pipette from the whole-cell configuration, where the outside of the membrane is exposed to the bath solution.

To functionally characterize endolysosomal ion channels in detail, electrophysiological methods are necessary and inevitable. Because of the intracellular localization and the relatively small size of vesicles, it was not been feasible to directly measure the electrical activity of endolysosomal channels in the past. Therefore, several indirect alternative approaches had been employed to resolve the biophysical properties of ion channels in intracellular membrane systems. One approach is to redirect endolysosomal channels to the plasma membrane by introducing mutation to delete two major classes of lysosomal sorting signals which are “tyrosine-based” (NPXY or YXXØ) and “dileucine-based” ([DE]XXXL[LI] or DXXLL) consensus motifs [153-156]. Thus, endolysosomal ion channels translocate to the plasma membrane, where they are accessible to conventional patch-clamp analysis [51, 101, 140]. The other approach is to reconstitute lysosomal channels into artificial membranes or synthetic phospholipid bilayers [91, 157-159]. Besides, Ca²⁺-conducting endolysosomal ion channels can be analyzed by Ca²⁺-imaging techniques using small molecular fluorescent Ca²⁺ indicator dyes such as Fura-2 [160, 161] or genetically encoded Ca²⁺ indicators (GECIs) such as GCaMP [162, 163].

The weakness of these indirect electrophysiological methods is that ion channel proteins are extracted from their physiological environment and studied in nonnative membranes. This procedure bears a high risk of losing important factors, such as critical components of the lipid membrane, as well as specific modulators and accessory subunits that are associated in vivo with the ion channel proteins. On the other hand, factors in the plasma membrane can potentially interfere with the activity of the translocated endolysosomal ion channel. Furthermore, the procedure of purification of proteins can possibly affect the ion channel or form additional conductances that lead to incorrect interpretation of current recordings from bilayers.

In addition, a planar patch-clamp approach has been established to electrophysiologically analyze endolysosomal ion channels, which allows reliable and efficient characterization of currents from isolated endolysosomes [164]. The advantages of planar patch-clamp are that even small and native endolysosomes that have not been enlarged can be analyzed, and there is no selection bias in planar patch-clamp since there is inherently no visualization by a microscope or

micromanipulation system. Disadvantages of planar patch-clamp are that purification of endolysosomal vesicles is required and that the method lacks visual control by microscopy optics and mechanical control via a micromanipulator. Furthermore, no inside-out or outside-out patches can be produced. The most substantial limitation of this method is that high Ca^{2+} cannot be omitted on one side of the endolysosomal membrane as high Ca^{2+} is required for successful gigaseal formation, which limits the degree of freedom of experimental design. In order to overcome these abovementioned problems, a conventional whole-lysosome patch-clamp approach was developed [73, 92, 98, 101], in combination with pharmacological tools to enlarge endolysosomal vesicles to a degree suitable for manual patch-clamp ($>4 \mu\text{m}$), detailed information of which is fully described in **Manuscript 1**.

Aims of the thesis

After establishing the manual conventional modified endolysosomal patch-clamp technique in **Manuscript 1**, we applied this technique to better understand the functional roles of endolysosomal ion channels in the human body under physiological and pathophysiological conditions. The objective of the thesis was to investigate and characterize intracellular ion channels by using the manual conventional modified endolysosomal patch-clamp on the following subjects:

Aim 1

Functional characterization of TRPML3 activities in early endosomes, late endosomes, and lysosomes by using a combination of chemicals to specifically enlarge different intracellular organelles. **(Manuscript 2)**

Aim 2

Investigation of the role of intracellular ion channel TPC2 in the tumor cell metastasis formation process. **(Manuscript 3)**

Aim 3

Functional characterization of human TPC2 channel polymorphisms and their relation to hair color pigmentation. **(Manuscript 4)**

Short summary of manuscripts

1. Patch-clamp technique to characterize ion channels in enlarged individual endolysosomes

Cheng-Chang Chen*, Chunlei Cang*, Stefanie Fenske, Elisabeth Butz, **Yu-Kai Chao**, Martin Biel, Dejian Ren, Christian Wahl-Schott & Christian Grimm

Nature Protocol. 2017 Aug;12(8):1639-1658.

** equal contribution*

Electrophysiological techniques, especially patch-clamp, is the gold standard method to functionally characterize ion channels which are located on the plasma membrane. However, investigating ion channels embedded on the membranes of intracellular organelles such as endosomes and lysosomes was impossible in the past because of the lack of direct methods, inaccessibility of these channels by using the patch-clamp technique and the small size of endolysosomes.

To overcome these problems, we develop a manual conventional patch-clamp technique combined with pharmacological tools to enlarge endolysosomal vesicles to a size suitable for manual patch-clamping (>4 μm). Thus, endolysosomal ion channels can now be characterized after isolation of enlarged endolysosomes from the cell without technical restrictions or experimental constraints.

Declaration of contribution: I contributed the recordings of currents for the calculation of pipette resistance, sealing resistance, series resistance, and cell capacitance. And the representative whole-endolysosome recordings, both current traces and current-voltage relationships from HEK cells overexpressing endolysosomal TPC1 or TPC2.

2. Small Molecules for Early Endosome-Specific Patch Clamping

Cheng-Chang Chen*, Elisabeth S. Butz*, **Yu-Kai Chao**, Yulia Grishchuk, Lars Becker, Stefan Heller, Susan A. Slaugenhaupt, Martin Biel, Christian Wahl-Schott*, and Christian Grimm*

Cell Chemical Biology. 2017 Jul 20;24(7):907-916.

* *equal contribution*

Functional characterization of endolysosomal channels by using the patch clamp technique has been successfully performed in manuscript 1. However, the small molecule vacuolin-1 used to enlarge endolysosomal vesicles in manuscript 1 is not selective for specific endolysosomal organelles, i.e. EE, RE, LE, and LY are enlarged alike. Therefore, we deemed it important to identify tools to selectively enlarge the respective vesicles in the endolysosomal system.

This, in this work, we have developed an improved experimental approach to selectively patch clamp Rab5 positive early endosomes (EE) versus Rab7/LAMP1-positive late endosomes/lysosomes (LE/LY). We found that the combination of two small molecules, wortmannin and latrunculin B can specifically enlarge Rab5-positive EE but not Rab7-, LAMP1-, or Rab11 (RE)-positive vesicles. We applied these tools to measure currents mediated by TRPML3, confirming that TRPML3 is functionally active in both EE and LE/LY in overexpressing HEK cells and in endogenously expressing primary CD11b+ alveolar macrophages.

Declaration of contribution: I contributed the endolysosomal patch clamp experiments characterizing TRPML3 channel function in both EE and LE/LY under different ion and pH conditions in HEK cells overexpressing TRPML3.

3. Two-Pore Channel Function Is Crucial for the Migration of Invasive Cancer Cells

Ong Nam Phuong Nguyen*, Christian Grimm*, Lina S. Schneider, **Yu-Kai Chao**, Carina Atzberger, Karin Bartel, Anna Watermann, Melanie Ulrich, Doris Mayr, Christian Wahl-Schott, Martin Biel, and Angelika M. Vollmar

Cancer Research. 2017 Mar 15;77(6):1427-1438. *equal contribution

Metastatic invasion is the key feature that distinguishes cancer cells from all other cells. Metastases formation is the major cause of cancer-related deaths. The ability of cancer cells to migrate from primary disease sites is attributed to the mutation of genes that regulate the production of proteins that normally tether cells to their surrounding tissues. Decreased synthesis in cancer cells of a number of substances that bind them to neighboring cells, together with the abnormal synthesis of enzymes capable of degrading the bonds between cells and tissues, allow cancer cells to escape the primary tumor site.

In this study, we report the NAADP and PI(3,5)P2 sensitive Ca²⁺-permeable cation channels in the endolysosomal system of these cells, two-pore channels (TPC), as candidate targets for the treatment of invasive cancers because inhibition of TPCs was found to abrogate metastatic cancer cell migration. Disrupting TPC function halted trafficking of β 1-integrin and resulted in its accumulation in EEA1-positive early endosomes, therefore metastatic invasive cancer cells were rendered unable to form leading edges that are required for migration. Our findings link TPC to cancer cell migration and provide a preclinical proof of concept for their candidacy as targets to treat metastatic cancers.

Declaration of contribution: I performed endolysosomal patch clamp experiments characterizing TPC2 channel function and the inhibitory effect of tetrandrine on TPC2 in T24 cancer cell.

4. TPC2 polymorphisms associated with a hair pigmentation phenotype in humans result in gain of channel function by independent mechanisms

Yu-Kai Chao*, Verena Schludi*, Cheng-Chang Chen, Elisabeth Butz, O. N. Phuong Nguyen, Martin Müller, Jens Krüger, Claudia Kammerbauer, Manu Ben-Johny, Angelika M. Vollmar, Carola Berking, Martin Biel, Christian A. Wahl-Schotta, and Christian Grimm

PNAS. 2017 Oct 10;114(41):E8595-E8602.

** equal contribution*

Two polymorphisms (M484L and G734E) in the endolysosomal ion channel TPC2 have been reported to be associated with a shift in hair color from brown to blond in a genome-wide association study. Later on the role of TPC2 in hair color pigmentation had also been described showing that TPC2 regulates the pH and size of melanosomes inside the melanocytes and that loss of TPC2 activity by knockout or knockdown leads to a strong increase of melanosomal pH, resulting in the higher melanin production. However functional, i.e. electrophysiological data of how TPC2 polymorphisms affect channel function was still missing.

In this study, we characterized these two TPC2 polymorphisms by using the endolysosomal patch-clamp technique and found that both polymorphisms result in TPC2 channel gain-of-function by different mechanisms. TPC2 M484L polymorphic variant shows increased sensitivity to the endogenous ligand PI(3,5)P₂ because of a channel pore dilation; besides, TPC2 G734E polymorphic variant shows less sensitivity to ATP-Mg inhibition due to the weaker interaction between mTOR complex and the TPC2 channel. Electrophysiological data from fibroblast cell lines isolated from human donors carrying the different polymorphic variants further validated our findings in HEK cells expressing the different TPC2 polymorphisms.

Declaration of contribution: In this study I contributed the lysosomal patch clamp recordings on HEK cells expressing hTPC2 with different polymorphic variants. In addition I performed recordings on different human fibroblast cell lines isolated

from donors with distinct TPC2 polymorphisms, contributed dose response curves of PI(3,5)P₂ and assessed ATP-Mg as well as mTOR inhibitor effects on TPC2 in HEK cells.

References

1. Grant, B.D. and J.G. Donaldson, *Pathways and mechanisms of endocytic recycling*. Nat Rev Mol Cell Biol, 2009. **10**(9): p. 597-608.
2. Luzio, J.P., N.A. Bright, and P.R. Pryor, *The role of calcium and other ions in sorting and delivery in the late endocytic pathway*. Biochem Soc Trans, 2007. **35**(Pt 5): p. 1088-91.
3. Repnik, U., M.H. Cesen, and B. Turk, *The endolysosomal system in cell death and survival*. Cold Spring Harb Perspect Biol, 2013. **5**(1): p. a008755.
4. Goody, R.S., M.P. Muller, and Y.W. Wu, *Mechanisms of action of Rab proteins, key regulators of intracellular vesicular transport*. Biol Chem, 2017. **398**(5-6): p. 565-575.
5. Gomez-Navarro, N. and E.A. Miller, *COP-coated vesicles*. Curr Biol, 2016. **26**(2): p. R54-R57.
6. Kirchhausen, T., D. Owen, and S.C. Harrison, *Molecular structure, function, and dynamics of clathrin-mediated membrane traffic*. Cold Spring Harb Perspect Biol, 2014. **6**(5): p. a016725.
7. Mayor, S., R.G. Parton, and J.G. Donaldson, *Clathrin-independent pathways of endocytosis*. Cold Spring Harb Perspect Biol, 2014. **6**(6).
8. Maxfield, F.R. and T.E. McGraw, *Endocytic recycling*. Nat Rev Mol Cell Biol, 2004. **5**(2): p. 121-32.
9. Luzio, J.P., P.R. Pryor, and N.A. Bright, *Lysosomes: fusion and function*. Nat Rev Mol Cell Biol, 2007. **8**(8): p. 622-32.
10. Raposo, G., M.S. Marks, and D.F. Cutler, *Lysosome-related organelles: driving post-Golgi compartments into specialisation*. Curr Opin Cell Biol, 2007. **19**(4): p. 394-401.
11. Zampese, E. and P. Pizzo, *Intracellular organelles in the saga of Ca²⁺ homeostasis: different molecules for different purposes?* Cell Mol Life Sci, 2012. **69**(7): p. 1077-104.
12. Stael, S., et al., *Plant organellar calcium signalling: an emerging field*. J Exp Bot, 2012. **63**(4): p. 1525-42.
13. Clapham, D.E., L.W. Runnels, and C. Strubing, *The TRP ion channel family*. Nat Rev Neurosci, 2001. **2**(6): p. 387-96.

14. Clapham, D.E., *TRP channels as cellular sensors*. Nature, 2003. **426**(6966): p. 517-24.
15. Ramsey, I.S., M. Delling, and D.E. Clapham, *An introduction to TRP channels*. Annu Rev Physiol, 2006. **68**: p. 619-47.
16. Jentsch, T.J., I. Neagoe, and O. Scheel, *CLC chloride channels and transporters*. Curr Opin Neurobiol, 2005. **15**(3): p. 319-25.
17. Huang, P., et al., *P2X4 forms functional ATP-activated cation channels on lysosomal membranes regulated by luminal pH*. J Biol Chem, 2014. **289**(25): p. 17658-67.
18. Cang, C., et al., *TMEM175 Is an Organelle K(+) Channel Regulating Lysosomal Function*. Cell, 2015. **162**(5): p. 1101-12.
19. Cao, Q., et al., *BK Channels Alleviate Lysosomal Storage Diseases by Providing Positive Feedback Regulation of Lysosomal Ca²⁺ Release*. Dev Cell, 2015. **33**(4): p. 427-41.
20. Morgan, A.J., et al., *Molecular mechanisms of endolysosomal Ca²⁺ signalling in health and disease*. Biochem J, 2011. **439**(3): p. 349-74.
21. Koivusalo, M., et al., *In situ measurement of the electrical potential across the lysosomal membrane using FRET*. Traffic, 2011. **12**(8): p. 972-82.
22. Minke, B., C. Wu, and W.L. Pak, *Induction of photoreceptor voltage noise in the dark in Drosophila mutant*. Nature, 1975. **258**(5530): p. 84-7.
23. Montell, C. and G.M. Rubin, *Molecular characterization of the Drosophila trp locus: a putative integral membrane protein required for phototransduction*. Neuron, 1989. **2**(4): p. 1313-23.
24. Hardie, R.C. and B. Minke, *The trp gene is essential for a light-activated Ca²⁺ channel in Drosophila photoreceptors*. Neuron, 1992. **8**(4): p. 643-51.
25. Wes, P.D., et al., *TRPC1, a human homolog of a Drosophila store-operated channel*. Proc Natl Acad Sci U S A, 1995. **92**(21): p. 9652-6.
26. Zhu, X., et al., *Molecular cloning of a widely expressed human homologue for the Drosophila trp gene*. FEBS Lett, 1995. **373**(3): p. 193-8.
27. Harteneck, C., T.D. Plant, and G. Schultz, *From worm to man: three subfamilies of TRP channels*. Trends Neurosci, 2000. **23**(4): p. 159-66.
28. Wu, L.J., T.B. Sweet, and D.E. Clapham, *International Union of Basic and Clinical Pharmacology. LXXVI. Current progress in the mammalian TRP ion channel family*. Pharmacol Rev, 2010. **62**(3): p. 381-404.
29. Nilius, B. and A. Szallasi, *Transient receptor potential channels as drug*

- targets: from the science of basic research to the art of medicine.* Pharmacol Rev, 2014. **66**(3): p. 676-814.
30. Li, M., Y. Yu, and J. Yang, *Structural biology of TRP channels.* Adv Exp Med Biol, 2011. **704**: p. 1-23.
 31. Nilius, B., *Transient receptor potential (TRP) cation channels: rewarding unique proteins.* Bull Mem Acad R Med Belg, 2007. **162**(3-4): p. 244-53.
 32. Nilius, B., et al., *Regulation of TRP channels: a voltage-lipid connection.* Biochem Soc Trans, 2007. **35**(Pt 1): p. 105-8.
 33. Hoenderop, J.G., et al., *Homo- and heterotetrameric architecture of the epithelial Ca²⁺ channels TRPV5 and TRPV6.* EMBO J, 2003. **22**(4): p. 776-85.
 34. Cao, E., et al., *TRPV1 structures in distinct conformations reveal activation mechanisms.* Nature, 2013. **504**(7478): p. 113-8.
 35. Paulsen, C.E., et al., *Structure of the TRPA1 ion channel suggests regulatory mechanisms.* Nature, 2015. **525**(7570): p. 552.
 36. Chen, Q., et al., *Structure of mammalian endolysosomal TRPML1 channel in nanodiscs.* Nature, 2017. **550**(7676): p. 415-418.
 37. Tang, Q., et al., *Structure of the receptor-activated human TRPC6 and TRPC3 ion channels.* Cell Res, 2018. **28**(7): p. 746-755.
 38. Yin, Y., et al., *Structure of the cold- and menthol-sensing ion channel TRPM8.* Science, 2018. **359**(6372): p. 237-241.
 39. Schaefer, M., *Homo- and heteromeric assembly of TRP channel subunits.* Pflugers Arch, 2005. **451**(1): p. 35-42.
 40. Venkatachalam, K. and C. Montell, *TRP channels.* Annu Rev Biochem, 2007. **76**: p. 387-417.
 41. Owsianik, G., et al., *Structure-function relationship of the TRP channel superfamily.* Rev Physiol Biochem Pharmacol, 2006. **156**: p. 61-90.
 42. Grimm, C., et al., *Role of TRPML and two-pore channels in endolysosomal cation homeostasis.* J Pharmacol Exp Ther, 2012. **342**(2): p. 236-44.
 43. Dong, X.P., X. Wang, and H. Xu, *TRP channels of intracellular membranes.* J Neurochem, 2010. **113**(2): p. 313-28.
 44. Xu, H. and D. Ren, *Lysosomal physiology.* Annu Rev Physiol, 2015. **77**: p. 57-80.
 45. Grimm, C. and M.P. Cuajungco, *TRPML Channels and Mucopolipidosis Type IV,* in *Pathologies of Calcium Channels*, N. Weiss and A. Koschak, Editors. 2014,

- Springer Berlin Heidelberg: Berlin, Heidelberg. p. 365-379.
46. Calcraft, P.J., et al., *NAADP mobilizes calcium from acidic organelles through two-pore channels*. *Nature*, 2009. **459**(7246): p. 596-600.
 47. Brailoiu, E., et al., *Essential requirement for two-pore channel 1 in NAADP-mediated calcium signaling*. *J Cell Biol*, 2009. **186**(2): p. 201-9.
 48. Zong, X., et al., *The two-pore channel TPCN2 mediates NAADP-dependent Ca(2+)-release from lysosomal stores*. *Pflugers Arch*, 2009. **458**(5): p. 891-9.
 49. Peiter, E., et al., *The vacuolar Ca²⁺-activated channel TPC1 regulates germination and stomatal movement*. *Nature*, 2005. **434**(7031): p. 404-8.
 50. Ishibashi, K., M. Suzuki, and M. Imai, *Molecular cloning of a novel form (two-repeat) protein related to voltage-gated sodium and calcium channels*. *Biochem Biophys Res Commun*, 2000. **270**(2): p. 370-6.
 51. Brailoiu, E., et al., *An NAADP-gated two-pore channel targeted to the plasma membrane uncouples triggering from amplifying Ca²⁺ signals*. *J Biol Chem*, 2010. **285**(49): p. 38511-6.
 52. Grimm, C., et al., *From mucopolipidosis type IV to Ebola: TRPML and two-pore channels at the crossroads of endo-lysosomal trafficking and disease*. *Cell Calcium*, 2017. **67**: p. 148-155.
 53. Guo, J., et al., *Structure of the voltage-gated two-pore channel TPC1 from *Arabidopsis thaliana**. *Nature*, 2016. **531**(7593): p. 196-201.
 54. Zhu, M.X., et al., *Two-pore channels for integrative Ca signaling*. *Commun Integr Biol*, 2010. **3**(1): p. 12-7.
 55. Cai, X. and S. Patel, *Degeneration of an intracellular ion channel in the primate lineage by relaxation of selective constraints*. *Mol Biol Evol*, 2010. **27**(10): p. 2352-9.
 56. Morgan, A.J. and A. Galione, *Two-pore channels (TPCs): current controversies*. *Bioessays*, 2014. **36**(2): p. 173-83.
 57. Yu, F.H. and W.A. Catterall, *The VGL-kanome: a protein superfamily specialized for electrical signaling and ionic homeostasis*. *Sci STKE*, 2004. **2004**(253): p. re15.
 58. Galione, A., et al., *The acid test: the discovery of two-pore channels (TPCs) as NAADP-gated endolysosomal Ca(2+) release channels*. *Pflugers Arch*, 2009. **458**(5): p. 869-76.
 59. Churamani, D., et al., *Domain assembly of NAADP-gated two-pore channels*.

- Biochem J, 2012. **441**(1): p. 317-23.
60. Rietdorf, K., et al., *Two-pore channels form homo- and heterodimers*. J Biol Chem, 2011. **286**(43): p. 37058-62.
 61. Hooper, R., et al., *Membrane topology of NAADP-sensitive two-pore channels and their regulation by N-linked glycosylation*. J Biol Chem, 2011. **286**(11): p. 9141-9.
 62. Churamani, D., et al., *The N-terminal region of two-pore channel 1 regulates trafficking and activation by NAADP*. Biochem J, 2013. **453**(1): p. 147-51.
 63. Patel, S., *Function and dysfunction of two-pore channels*. Sci Signal, 2015. **8**(384): p. re7.
 64. Ruas, M., et al., *Purified TPC isoforms form NAADP receptors with distinct roles for Ca(2+) signaling and endolysosomal trafficking*. Curr Biol, 2010. **20**(8): p. 703-9.
 65. Lin-Moshier, Y., et al., *Photoaffinity labeling of nicotinic acid adenine dinucleotide phosphate (NAADP) targets in mammalian cells*. J Biol Chem, 2012. **287**(4): p. 2296-307.
 66. Grimm, C., et al., *High susceptibility to fatty liver disease in two-pore channel 2-deficient mice*. Nat Commun, 2014. **5**: p. 4699.
 67. Hockey, L.N., et al., *Dysregulation of lysosomal morphology by pathogenic LRRK2 is corrected by TPC2 inhibition*. J Cell Sci, 2015. **128**(2): p. 232-8.
 68. Lin-Moshier, Y., et al., *The Two-pore channel (TPC) interactome unmasks isoform-specific roles for TPCs in endolysosomal morphology and cell pigmentation*. Proc Natl Acad Sci U S A, 2014. **111**(36): p. 13087-92.
 69. Ruas, M., et al., *TPC1 has two variant isoforms, and their removal has different effects on endo-lysosomal functions compared to loss of TPC2*. Mol Cell Biol, 2014. **34**(21): p. 3981-92.
 70. Castonguay, J., et al., *The two-pore channel TPC1 is required for efficient protein processing through early and recycling endosomes*. Sci Rep, 2017. **7**(1): p. 10038.
 71. Pereira, G.J., et al., *Nicotinic acid adenine dinucleotide phosphate (NAADP) regulates autophagy in cultured astrocytes*. J Biol Chem, 2011. **286**(32): p. 27875-81.
 72. Lin, P.H., et al., *Lysosomal two-pore channel subtype 2 (TPC2) regulates skeletal muscle autophagic signaling*. J Biol Chem, 2015. **290**(6): p. 3377-89.

73. Cang, C., et al., *mTOR regulates lysosomal ATP-sensitive two-pore Na(+)* channels to adapt to metabolic state. *Cell*, 2013. **152**(4): p. 778-790.
74. Davis, L.C., et al., *NAADP activates two-pore channels on T cell cytolytic granules to stimulate exocytosis and killing*. *Curr Biol*, 2012. **22**(24): p. 2331-7.
75. Arndt, L., et al., *NAADP and the two-pore channel protein 1 participate in the acrosome reaction in mammalian spermatozoa*. *Mol Biol Cell*, 2014. **25**(6): p. 948-64.
76. Favia, A., et al., *VEGF-induced neoangiogenesis is mediated by NAADP and two-pore channel-2-dependent Ca²⁺ signaling*. *Proc Natl Acad Sci U S A*, 2014. **111**(44): p. E4706-15.
77. Pafumi, I., et al., *Naringenin Impairs Two-Pore Channel 2 Activity And Inhibits VEGF-Induced Angiogenesis*. *Sci Rep*, 2017. **7**(1): p. 5121.
78. Ramos, I., A. Reich, and G.M. Wessel, *Two-pore channels function in calcium regulation in sea star oocytes and embryos*. *Development*, 2014. **141**(23): p. 4598-609.
79. Horton, J.S., et al., *Two-pore channel 1 interacts with citron kinase, regulating completion of cytokinesis*. *Channels (Austin)*, 2015. **9**(1): p. 21-9.
80. Sakurai, Y., et al., *Ebola virus. Two-pore channels control Ebola virus host cell entry and are drug targets for disease treatment*. *Science*, 2015. **347**(6225): p. 995-8.
81. Gunaratne, G.S., et al., *NAADP-dependent Ca(2+) signaling regulates Middle East respiratory syndrome-coronavirus pseudovirus translocation through the endolysosomal system*. *Cell Calcium*, 2018. **75**: p. 30-41.
82. Sulem, P., et al., *Two newly identified genetic determinants of pigmentation in Europeans*. *Nat Genet*, 2008. **40**(7): p. 835-7.
83. Ambrosio, A.L., et al., *TPC2 controls pigmentation by regulating melanosome pH and size*. *Proc Natl Acad Sci U S A*, 2016. **113**(20): p. 5622-7.
84. Bellono, N.W., I.E. Escobar, and E. Oancea, *A melanosomal two-pore sodium channel regulates pigmentation*. *Sci Rep*, 2016. **6**: p. 26570.
85. Brailoiu, E., et al., *An ancestral deuterostome family of two-pore channels mediates nicotinic acid adenine dinucleotide phosphate-dependent calcium release from acidic organelles*. *J Biol Chem*, 2010. **285**(5): p. 2897-901.

86. Dionisio, N., et al., *Acidic NAADP-releasable Ca(2+) compartments in the megakaryoblastic cell line MEG01*. *Biochim Biophys Acta*, 2011. **1813**(8): p. 1483-94.
87. Ogunbayo, O.A., et al., *Cyclic adenosine diphosphate ribose activates ryanodine receptors, whereas NAADP activates two-pore domain channels*. *J Biol Chem*, 2011. **286**(11): p. 9136-40.
88. Tugba Durlu-Kandilci, N., et al., *TPC2 proteins mediate nicotinic acid adenine dinucleotide phosphate (NAADP)- and agonist-evoked contractions of smooth muscle*. *J Biol Chem*, 2010. **285**(32): p. 24925-32.
89. Yamaguchi, S., et al., *Transient receptor potential mucolipin 1 (TRPML1) and two-pore channels are functionally independent organellar ion channels*. *J Biol Chem*, 2011. **286**(26): p. 22934-42.
90. Walseth, T.F., et al., *Photoaffinity labeling of high affinity nicotinic acid adenine dinucleotide phosphate (NAADP)-binding proteins in sea urchin egg*. *J Biol Chem*, 2012. **287**(4): p. 2308-15.
91. Pitt, S.J., et al., *TPC2 is a novel NAADP-sensitive Ca²⁺ release channel, operating as a dual sensor of luminal pH and Ca²⁺*. *J Biol Chem*, 2010. **285**(45): p. 35039-46.
92. Wang, X., et al., *TPC proteins are phosphoinositide- activated sodium-selective ion channels in endosomes and lysosomes*. *Cell*, 2012. **151**(2): p. 372-83.
93. Jha, A., et al., *Convergent regulation of the lysosomal two-pore channel-2 by Mg(2)(+), NAADP, PI(3,5)P(2) and multiple protein kinases*. *EMBO J*, 2014. **33**(5): p. 501-11.
94. Ruas, M., et al., *Expression of Ca(2)(+)-permeable two-pore channels rescues NAADP signalling in TPC-deficient cells*. *EMBO J*, 2015. **34**(13): p. 1743-58.
95. Rahman, T., et al., *Two-pore channels provide insight into the evolution of voltage-gated Ca²⁺ and Na⁺ channels*. *Sci Signal*, 2014. **7**(352): p. ra109.
96. Guo, J., W. Zeng, and Y. Jiang, *Tuning the ion selectivity of two-pore channels*. *Proc Natl Acad Sci U S A*, 2017. **114**(5): p. 1009-1014.
97. She, J., et al., *Structural insights into the voltage and phospholipid activation of the mammalian TPC1 channel*. *Nature*, 2018. **556**(7699): p. 130-134.
98. Dong, X.P., et al., *PI(3,5)P(2) controls membrane trafficking by direct activation of mucolipin Ca(2+) release channels in the endolysosome*. *Nat*

- Commun, 2010. **1**: p. 38.
99. Cheng, X., et al., *Mucolipins: Intracellular TRPML1-3 channels*. FEBS Lett, 2010. **584**(10): p. 2013-21.
 100. Venkatachalam, K., C.O. Wong, and M.X. Zhu, *The role of TRPMLs in endolysosomal trafficking and function*. Cell Calcium, 2015. **58**(1): p. 48-56.
 101. Dong, X.P., et al., *The type IV mucopolidosis-associated protein TRPML1 is an endolysosomal iron release channel*. Nature, 2008. **455**(7215): p. 992-6.
 102. Feng, X., et al., *Drosophila TRPML forms PI(3,5)P2-activated cation channels in both endolysosomes and plasma membrane*. J Biol Chem, 2014. **289**(7): p. 4262-72.
 103. Xiong, J. and M.X. Zhu, *Regulation of lysosomal ion homeostasis by channels and transporters*. Sci China Life Sci, 2016. **59**(8): p. 777-91.
 104. Schmiege, P., et al., *Human TRPML1 channel structures in open and closed conformations*. Nature, 2017. **550**(7676): p. 366-370.
 105. Vergarajauregui, S. and R. Puertollano, *Two di-leucine motifs regulate trafficking of mucolipin-1 to lysosomes*. Traffic, 2006. **7**(3): p. 337-53.
 106. Miedel, M.T., et al., *Posttranslational cleavage and adaptor protein complex-dependent trafficking of mucolipin-1*. J Biol Chem, 2006. **281**(18): p. 12751-9.
 107. Pryor, P.R., et al., *Mucolipin-1 is a lysosomal membrane protein required for intracellular lactosylceramide traffic*. Traffic, 2006. **7**(10): p. 1388-98.
 108. Puertollano, R. and K. Kiselyov, *TRPMLs: in sickness and in health*. Am J Physiol Renal Physiol, 2009. **296**(6): p. F1245-54.
 109. Li, X., et al., *A molecular mechanism to regulate lysosome motility for lysosome positioning and tubulation*. Nat Cell Biol, 2016. **18**(4): p. 404-17.
 110. Zhang, X., et al., *MCOLN1 is a ROS sensor in lysosomes that regulates autophagy*. Nat Commun, 2016. **7**: p. 12109.
 111. Settembre, C., et al., *TFEB links autophagy to lysosomal biogenesis*. Science, 2011. **332**(6036): p. 1429-33.
 112. Shen, D., et al., *Lipid storage disorders block lysosomal trafficking by inhibiting a TRP channel and lysosomal calcium release*. Nat Commun, 2012. **3**: p. 731.
 113. Zhang, X., X. Li, and H. Xu, *Phosphoinositide isoforms determine compartment-specific ion channel activity*. Proc Natl Acad Sci U S A, 2012.

- 109**(28): p. 11384-9.
114. De Leo, M.G., et al., *Autophagosome-lysosome fusion triggers a lysosomal response mediated by TLR9 and controlled by OCRL*. *Nat Cell Biol*, 2016. **18**(8): p. 839-850.
 115. Miao, Y., et al., *A TRP Channel Senses Lysosome Neutralization by Pathogens to Trigger Their Expulsion*. *Cell*, 2015. **161**(6): p. 1306-19.
 116. Li, R.J., et al., *Regulation of mTORC1 by lysosomal calcium and calmodulin*. *Elife*, 2016. **5**.
 117. Onyenwoke, R.U., et al., *The mucopolidosis IV Ca²⁺ channel TRPML1 (MCOLN1) is regulated by the TOR kinase*. *Biochem J*, 2015. **470**(3): p. 331-42.
 118. Sun, X., et al., *A negative feedback regulation of MTORC1 activity by the lysosomal Ca(2+) channel MCOLN1 (mucolipin 1) using a CALM (calmodulin)-dependent mechanism*. *Autophagy*, 2018. **14**(1): p. 38-52.
 119. Medina, D.L., et al., *Lysosomal calcium signalling regulates autophagy through calcineurin and TFEB*. *Nat Cell Biol*, 2015. **17**(3): p. 288-99.
 120. Bassi, M.T., et al., *Cloning of the gene encoding a novel integral membrane protein, mucolipidin-and identification of the two major founder mutations causing mucopolidosis type IV*. *Am J Hum Genet*, 2000. **67**(5): p. 1110-20.
 121. Sun, M., et al., *Mucopolidosis type IV is caused by mutations in a gene encoding a novel transient receptor potential channel*. *Hum Mol Genet*, 2000. **9**(17): p. 2471-8.
 122. Bretou, M., et al., *Lysosome signaling controls the migration of dendritic cells*. *Sci Immunol*, 2017. **2**(16).
 123. Xu, M., et al., *The lysosomal TRPML1 channel regulates triple negative breast cancer development by promoting mTORC1 and purinergic signaling pathways*. *Cell Calcium*, 2019. **79**: p. 80-88.
 124. Jung, J., et al., *HRAS-driven cancer cells are vulnerable to TRPML1 inhibition*. *EMBO Rep*, 2019. **20**(4).
 125. Kim, M.S., et al., *Exosomal release through TRPML1-mediated lysosomal exocytosis is required for adipogenesis*. *Biochem Biophys Res Commun*, 2019. **510**(3): p. 409-415.
 126. Di Paola, S. and D.L. Medina, *TRPML1-/TFEB-Dependent Regulation of Lysosomal Exocytosis*. *Methods Mol Biol*, 2019. **1925**: p. 143-144.
 127. Lev, S., et al., *Constitutive activity of the human TRPML2 channel induces*

- cell degeneration*. J Biol Chem, 2010. **285**(4): p. 2771-82.
128. Cuajungco, M.P., et al., *The mucolipin-2 (TRPML2) ion channel: a tissue-specific protein crucial to normal cell function*. Pflugers Arch, 2016. **468**(2): p. 177-92.
129. Garcia-Anoveros, J. and T. Wiwatpanit, *TRPML2 and mucolipin evolution*. Handb Exp Pharmacol, 2014. **222**: p. 647-58.
130. Sun, L., et al., *Novel Role of TRPML2 in the Regulation of the Innate Immune Response*. J Immunol, 2015. **195**(10): p. 4922-32.
131. Valadez, J.A. and M.P. Cuajungco, *PAX5 is the transcriptional activator of mucolipin-2 (MCOLN2) gene*. Gene, 2015. **555**(2): p. 194-202.
132. Venkatachalam, K., T. Hofmann, and C. Montell, *Lysosomal localization of TRPML3 depends on TRPML2 and the mucopolidosis-associated protein TRPML1*. J Biol Chem, 2006. **281**(25): p. 17517-27.
133. Karacsonyi, C., A.S. Miguel, and R. Puertollano, *Mucolipin-2 localizes to the Arf6-associated pathway and regulates recycling of GPI-APs*. Traffic, 2007. **8**(10): p. 1404-14.
134. Plesch, E., et al., *Selective agonist of TRPML2 reveals direct role in chemokine release from innate immune cells*. Elife, 2018. **7**.
135. Rinkenberger, N. and J.W. Schoggins, *Mucolipin-2 Cation Channel Increases Trafficking Efficiency of Endocytosed Viruses*. MBio, 2018. **9**(1).
136. Grimm, C., et al., *A helix-breaking mutation in TRPML3 leads to constitutive activity underlying deafness in the varitint-waddler mouse*. Proc Natl Acad Sci U S A, 2007. **104**(49): p. 19583-8.
137. Grimm, C., et al., *Small molecule activators of TRPML3*. Chem Biol, 2010. **17**(2): p. 135-48.
138. Kim, C., *TRPV Family Ion Channels and Other Molecular Components Required for Hearing and Proprioception in Drosophila*, in *TRP Ion Channel Function in Sensory Transduction and Cellular Signaling Cascades*, W.B. Liedtke and S. Heller, Editors. 2007: Boca Raton (FL).
139. Kim, H.J., et al., *Properties of the TRPML3 channel pore and its stable expansion by the Varitint-Waddler-causing mutation*. J Biol Chem, 2010. **285**(22): p. 16513-20.
140. Xu, H., et al., *Activating mutation in a mucolipin transient receptor potential channel leads to melanocyte loss in varitint-waddler mice*. Proc Natl Acad Sci U S A, 2007. **104**(46): p. 18321-6.

141. Nagata, K., et al., *The varitint-waddler (Va) deafness mutation in TRPML3 generates constitutive, inward rectifying currents and causes cell degeneration*. Proc Natl Acad Sci U S A, 2008. **105**(1): p. 353-8.
142. Dong, X.P., et al., *Activating mutations of the TRPML1 channel revealed by proline-scanning mutagenesis*. J Biol Chem, 2009. **284**(46): p. 32040-52.
143. Samie, M.A., et al., *The tissue-specific expression of TRPML2 (MCOLN-2) gene is influenced by the presence of TRPML1*. Pflugers Arch, 2009. **459**(1): p. 79-91.
144. Di Palma, F., et al., *Mutations in Mcoln3 associated with deafness and pigmentation defects in varitint-waddler (Va) mice*. Proc Natl Acad Sci U S A, 2002. **99**(23): p. 14994-9.
145. Kim, H.J., et al., *The Ca(2+) channel TRPML3 regulates membrane trafficking and autophagy*. Traffic, 2009. **10**(8): p. 1157-67.
146. Kim, H.J., et al., *A novel mode of TRPML3 regulation by extracytosolic pH absent in the varitint-waddler phenotype*. EMBO J, 2008. **27**(8): p. 1197-205.
147. Jors, S., et al., *Genetic inactivation of Trpml3 does not lead to hearing and vestibular impairment in mice*. PLoS One, 2010. **5**(12): p. e14317.
148. Castiglioni, A.J., et al., *Expression and vesicular localization of mouse Trpml3 in stria vascularis, hair cells, and vomeronasal and olfactory receptor neurons*. J Comp Neurol, 2011. **519**(6): p. 1095-1114.
149. Remis, N.N., et al., *Mucolipin co-deficiency causes accelerated endolysosomal vacuolation of enterocytes and failure-to-thrive from birth to weaning*. PLoS Genet, 2014. **10**(12): p. e1004833.
150. Wiwatpanit, T., et al., *Codeficiency of Lysosomal Mucolipins 3 and 1 in Cochlear Hair Cells Diminishes Outer Hair Cell Longevity and Accelerates Age-Related Hearing Loss*. J Neurosci, 2018. **38**(13): p. 3177-3189.
151. Neher, E. and B. Sakmann, *Single-channel currents recorded from membrane of denervated frog muscle fibres*. Nature, 1976. **260**(5554): p. 799-802.
152. Hamill, O.P., et al., *Improved patch-clamp techniques for high-resolution current recording from cells and cell-free membrane patches*. Pflugers Arch, 1981. **391**(2): p. 85-100.
153. Trowbridge, I.S., J.F. Collawn, and C.R. Hopkins, *Signal-dependent membrane protein trafficking in the endocytic pathway*. Annu Rev Cell Biol, 1993. **9**: p. 121-164.

1993. **9**: p. 129-61.
154. Sandoval, I.V. and O. Bakke, *Targeting of membrane proteins to endosomes and lysosomes*. Trends Cell Biol, 1994. **4**(8): p. 292-7.
155. Bonifacino, J.S. and E.C. Dell'Angelica, *Molecular bases for the recognition of tyrosine-based sorting signals*. J Cell Biol, 1999. **145**(5): p. 923-6.
156. Bonifacino, J.S. and L.M. Traub, *Signals for sorting of transmembrane proteins to endosomes and lysosomes*. Annu Rev Biochem, 2003. **72**: p. 395-447.
157. Zhang, F. and P.L. Li, *Reconstitution and characterization of a nicotinic acid adenine dinucleotide phosphate (NAADP)-sensitive Ca²⁺ release channel from liver lysosomes of rats*. J Biol Chem, 2007. **282**(35): p. 25259-69.
158. Zhang, F., et al., *TRP-ML1 functions as a lysosomal NAADP-sensitive Ca²⁺ release channel in coronary arterial myocytes*. J Cell Mol Med, 2009. **13**(9B): p. 3174-85.
159. Pitt, S.J., et al., *Reconstituted human TPC1 is a proton-permeable ion channel and is activated by NAADP or Ca²⁺*. Sci Signal, 2014. **7**(326): p. ra46.
160. Grynkiewicz, G., M. Poenie, and R.Y. Tsien, *A new generation of Ca²⁺ indicators with greatly improved fluorescence properties*. J Biol Chem, 1985. **260**(6): p. 3440-50.
161. Takahashi, A., et al., *Measurement of intracellular calcium*. Physiol Rev, 1999. **79**(4): p. 1089-125.
162. Demaurex, N., *Calcium measurements in organelles with Ca²⁺-sensitive fluorescent proteins*. Cell Calcium, 2005. **38**(3-4): p. 213-22.
163. McCombs, J.E. and A.E. Palmer, *Measuring calcium dynamics in living cells with genetically encodable calcium indicators*. Methods, 2008. **46**(3): p. 152-9.
164. Schieder, M., et al., *Planar patch clamp approach to characterize ionic currents from intact lysosomes*. Sci Signal, 2010. **3**(151): p. pl3.

Curriculum vitae

Personal information

Name: Yu-Kai, Chao
Place of birth: Kaohsiung, Taiwan
Date of birth: 07.01.1986
Email: Yu-Kai.Chao@cup.uni-muenchen.de

Education

Ludwig-Maximilian University (LMU), Munich, Germany (2014-Present)
PhD student. Department of Pharmacy – Center for Drug Research, concentration in ion channel field
Supervisor – Prof. Dr. Dr. Christian Michael Grimm (Dr. rer. nat.)

College of Medicine, National Taiwan University (NTU), Taipei, Taiwan (2008-2010)
Master of Science, Clinical Laboratory Science & Medical Biotechnology, concentration in virology
Supervisor – Dr. Chang, Sui-Yuan (Sc.D.)
Master thesis – The Role of Annexin II in Human Herpes Simplex Virus Type 1 Production.

College of Medicine, Chang Gung University, Taoyuan, Taiwan (2004-2008)
Bachelor of Science, Medical Laboratory Science
Supervisor – Dr. Chong, Kowit-Yu (Ph.D.)
Bachelor thesis – Investigation of gene expression level triggered by different promoters in Lentiviral vector

Working experience

Quality Engineer, Department of Quality Assurance, IMPAX Laboratories, Inc.
Zhunan, Taiwan (2012–2014)

Researcher, Department of Clinical Laboratory Science & Medical Biotechnology, National Taiwan University
Taipei, Taiwan (2011–2012)

Second Lieutenant, Armed Forces Zuoying General Hospital
Kaohsiung, Taiwan (2010–2011)

Teaching Assistant, Introductory Clinical Virology, National Taiwan University
Taipei, Taiwan (2008–2009)

Medical Technologist Intern, Chang Gung Memorial Hospital
LinKou, Taiwan (2007–2008)

Complete list of original publications

1. Villella VR, Venerando A, Cozza G, Esposito S, Ferrari E, Monzani R, Spinella MC, Oikonomou V, Renga G, Tosco A, Rossin F, Guido S, Silano M, Garaci E, **Chao YK**, Grimm C, Luciani A, Romani L, Piacentini M, Raia V, Kroemer G, Maiuri L. "A pathogenic role for cystic fibrosis transmembrane conductance regulator in celiac disease." *EMBO J.* 2019 Jan 15;38(2).
2. **Chao YK***, Schludi V*, Chen CC, Butz E, Nguyen ONP, Müller M, Krüger J, Kammerbauer C, Ben-Johny M, Vollmar AM, Berking C, Biel M, Wahl-Schott CA, Grimm C. "TPC2 polymorphisms associated with a hair pigmentation phenotype in humans result in gain of channel function by independent mechanisms." *Proc Natl Acad Sci U S A.* 2017 Oct 10;114(41):E8595-E8602.
3. Chen CC*, Butz ES*, **Chao YK**, Grishchuk Y, Becker L, Heller S, Slaugenhaupt SA, Biel M, Wahl-Schott C, Grimm C. "Small Molecules for Early Endosome-Specific Patch Clamping." *Cell Chem Biol.* 2017 Jul 20;24(7):907-916.
4. Chen CC*, Cang C*, Fenske S, Butz E, **Chao YK**, Biel M, Ren D, Wahl-Schott C, Grimm C. "Patch-clamp technique to characterize ion channels in enlarged individual endolysosomes." *Nat Protoc.* 2017 Aug;12(8):1639-1658.
5. Nguyen ON*, Grimm C*, Schneider LS, **Chao YK**, Atzberger C, Bartel K, Watermann A, Ulrich M, Mayr D, Wahl-Schott C, Biel M, Vollmar AM. "Two-Pore Channel Function Is Crucial for the Migration of Invasive Cancer Cells." *Cancer Res.* 2017 Mar 15;77(6):1427-1438.
6. Beck S, Henß L, Weidner T, Herrmann J, Müller R, **Chao YK**, Grimm C, Weber C, Sliva K, Schnierle BS. "Identification of entry inhibitors of Ebola virus pseudotyped vectors from a myxobacterial compound library." *Antiviral Res.* 2016 Aug;132:85-91.
7. Lin PH, Ke YY, Su CT, Shiao HY, Hsieh HP, **Chao YK**, Lee CN, Kao CL, Chao YS, Chang SY. "Inhibition of HIV-1 Tat-mediated transcription by a coumarin derivative, BPRHIV001, through the Akt pathway." *J Virol.* 2011 Sep;85(17):9114-26.

* These authors contributed equally

Acknowledgement

I would like to express the deepest appreciation to my supervisors Prof. Dr. Dr. Christian Grimm and Prof. Dr. Martin Biel for the best opportunity to join the group in Germany, this dissertation would not have been possible without their guidance and persistent help. I would particularly like to acknowledge Dr. Cheng-Chang (Maxo) Chen for his wonderful collaboration, Maxo supported me greatly and were always willing to help me not only in the work but also the living in Germany, besides, I won't have the ability to conduct lysosomal patch-clamp without his guidance. Sincerely acknowledgement for the time and interest to my examination committee member, Prof. Dr. Angelika Vollmar, Prof. Dr. Alexander Dietrich, Prof. Dr. Franz Bracher, and Prof. Dr. Stefan Zahler, it is my pleasure to have you be in the board. Verena and Elisabeth, I'm glad to work with you and I cherished all the memories we had together. Phuong, Martin, and Karin, thank you for all the efforts and supports, and also the contribution from Martin to the science work. Susi and Eva, it's my pleasure to have the chance cooperating with you on those amazing chemical compounds. Marc, thank you for your caring and all the accompany in the lab. My sincere thanks also go to all the current and past members in the wonderful group from Prof. Biel's lab, Prof. Wahl-Schott, Dr. Michalakis, Dr. Becirovic, Dr. Fenske, Dr. Hammelmann, Dr. Schön, Dr. Le Meur, Dr. Murenu, Dr. Perera, Dr. Koch, Dr. Spahn, Dr. Böhm, Dr. Splith, Dr. Geserich, Ella, Grazia, Rasmus, Konstantin, Henrik, Jennifer, Anna, Marina, Lisa, Rene, Constanze, Sebastian, Verena, and Johanna. Many thanks to Elisabeth, Berit, Melanie, Kerstin, Jojo, Tamara, Mariella, Selina, and Monika. I will never forget their great support. I also owe my gratitude to those lovely colleagues from Prof. Grimm's group, Anna, Barbara, Carla, Einar, Iria, Julia, Judith, Marcel, Ness, Rachael, Thiemo, it's really nice to work with you. Xiangang, Zhuolu, Shuaijun, and Yanfen, I'm glad to work with you despite the political issue between our countries. Many thanks to all my friends, especially Kathi, Shuan-Hsiao, James, Yi-Li, and Bei-bei, who support my life during thesis period and also provide happy distraction to rest my mind outside of my research. Last but not least, I would like to thank my parents and my sister for sympathetic ear and mental supports. Most importantly, I wish to thank my loving and supportive wife, Hsin-Hsuan, you are always there for me.

Appendix

In the following, manuscripts 1 to 4 are reprinted:

1. Chen CC*, Cang C*, Fenske S, Butz E, **Chao YK**, Biel M, Ren D, Wahl-Schott C, Grimm C. "Patch-clamp technique to characterize ion channels in enlarged individual endolysosomes." *Nat Protoc.* 2017 Aug;12(8):1639-1658.
2. Chen CC*, Butz ES*, **Chao YK**, Grishchuk Y, Becker L, Heller S, Slaugenhaupt SA, Biel M, Wahl-Schott C, Grimm C. "Small Molecules for Early Endosome-Specific Patch Clamping." *Cell Chem Biol.* 2017 Jul 20;24(7):907-916.
3. Nguyen ON*, Grimm C*, Schneider LS, **Chao YK**, Atzberger C, Bartel K, Watermann A, Ulrich M, Mayr D, Wahl-Schott C, Biel M, Vollmar AM. "Two-Pore Channel Function Is Crucial for the Migration of Invasive Cancer Cells." *Cancer Res.* 2017 Mar 15;77(6):1427-1438.
4. **Chao YK***, Schludi V*, Chen CC, Butz E, Nguyen ONP, Müller M, Krüger J, Kammerbauer C, Ben-Johny M, Vollmar AM, Berking C, Biel M, Wahl-Schott CA, Grimm C. "TPC2 polymorphisms associated with a hair pigmentation phenotype in humans result in gain of channel function by independent mechanisms." *Proc Natl Acad Sci U S A.* 2017 Oct 10;114(41):E8595-E8602.

Patch-clamp technique to characterize ion channels in enlarged individual endolysosomes

Cheng-Chang Chen^{1,4}, Chunlei Cang^{2,4} , Stefanie Fenske¹, Elisabeth Butz¹, Yu-Kai Chao¹ , Martin Biel¹, Dejian Ren³, Christian Wahl-Schott¹ & Christian Grimm¹

¹Department of Pharmacy – Center for Drug Research and Center for Integrated Protein Science Munich (CIPSM), Ludwig-Maximilians-Universität München, München, Germany. ²School of Life Sciences, University of Science & Technology of China, Hefei, China. ³Department of Biology, University of Pennsylvania, Philadelphia, Pennsylvania, USA. ⁴These authors contributed equally to this work. Correspondence should be addressed to C.G. (chgrph@cup.uni-muenchen.de) or C.W.-S. (christian.wahl@cup.uni-muenchen.de).

Published online 20 July 2017; doi:10.1038/nprot.2017.036

According to proteomics analyses, more than 70 different ion channels and transporters are harbored in membranes of intracellular compartments such as endosomes and lysosomes. Malfunctioning of these channels has been implicated in human diseases such as lysosomal storage disorders, neurodegenerative diseases and metabolic pathologies, as well as in the progression of certain infectious diseases. As a consequence, these channels have engendered very high interest as future drug targets. Detailed electrophysiological characterization of intracellular ion channels is lacking, mainly because standard methods to analyze plasma membrane ion channels, such as the patch-clamp technique, are not readily applicable to intracellular organelles. Here we present a protocol detailing how to implement a manual patch-clamp technique for endolysosomal compartments. In contrast to the alternatively used planar endolysosomal patch-clamp technique, this method is a visually controlled, direct patch-clamp technique similar to conventional patch-clamping. The protocol assumes basic knowledge and experience with patch-clamp methods. Implementation of the method requires up to 1 week, and material preparation takes ~2–4 d. An individual experiment (i.e., measurement of channel currents across the endolysosomal membrane), including control experiments, can be completed within 1 h. This excludes the time for endolysosome enlargement, which takes between 1 and 48 h, depending on the approach and cell type used. Data analysis requires an additional hour.

INTRODUCTION

The membranes of intracellular organelles make up the majority of the total cell membrane and harbor a large number of transmembrane proteins, including many ion channels. Among these intracellular channels, ion channels localized in endolysosomal membranes have recently generated particular interest. They are fundamental to the control of numerous physiological functions, including endolysosomal ion and pH homeostasis, regulation of endolysosomal resting membrane potential, catabolic export of amino acids, vesicle trafficking and vesicle fusion^{1–7}. Loss of function or dysfunction of endolysosomal ion channels underlies human metabolic diseases such as nonalcoholic fatty liver disease and hyperlipoproteinemia, affects the development of certain infectious diseases and is implicated in the development of congenital lysosomal storage disorders and neurodegenerative diseases such as Alzheimer's disease and Parkinson's disease^{1,6–11}. For example, Hockey *et al.* recently demonstrated that defects such as enlarged and aggregated lysosomes in fibroblasts from Parkinson's disease patients with the common G2019S mutation in LRRK2 (leucine-rich repeat kinase 2) could be corrected by molecular silencing of TPC2 (two-pore channel 2), pharmacological inhibition of TPC regulators (Rab7, NAADP and PtdIns(3,5)P2) and buffering local Ca²⁺ increases¹¹. The strong link between dysfunction or loss of function of these channels and the pathophysiology of human disease indicates that these ion channels have a high potential to become clinically relevant drug targets. In addition, organelle proteomic studies suggest that there is a plethora of other putative ion channels and transporters (>70) in endolysosomes that remain to be characterized^{12,13}.

Development of the protocol

To functionally characterize endolysosomal ion channels in detail, electrophysiological methods are inevitable. In the past,

these channels could not be analyzed in detail because of the lack of direct methods, in particular because of the inaccessibility of these channels by the patch-clamp method. In addition to technical problems arising from the intracellular localization of these channels *per se*, the small sizes (~0.5 μm) of endosomes and lysosomes preclude the use of standard patch-clamp electrodes. To circumvent this, endolysosomal channel proteins can be purified and reconstituted in artificial membranes or bilayers^{14–17}. Alternatively, Ca²⁺-conducting endolysosomal ion channels can be analyzed by Ca²⁺-imaging techniques. However, all these methods suffer from methodological drawbacks (see 'Comparison with alternative approaches' section). Recently, we used a planar patch-clamp approach that is well suited to direct analysis of endolysosomal ion channels such as TRPML channels (also called MCOLN channels or mucopolipins) and TPCs^{18–22}, and also to characterization of bacterial and mitochondrial ion channels. Although the planar patch-clamp method is technically straightforward to perform even at high efficiency, the most substantial limitation of this method is that Ca²⁺ cannot be omitted on one side of the endolysosomal membrane (a high Ca²⁺ concentration is required for successful gigaseal formation, as described previously²³), which limits the degree of freedom of experimental design. Here, we describe a method that overcomes this problem by using the conventional patch-clamp technique. In combination with pharmacological tools to enlarge endolysosomal vesicles to a degree suitable for manual patch-clamp (>4 μm), this method is very powerful. In this protocol, a set of techniques is provided that is well suited to the characterization of ionic currents from endolysosomes and that does not have major technical restrictions or experimental restraints. The protocol assumes basic knowledge of patch-clamp methods.

PROTOCOL

Overview of the procedure

In our recent studies^{1,8}, we adopted a robust methodology that has recently been used by other groups^{2,24}. This approach permits efficient endolysosomal patch-clamping of ion channels from heterologous expression, as well as from native cells such as cardiomyocytes, hippocampal neurons or macrophages. Initially, a suitable cell system for endolysosomal patch-clamping must be selected. Then, the specific expression of the ion channel in question must be confirmed in the endolysosomal system. This can be done by standard molecular biology and cell culture methods, and will not be described in this protocol. Once a suitable cell system is selected and the expression of the ion channels in question is verified, the actual patch-clamp experiment can be performed. The following five stages, most of which are also applied in conventional patch-clamping, have been specifically optimized (see Fig. 1 for an overview of the PROCEDURE): enlargement of endolysosomal vesicles using one of the described approaches (Steps 11 and 12), the design and production of high-end glass electrodes (Steps 13–27), the dissection and release of endolysosomal vesicles from the cells into the culture dish (Steps 28–38) and the actual patch-clamp experiment (39–55). As a whole, the technique provides a valuable tool for high-efficiency state-of-the-art recordings from endolysosomal ion channels. In the ‘Experimental design’ section, we outline the key modifications that are central to the optimal performance of the protocol.

Applications of the assay and target audience

This protocol is dedicated to scientists working on endolysosomal ion channels. Using endolysosomal patch-clamp technology, known endolysosomal ion channels can be analyzed, and novel channels and transporters can be discovered and characterized. The technique outlined in this protocol will open a broad spectrum of novel applications dealing with endolysosomal ion channel function and dysfunction. The method can also complement drug screening to identify new drugs for lysosomal ion channels. Compounds identified in such a screen could be validated individually using the robustness of lysosomal patch-clamp. Our protocol provides the scientific framework that enables the experimenter to establish direct methodologies for electrophysiological recordings of endolysosomal ion channels and to directly address related scientific questions. The technology can be modified for recordings of other endolysosomal-like organelles, such as phagosomes²⁵ or melanosomes²⁶, and, potentially, of other intracellular vesicles and organelles, such as secretory granules or Golgi-derived vesicles. However, the technique might not be applicable to very large organelles with a more complex architecture—in particular, endoplasmic reticulum (ER).

Advantages and limitations of the assay

The key advantages of this method for recording endolysosomal ion channels are as follows:

- The method is direct. It allows for direct measurements of endolysosomal ion channels in their quasi-native environment. There is no need for biochemical isolation or purification of endolysosomal vesicles. The method is suitable for studies of already-known endolysosomal ion channels and, more importantly, for the discovery and characterization of new ones.
- The method is very robust. It is possible to control most parameters just as in conventional patch-clamp.

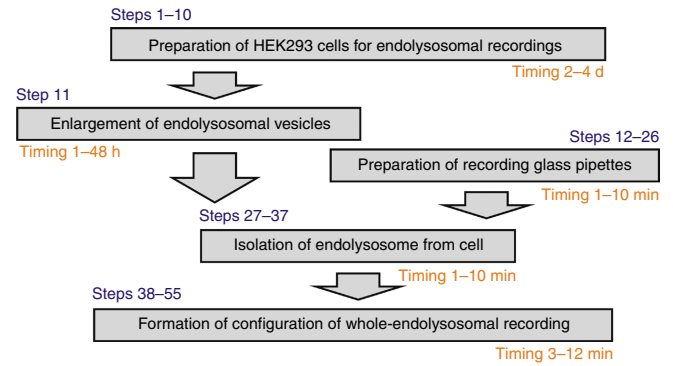


Figure 1 | Overview of the Procedure: whole-organelle patch-clamp approach.

- The protocol has broad applications in cell lines such as HEK293 cells and native cells.
- The level of technical challenge is comparable to that of conventional patch-clamp.
- The protocol generally does not require specific equipment (requires only standard electrophysiological equipment); one exception is the electrode puller. We recommend using a Sutter model P-97.
- Visual control allows identification of specific target vesicles expressing fluorescent-protein-tagged channel variants using epifluorescence microscopy. Enlarged lysosomes are fragile spherical vesicles that can be discriminated from other intracellular organelles. Visual control is vital for selecting the correct vesicles and for monitoring during the subsequent patch-clamp experiment.

The method also has some potential drawbacks and pitfalls:

- Enlargement of endolysosomes using small molecules or expression of mutant Rab variants bears the risk of potential artifacts. First, artifacts could result from changes in endolysosomal membrane structure and/or composition of lipids and proteins. Second, small molecules could directly interact with the ion channel in question and affect the properties. The mechanisms regarding how vacuolin-1 and the other molecules enlarge endolysosomes are still not fully understood.
- Similar to conventional patch-clamp in general, there is a potential risk for selection bias. Given that dissection, seal formation and recording of large lysosomes are much easier as compared with those of small ones with this protocol, the experimenter might be tempted to preferentially select very large endolysosomes (as opposed to planar patch-clamp).
- It is difficult to exchange the electrode solution with this protocol (as opposed to planar patch-clamp).
- Production of patch pipettes is difficult, and optimization of the protocol for the P-97 puller is time-consuming.
- It is quite probable that cytosolic factors such as small molecules or proteins associated with endolysosomal membranes are altered or lost when cells are sliced and endolysosomes are dissected and released from the cytosol. This loss of factors could lead to a change or lack in regulation of properties of the channel in question.

Comparison with alternative approaches

A limited number of methods are currently available for the characterization of endolysosomal and other intracellular ion channels. The standard method used is to reconstitute purified ion channel

proteins or membranes of isolated cell organelles into synthetic phospholipid bilayers^{14,15}. Alternatively, purified channel proteins or membrane vesicles can be reconstituted into liposomes that are quite large and can be analyzed by means of conventional patch-clamp^{16,17}. The main conceptual drawback of these methods is that the ion channel proteins are extracted from their physiological environment. This procedure bears a high risk of losing important factors, such as critical components of the lipid membrane, as well as specific modulators and accessory subunits that are associated *in vivo* with the ion channel protein. Other approaches for investigating intracellular ion channels in organelles include Ca²⁺ imaging²⁷. This technique is an option only for ion channels permeable to Ca²⁺. For these experiments, either Ca²⁺ indicators or better genetically encoded Ca²⁺ sensors can be used. One option is to design fusion proteins that combine genetically encoded Ca²⁺ sensor proteins with endolysosomal ion channels. Most endolysosomal ion channels' N and C termini face the cytosolic side of the lysosomal membrane. Therefore, attaching genetically encoded Ca²⁺ channels to either the N or the C terminus resolves Ca²⁺ signals in the ultimate proximity of the cytoplasmic opening of the channel in question. However, these methods lack some advantages of patch-clamp analysis, including the ability to directly access ion channels. Furthermore, disrupting lysosomal targeting motifs has been shown to effectively (mis)target endolysosomal ion channels to the plasma membrane, where they are accessible to conventional patch-clamp experimentation²⁸. Finally, we recently applied a planar patch-clamp approach to electrophysiologically analyze endolysosomal ion channels. It is possible to efficiently obtain electrophysiological recordings using this approach. The planar patch-clamp method allows reliable and efficient characterization of currents from isolated endolysosomes. Furthermore, a direct side-by-side comparison of electrophysiological experiments using planar patch-clamp and endolysosomal patch-clamp (using the protocol described here) revealed similar functional properties for TRPML1, TRPML3, TPC1 and TPC2, which cross-validates these methods. The advantages of planar patch-clamp are that even small and native endolysosomes that have not been enlarged can be analyzed. Furthermore, in planar patch-clamp there is no selection bias, as there is inherently no visualization by a microscopy or micromanipulation system. Disadvantages of planar patch-clamp are that purification of endolysosomal vesicles is required and that the method lacks visual control by microscopy optics and mechanical control via a micromanipulator. Furthermore, no inside-out or outside-out patches can be produced. The most noteworthy drawback of planar patch-clamp is the low degree of freedom in the design of solutions—for example, it is not possible to record in Ca²⁺-free solution.

Experimental design

Here, we present a comprehensive protocol for endolysosomal patch-clamp. There are technical challenges in the experimental aspect of the protocol (expression of endolysosomal channels in heterologous systems, preparation of native cells, enlargement of endolysosomes, design of patch electrodes, dissection of endolysosomes), as well as in the acquisition and the analysis of patch-clamp data.

Generation and validation of heterologous and native cell systems suitable for endolysosomal patch-clamp.

In general,

any cell type, such as HEK293 cells, transiently or stably expressing endolysosomal ion channels, as well as native cells prepared from wild-type or genetically modified mouse lines, can be used for endolysosomal patch-clamp. For rules and considerations in regard to how to generate, express and validate expression of tagged and nontagged ion channel variants in different cell lines, we refer to standard literature for detailed protocols on transfection, generation of stable cell lines and preparation and cultivation of native cells from mice. In this protocol, we will focus on HEK293 cells expressing endolysosomal ion channels to describe the endolysosomal patch-clamp approach.

Cell lines transiently or stably expressing channel variants tagged by fluorescent proteins attached to the N- or C-terminal cytosolic part of the channel protein are useful because the specific expression in the correct vesicle system can be confirmed by confocal imaging in living cells. This can be done by coexpressing marker proteins such as Rab5 for early/sorting endosomes, Rab11 for recycling endosomes, and Rab7 or LAMP1 for late endosomes and lysosomes. Here, it should be taken into consideration that overexpression of channel proteins or marker proteins may change endolysosomal morphology (e.g., diameter). Cells can also be fixed and immunocytochemistry can be performed to find out which specific vesicle type expresses the desired ion channel. There are excellent commercially available antibodies that selectively stain early/sorting endosomes (Rab5), recycling endosomes (Rab11) or late endosomes/lysosomes (Rab7/LAMP1). For these experiments, either tagged or untagged channel proteins can be used. If specific antibodies are available to reliably detect the desired endolysosomal channel, immunocytochemistry can be performed in cells expressing untagged channel variants or in native cells.

It is reasonable to start with cell lines stably expressing tagged channel variants. As soon as it is clear in which vesicle the channel is expressed, the tag can be omitted and cell lines stably expressing the untagged channel variant can be used for further experiments. The advantage is that potential artifacts associated with fusion of fluorophores to channels can be ruled out. Alternatively, bicistronic expression plasmids can be used, which lead to expression of the untagged channel protein in one reading frame and a fluorophore in another reading frame. By this approach, cells expressing the channel are marked by the fluorophore.

We also use native cell lines for endolysosomal patch-clamp experiments. For example, immortalized mouse embryonal fibroblasts (MEF cells) are very convenient cell lines for endolysosomal research in general. We produced and patch-clamped MEF cells from wild-type mice and genetically modified mouse models lacking TRPML channels or TPCs. These lines can be cultured for 4–8 passages for endolysosomal patch-clamp experiments. Mutant MEFs can also be engineered using the CRISPR/Cas system or standard shRNA-mediated knockdown approaches. In addition to MEFs, we use primary cells such as cardiomyocytes, hippocampal neurons, glial cells, peritoneal and other tissue macrophages, hepatocytes, and kidney and bladder epithelial cells. For native cells, specific expression of the desired ion channel in distinct endolysosomal vesicles is determined as described above for cell lines.

We will outline five important stages that must be optimized for endolysosomal patch-clamp. These stages are described in step-by-step detail in the PROCEDURE.

Enlargement of endolysosomal vesicles. For manual endolysosomal patch-clamp experiments, it is very important to enlarge endolysosomes to a degree sufficient for manual experimentation. To enlarge late endosomes and lysosomes, either PIKfyve inhibitor YM201636 (ref. 9) or vacuolin-1 (ref. 2) can be used. However, the latter is less specific because it also increases the size of early endosomes and possibly other vesicle populations²⁹. Transient transfection of mutated marker proteins such as Rab5Q79L (for early endosomes) can also be applied to enlarge distinct endolysosomal vesicles. However, one noteworthy advantage of pharmacological tools is that they are acutely applied and can lead to substantial vesicle enlargement within a few hours. Furthermore, these compounds do not seem to have an impact on membrane proteins and membrane components during measurements.

Results of effective treatment are shown in **Figure 2**. A video demonstrating the enlargement process over a period of 1 h is shown for vacuolin-1 (**Supplementary Video 1** and **Supplementary Fig. 1**; scale bar, 10 μm). It is very important to determine the optimal concentration and time required to enlarge specific vesicles in different cell types. These parameters must be optimized for individual cell types. We recommend starting with testing more than one method for enlarging endolysosomes. Begin with cell lines expressing tagged channel variants and analyze the effect of the procedure by live-cell confocal microscopy. Confirm the identity of enlarged vesicles either by coexpression of tagged ion channels or by measurement of marker proteins. Alternatively, use immunocytochemistry and specific antibodies that detect the tagged or native ion channel along with antibodies that specifically detect marker proteins for early endosomes, recycling endosomes or late endosomes/lysosomes. In patch-clamp experiments, results obtained with different methods of enlarging endolysosomes should be compared to ensure that there are no artifacts relating to a particular substance.

Design and fabrication of glass pipettes for endolysosomal patch-clamp. The greatest challenge with endolysosomal patch-clamp is the production of suitable electrodes. In fact, in our experience 65% of the time required for endolysosomal patch-clamp is spent on the production of these electrodes. Several puller systems are available that can reliably be used for the production of high-end patch-clamp electrodes. We use a Sutter model P-97 puller. Alternatively, pipettes may be produced using other pullers such as the Narishige puller (PC-10). However, we have used this puller with very limited success, and therefore we cannot recommend this puller to generate pipettes for endolysosomal patch-clamping. To patch large or medium-sized native endolysosomes, the DMZ puller, in combination with thick-walled glass electrodes with a very small opening diameter, may be used. Optimal pipette geometry and pipette resistance are essential to the formation of high-resistance seals (gigaseals) with the membrane of the lysosome or organelle of interest. The optimal geometry of patch pipettes for endolysosomal patch-clamp is shown in **Figures 3** and **4**. To obtain highly efficient pipettes, we use a six-cycle pulling program (**Table 1**; **Fig. 3c**). On the basis of our experience, patch electrodes optimal for endolysosomal recordings have a pipette resistance of 5–8 $\text{M}\Omega$ (**Table 2**). The resistance of the pipette used for recordings is mainly the result of the geometry of the pipette, the characteristics of the glass and the internal solution used. Thick-walled glass capillaries should

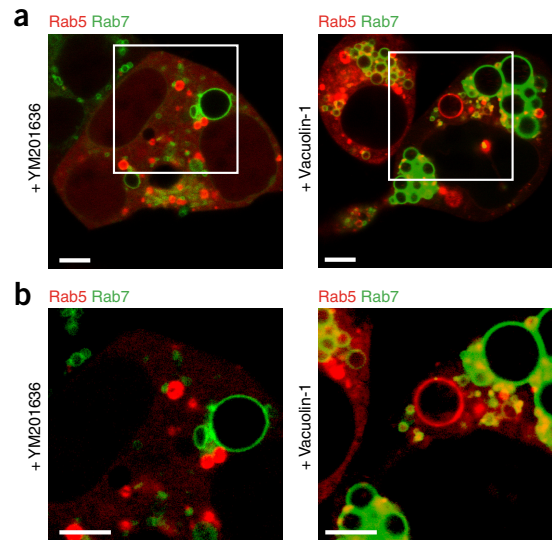


Figure 2 | Enlargement of intracellular organelles in HEK293 cells upon treatment. (a) Representative confocal images showing the effects of YM201636 (800 nM; 5 h) and vacuolin-1 (1 μM , overnight) on the enlargement of intracellular vesicles in HEK293 cells transfected with Rab5-mCherry (red) and Rab7-GFP (green). Scale bars, 5 μm . (b) Zoom-in images of the areas within the white squares shown in a. Note that a subpopulation of organelles increases to a size allowing successful patch-clamp experimentation. Scale bars, 5 μm . All cells were transfected for at least 24 h before application of reagents and incubated in a 10% CO_2 atmosphere and at 37 $^\circ\text{C}$ during the time of treatment.

be used for pipette fabrication. In comparison with pipettes used for whole-cell recording, pipettes used for endolysosomal patch-clamp have much higher resistance.

Dissection and release of endolysosomal vesicles. The next important stage is the dissection and release of enlarged endolysosomes using glass electrodes and patch-clamp micro-manipulators. For successful dissection, it is important that cells be tightly attached to the coverslip. This is done by coating the coverslips with poly-L-lysine. The entire procedure is shown in **Supplementary Videos 2** and **3**. **Figure 5** gives an overview of the dissection procedure in two planes.

Patch-clamp experiments in whole-endolysosome configuration. After dissection of lysosomes, the dissection electrode is exchanged for a recording electrode. As in whole-cell patch-clamp, the pipette is attached to the endolysosomal membrane using micromanipulators. We recommend using a water objective with 40 \times or 60 \times magnification to visualize endolysosomes. Seal formation is monitored in a manner similar to whole-cell patch-clamp by applying a voltage step pulse of 5 mV (pulse duration 5 ms) from a holding potential of 0 mV. During this step, slight suction is applied via a plastic pipette pressure system connected to the pipette holder (the pipette pressure system includes plastic three-way blood transfusion taps and 1-ml syringes). Successful gigaseal formation is indicated by a decrease to <10 pA of the current amplitude evoked by the voltage pulse of 5 mV. Endolysosome-attached configuration is established once a stable gigaseal has been reached. From this configuration, the whole-endolysosomal configuration can be established by rupturing the membrane by a

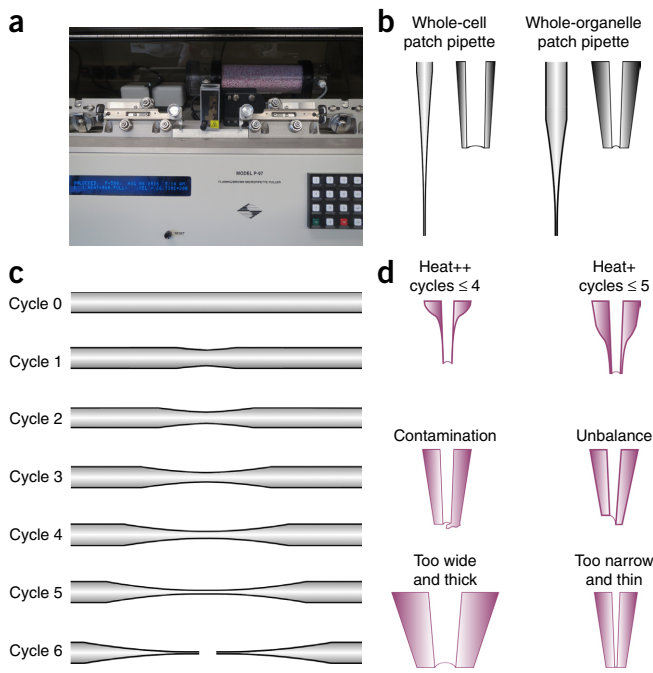


Figure 3 | Equipment used for the fabrication of optimal patch pipette tips. (a) A commercially available pipette puller. (b) Diagram of a conventional whole-cell patch-clamp pipette (left) and a whole-endolysosomal patch-clamp pipette. (c) Pipettes for endolysosomal patch-clamp after each individual pulling cycle are shown. (d) Examples of failed pipettes after pulling process are shown. Too much HEAT during the pulling process results in too-sharp tips (upper panel), which break the endolysosomal membrane. Pipettes may also be contaminated or unbalanced (middle panel). Suboptimal pulling conditions can result in pipette tips that are too wide or too narrow (lower panel). Heat+ and Heat++, too much heat.

ZAP pulse (fast voltage pulse—i.e., 0.1–50 ms with –200 to –1,000 mV). In our experience, suction pulse applied via the mouthpiece, similar to that used in whole-cell patch-clamp, does not work.

To conduct the protocol, we assume a basic understanding of and as well as experience in performing patch-clamp experiments. Details in regard to performance of patch-clamp recordings and data analysis are not described (for details see, e.g., *The Axon Guide for Electrophysiology & Biophysics Laboratory Techniques*³⁰). Only steps specific to recording endolysosomal preparations are described in detail. Conventions for endolysosomal current presentation are as in standard patch-clamp experimentation. Inward cationic currents are defined as currents flowing out of the vesicle lumen into the cytosol; outward cationic currents are those flowing from the cytosol into the organelle lumen. Therefore, current value reads from the amplifier for endolysosomal patch-clamp must be inverted (invert the y axes by multiplying by –1). Furthermore, endolysosomal membrane voltage is defined as cytosolic potential with respect to luminal (conventional: extracellular) potential (**Supplementary Fig. 2**). Therefore, the voltage axes must also be inverted. Thus, endolysosomal data are handled in the same way as inside-out patch data (for details see ref. 30).

Voltage-clamp mode. In endolysosomal voltage-clamp patch experiments, current flowing across the endolysosomal membrane is recorded as a function of the controlled input voltage delivered by either voltage steps or voltage ramps. For endolysosomal

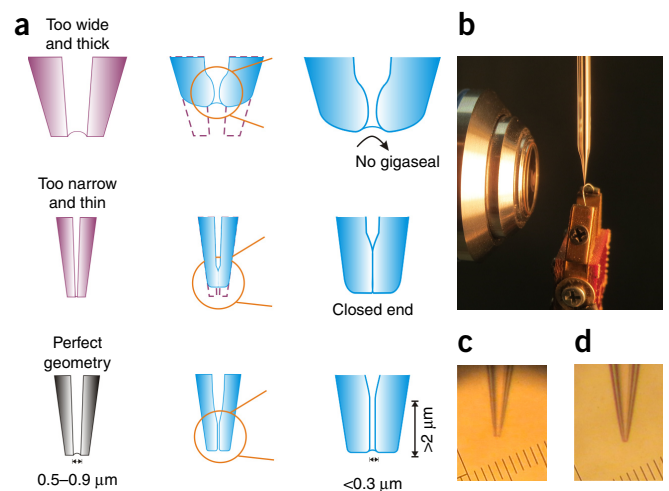


Figure 4 | Fire-polishing of patch-clamp pipettes. (a) Comparison of geometrical properties of recording pipettes for patch-clamp before polishing (left column) and after polishing (middle and right columns). Pipettes that are too wide and thick can result in no gigaseal formation (first row). Closed-end tip pipettes are produced from tips that are too narrow (second row) or by overpolishing. Third row shows ideal pipette geometry. (b) A commercially available fire polisher is shown. (c, d) Ideal pipette seen in the vision field of the 35× objective microscope lens of the fire polisher before polishing (c) and after polishing (d).

voltage-clamp experiments, a large range of input voltages (e.g., –100 mV to +100 mV) are used.

Passive current components may be present in endolysosomes from leak conductance and specific ion-channel-dependent background currents. Leak currents are characterized by linear current (I)–voltage (V) relations crossing the origin. Leak currents of endolysosomes isolated from nontransfected HEK293 cells are in the range of <50 pA (at 100 mV); the underlying ion channels are most likely potassium/sodium conductance channels and chloride channels.

In case of voltage-activated ion channels, leak current components could be subtracted from the measured currents by recording a series of scaled voltage pulses just before or after the voltage pulse used to elicit voltage-gated endolysosomal currents. These scaled pulses are typically one-fourth or one-fifth of the amplitude of the experimental pulses, and the subtraction process is referred to as P/4 or P/5 leak subtraction (for details see Cummins *et al.*³¹). Because of the very small amplitude of leak currents, we normally do not use P/4 or P/5 subtraction.

Once high-quality seals are established and background signals are minimized, specific endolysosomal conductance can be recorded. Several ion channels and transporters have been reported to be expressed in intracellular vesicles or endolysosomes (**Fig. 6; Table 3**), including TRPML1-3, TRPM2, TRPV2, TPC1-2, the potassium channel TMEM175, BK (big potassium) potassium channels, P2X4, CAX and chloride channels (CLCs)^{1,3,5,6,20,22,32–43}. Although most of these proteins have been reported to be localized in certain subsets of endolysosomal vesicles, it is not clear whether they are restricted to these vesicles or are more broadly distributed and also present in LROs (lysosome related organelles) or other vesicles and vice versa. In addition, the distribution of these channels may differ from one specific cell type to the other.

PROTOCOL

TABLE 1 | Comparison of pulling programs for endolysosomal patch pipettes and conventional patch pipettes.

Cycle	Endolysosomal patch pipette				Whole-cell patch pipette				
	HEAT	PULL	VEL	TIME	HEAT	PULL	VEL	TIME	
1	Value determined by ramp protocol	Blank	30	150	Value determined by ramp protocol +10	Blank	40	150	
2			25	150			40	150	
3			25	150			40	150	
4			25	150			40	150	
5			25	150			–*	–	
6			16	150			–	–	

Air jet $P = 400$ was applied in all cases. *Polishing is not necessary for conventional patch pipettes.

To establish the method and to familiarize yourself with endolysosomal ion channels present in the cell and vesicle types of interest, we recommend starting with native endolysosomes dissected from HEK293 or MEF cells. To monitor total currents present in endolysosomes, voltage ramps are useful. We start with ramps of different durations, ranging from 100 to 500 ms, and different time intervals between the application of individual ramps to account for dynamic activation and inactivation gating of endolysosomal ion channels. Typical shapes of $I-V$ relations for endolysosomal ion channels are shown in **Figure 6**. TPC1 channels are voltage-dependent, with an $I-V$ relationship resembling those of voltage-gated Ca^{2+} channels and Na^{+} channels³⁷. TPC2 channels do not display voltage-dependent gating and therefore display linear $I-V$ relations that can be distinguished from non-selective linear leak currents by a positive reversal potential of $\sim +60-80$ mV for standard recording solutions¹. There are also outwardly rectifying channels such as the BK⁴³ channel and CLC⁵ channel currents, and inwardly rectifying ion channels such as TRPML1-3 (ref. 6; **Fig. 6**). Protocols with a family of voltage steps separated by a pause interval can also be used. Using these protocols, specific aspects of channel gating, such as $I-V$ characteristics, kinetics and voltage dependence of activation, deactivation and inactivation of channels in question, can be examined (see the **Supplementary Note** and **Supplementary Table 1** for basic theoretical information and equations for patch-clamp).

Depending on the ion channels of interest, intra- and extraluminal patch-clamp solutions and voltage-clamp protocols must be designed. The specific composition of patch-clamp solutions must be adapted to the current of interest. If anionic conductance is not the major focus, the currents can be reduced by replacing chloride with impermeable anions such as aspartate, gluconate or methane sulfonate. In this case, agar bridges, instead of AgCl wire, may be used. With anionic conductance reduced, cationic currents of interest can be isolated from contaminating currents

by removal of individual cations. If pharmacological activators or blockers of the conductance of interest are available, these can be used to dissect currents from contaminating currents. For such experiments, initial measurements of the total current are performed, after which the endolysosome is exposed to a drug that selectively blocks or activates the current of interest. The current of interest is then extracted by calculating the difference between currents obtained before and after the exposure to drug. Finally, current recordings obtained from cell lines or primary native cells prepared from wild-type or knockout mouse lines lacking the channel of interest can be compared.

For endolysosomal current recordings, configurations similar to those used in whole-cell patch-clamp experiments can be used. Endolysosome-attached, whole-endolysosome, inside-out and outside-out configurations can be used². In the first two configurations, total current passing through all the channels in a particular intracellular vesicle can be measured. By contrast, in inside-out and outside-out patches, only currents through channels contained in the patch are measured.

Single-channel voltage-clamp recording. In voltage-clamp mode, single-channel activity can be recorded using the available configurations. The typical low density of endolysosomal ion channels can make it difficult to obtain patches containing a single channel. Thick-walled pipette glass seems to work best for manufacturing electrodes with small pipette tips and low capacitance. Coating of the glass with Sylgard or wax can be used to lower the pipette capacitance.

Potential experimental problems and specific considerations. Current recordings with whole-endolysosomal configuration are problematic because of the potential loss of factors from either side of the endolysosomal membrane, which could lead to changes in gating properties over the time course of the recording period.

TABLE 2 | Common ranges of electrical parameters for endolysosomal patch-clamp.

Parameter	R_{pipette}	R_{access}	R_{seal}	Capacitance	Leak currents
Range	5–8 M Ω	15–90 M Ω	1–20 G Ω	0.1–5 pF	<50 pA

Ω , ohm, F, farad.

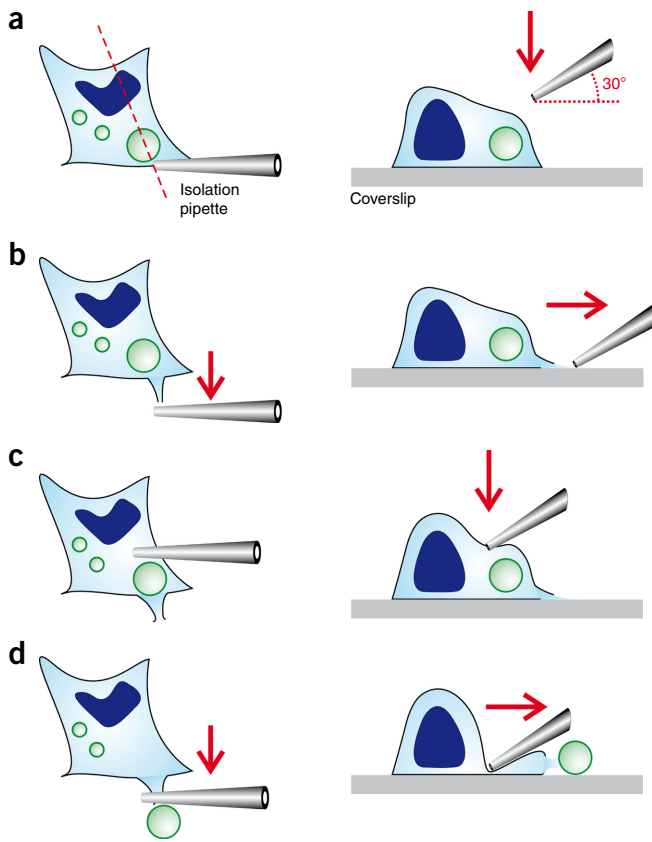


Figure 5 | Dissection procedure for preparation of individual enlarged endolysosomes from a single cell. Left panels show the top view of the target cell (view via eyepiece). Right panels show the section of the target cell along the red dotted line. (a) The glass pipette is pressed against the edge of a cell that is close to the enlarged target endolysosome. (b) The pipette is quickly pulled away to cut open the cell membrane. (c) The top of the cell is pushed with the same glass pipette. (d) The enlarged endolysosome is squeezed out through the incision.

First, the pipette solution could dilute or lead to a loss of specific modulators (small molecules or other factors) on the luminal side of the lysosome lumen and cause time-dependent changes in current properties. In addition, components of the pipette or cytosolic solution could activate or inhibit specific second messenger pathways regulating endolysosomal ion channels. Using the endolysosome-attached mode in conjunction with perforated patch would be well suited to solving specific problems arising from the luminal side of the endolysosomal membrane. Second, in endolysosomal patch-clamp there is the possibility of washout of small molecules or factors associated with the cytosolic side of the endolysosomal membrane, as this side of the membrane faces the recording solution (cytosolic solution). This possibility has been shown for ATP, which blocks TPCs from the cytosolic side of the membrane. This particular problem can be minimized by careful design of bath solutions (e.g., make sure not to include ATP in the cytosolic recording solution)¹ or controlled for by running time-dependent controls and starting specific protocols at consistent times after establishing the whole-endolysosome recording configuration. Another problem could be loss because of washout of regulatory proteins associated with endolysosomal ion channels. If these regulatory factors are part of signaling cascades, the

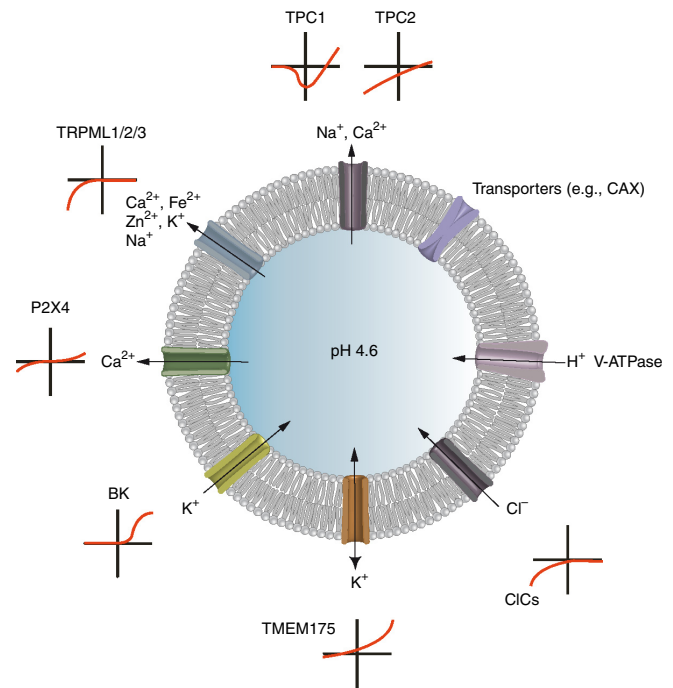


Figure 6 | Schematic showing ion channels that have been measured with the endolysosomal patch-clamp technique. The cross-shaped graphs show the IV curves (current–voltage plots; x axis = voltage, y axis = current) of six types of endolysosomal ion channels (TPCs, TRPMLs, P2X4, ClCs, TMEM175 and BK) measured with this technique. H⁺ and Ca²⁺ gradients in endolysosomes are established and maintained by V-ATPases and putative Ca²⁺ transporters (e.g., CAX). Inward current stands for cation flux from the lysosomal lumen to the cytosol. ClC, chloride channel; V, vacuolar-type.

physiological regulation of the endolysosomal channel is lost. For example, the regulation of TPCs by NAADP may depend on such a factor that is lost in some preparations whereas it is present in other preparations, which could potentially explain the presence of NAADP responses in some preparations and not others.

Current-clamp mode. Changes in membrane voltage of endolysosomal vesicles can be recorded using current-clamp experiments. In this recording mode, changes in the membrane potential are recorded as a function of the size of currents injected into the endolysosome. It is important to note that the endolysosomal membrane potential is defined as the outside potential (i.e., cytosolic potential) minus the luminal potential facing the inside of the intracellular vesicle ($\Delta\Psi = V_m = V_{\text{cytosol}} - V_{\text{lumen}}$ (ref. 44)). Endolysosomal current-clamp recordings can be used to study the resting membrane potential, dynamic changes of the endolysosomal membrane potential and the contribution of distinct ion channels to this potential. In addition, active changes of endolysosomal membrane potential upon opening or closing of the channel by specific activators or inhibitors can be analyzed. Furthermore, spontaneous and evoked active firing patterns can be recorded using current-clamp experiments. Recently, it has been shown that in endolysosomes action potential-like firing can be evoked¹⁰.

For current-clamp experiments we use MEFs or native cells generated from wild-type and genetic mouse lines lacking specific endolysosomal ion channels. It is important to use native cells or MEFs directly after preparation.

TABLE 3 | Ion channels in intracellular vesicles, the endolysosomal system or lysosome-related organelles.

Ion channel	Expression	Function	Human disease
TRPM1 (ref. 32)	Skin and eyes	Tumor suppressor; potential role in mediating synaptic transmission in bipolar cells	Mutations in TRPM1 are associated with congenital stationary night blindness, metastasis and poor prognosis in melanoma
TRPM2 (ref. 33)	Brain	Oxidant stress sensor, mediates H ₂ O ₂ -dependent cell death; potential role in lysosomes (ADP-ribose-evoked calcium release from intracellular calcium stores)	Guamanian amyotrophic lateral sclerosis/parkinsonism dementia complex
TRPM7 (ref. 34)	Broad	Synaptic vesicle function, Anoxia-induced cell death	Guamanian amyotrophic lateral sclerosis/parkinsonism dementia complex
TRPML1 (refs. 2,4,6, 7,9,10, 15,20–22,25)	Broad	PI(3,5)P ₂ activation; PI(4,5)P ₂ and sphingomyelin inhibition; role in sorting/transport in late endocytic pathway; regulates lysosomal lipid and cholesterol trafficking; endolysosomal pH regulation and cation/heavy-metal (iron) homeostasis; lysosomal exocytosis; phagocytosis	Mucopolipidosis type IV (MLIV) is associated with mutations in TRPML1; symptoms include severe psychomotor retardation and retinal degeneration
TRPML2 (refs. 6,22)	Highest expression in lymphoid and myeloid lineage	Found in recycling endosomes; upregulation in macrophages in response to TLR activation	ND
TRPML3 (refs. 6,10,22,35)	Hair cells of the inner ear, organ of corti, utricle, stria vascularis, (skin) melanocytes, kidney, bladder, lung, liver, olfactory bulb, nasal cavity, thymus, colon, trachea, brain	Senses lysosome neutralization by pathogens to trigger their expulsion	Deafness, circling behavior, head bobbing and coat-color dilution is associated with mutations in MmTRPML3 (Varitint-waddler mutations Va and Va ^J), bacterial uropathogenic <i>Escherichia coli</i> (UPEC) infection
TRPA1 (ref. 36)	Primary afferent somatosensory neurons present in sensory ganglia-containing nociceptors	Thermosensation and inflammatory pain; role in lysosomes?	Episodic pain syndrome
TRPV2 (ref. 37)	Central nervous system, spleen and lung	Thermosensation and nociception; role in early endosomes?	ND
TRPV5 (ref. 37)	Intestine, kidney, placenta	Ca ²⁺ reabsorption; found in early/recycling endosomes; interaction with TRPML channels?	Osteoporosis, hypercalciuria
TRPV6 (ref. 37)	Kidney, intestine	Ca ²⁺ reabsorption; found in early/recycling endosomes; interaction with TRPML channels?	Alopecia, dermatitis, decreased intestinal Ca ²⁺ reabsorption
TRPC3 (ref. 37)	Heart tissue	BDNF-induced chemoattractive turning; regulation of mitochondrial calcium uptake?	Cerebellar ataxia (moonwalker mouse)

(continued)

TABLE 3 | Ion channels in intracellular vesicles, the endolysosomal system or lysosome-related organelles (continued).

Ion channel	Expression	Function	Human disease
TRPC5 (ref. 37)	Cerebral vascular tissue	Regulation of growth cone extension	Susceptibility to pyloric stenosis
TPC1 (refs. 2,38)	Broad; highest expression in heart and kidney	PI(3,5)P ₂ activation; ATP-sensor; vesicle fusion and transport; endolysosomal pH and Ca ²⁺ regulation	Virus (Ebola) infection
TPC2 (refs. 1,7,8,24,39,40)	Broad	NAADP and PI(3,5)P ₂ activation; ATP-sensor; vesicle fusion and transport; endolysosomal pH? and Ca ²⁺ regulation; melanosomal pH regulation?	Virus (Ebola) infection, LDL-cholesterol and serum cholesterol accumulation, neurodegenerative diseases (e.g., Parkinson's disease)
CLC3 (ref. 5)	Broad	Acidification of synaptic vesicles, endosomes	
CLC4 (ref. 5)	Broad	ND	
CLC5 (refs. 5,41)	Kidney, intestine	Acidification of endosomes	Dent's disease (proteinuria, kidney stones)
CLC6 (ref. 5)	Nervous system	Acidification of late endosomes	
CLC7 (ref. 5)	Broad	Acidification of osteoclast resorption lacuna	Osteopetrosis, retinal degeneration, lysosomal storage
P2X4 (ref. 42)	Broad	ATP activation; pH and Ca ²⁺ regulation	Neuropathic pain
BK (ref. 43)	Neuron, smooth muscle, cochlea	Ca ²⁺ regulation	Epilepsy, neurological disorders
TMEM175 (ref. 3)	Nervous system	Regulation of lysosomal membrane potential and pH	Parkinson's disease

Tissue expression, function and associated human diseases are summarized from recent studies. Some of these ion channels are also present in other organelles and/or in the plasma membrane. BK, big potassium channel; CLC, chloride channel; ND, not determined; P2X4, P2X purinoreceptor subunit 4; TMEM175, transmembrane protein 175; TRP, transient receptor potential channel; TRPC, TRP canonical channel; TRPM, TRP melastatin channel; TRPV, TRP vanilloid channel.

Analysis of patch-clamp data. Data obtained by endolysosomal patch-clamp experiments are analyzed in the same way as data from conventional patch-clamp. We assume that the reader is experienced in analyzing data obtained by this method. For

detailed information on basic patch-clamp and analysis, we refer to—e.g., ref. 30. Analysis depends on the properties of the ion channels of interest. Some examples how data are analyzed and graphically displayed are given in the ANTICIPATED RESULTS.

MATERIALS

REAGENTS

Chemicals

- Boric acid (VWR, cat. no. 20185.360) **! CAUTION** Boric acid is a dangerous chemical. Avoid skin contact. Avoid inhalation and contact with skin or eyes. Wear protective gear while handling.
- Borax decahydrate, sodium borate decahydrate (Sigma-Aldrich, cat. no. B9876) **! CAUTION** Borate may damage fertility or the unborn child.
- Calcium methanesulfonate (Ca-MSA; Tokyo Chemical Industry, cat. no. M0549)
- Calcium chloride (CaCl₂; VWR, cat. no. 22317.297)
- EGTA (Sigma-Aldrich, cat. no. E4378)
- HEPES (Carl Roth, cat. no. 6763)
- Hydrochloric acid (HCl; VWR, cat. no. 470301) **! CAUTION** Hydrochloric acid is a corrosive acid. Avoid contact with eyes and skin. Wear protective gear while handling it.

- 2-(*N*-Morpholino)-ethane sulfonic acid (MES; Carl Roth, cat. no. 4256)
 - Poly-L-Lysine hydrobromide (Sigma-Aldrich, cat. no. P1399)
 - Potassium methanesulfonate (K-MSA; Sigma-Aldrich, cat. no. 83000)
 - Potassium hydroxide (KOH; Carl Roth, cat. no. 6751) **! CAUTION** KOH is toxic if swallowed. Avoid direct contact, which may cause severe skin burns and eye damage. KOH is harmful to aquatic life.
 - Potassium chloride (KCl; Sigma-Aldrich, cat. no. p9333)
 - Potassium phosphate monobasic (KH₂PO₄; Sigma-Aldrich, cat. no. P5655)
 - Sodium chloride (NaCl; VWR, cat. no. 27810.295)
 - Sodium phosphate dibasic anhydrous (Na₂HPO₄; VWR, cat. no. 470302-660)
 - Sodium methanesulfonate (Na-MSA; Sigma-Aldrich, cat. no. 304506)
- Drugs**
- Vacuolin-1 (Santa Cruz, cat. no. sc-216045)
 - PI(3,5)P₂ (AG Scientific, cat. no. P-1123)

PROTOCOL

Cell culture

- Human embryonic kidney (HEK) 293 cells stably overexpressing the ion channels under investigation (DSMZ, cat. no. ACC 305) **! CAUTION** The cell lines used in your research should be regularly checked to ensure that the cells are authentic and that they are free from contamination such as mycoplasma.
- Dulbecco's modified Eagle medium containing 25 mM glucose (DMEM supplemented with 4.5 g/l glucose, pyruvate and GlutaMax; Invitrogen, cat. no. 31966-021)
- FBS (Biochrom, cat. no. S0615)
- Penicillin–streptomycin (penicillin 10,000 units/ml; streptomycin 10,000 µg/ml; Biochrom, cat. no. A2213)
- 0.5% Trypsin–EDTA (10×; Gibco, cat. no. 1699348)
- TurboFect transfection reagent (Thermo Fisher Scientific, cat. no. R0531)

EQUIPMENT

Cell Culture

- Humidified cell culture incubator set to 37 °C, 10% CO₂
- Water bath, 37 °C

Pipette preparation

- Capillary glass and filament (borosilicate glass with filament, fire polished, o.d. 1.5 mm, i.d. 0.75 mm, length 10 cm; Sutter Instrument, cat. no. BF150-75-10) **▲ CRITICAL** The correct glass type is essential to producing good patch pipettes.
- **▲ CRITICAL** The protocol is optimized for use in combination with the following equipment.
- Flaming/Brown-type micropipette puller (Sutter Instrument, cat. no. P-97)
- Trough filament, 3.0 mm wide (World Precision Instruments, cat. no. FT330B) **▲ CRITICAL** It is not possible to produce good patch pipettes with a box filament.
- Microforge with platinum heater (Narishige, cat. no. MF-830)

Patch-clamp setup

- Inverted microscope system (Olympus, model no. IX73)
- Light source (LEJ, model no. LQ-HXP 120)
- Patch-clamp amplifier. For single-channel recordings and whole-endolysosomal recordings in voltage-clamp mode, it is possible to use a HEKA EPC10 (HEKA Instruments, cat. no. 895000) or an Axopatch 200B (Molecular Devices). For current-clamp recordings, it is possible to use a HEKA EPC10 (HEKA Instruments, cat. no. 895000) or a Multiclamp 700B Amplifier (Molecular Devices, model no. 700B)
- Multi-micromanipulator systems (Sutter Instrument, model no. MPC-200-ROE)
- TMC 63-500 Series high-performance lab tables (TMC, model no. 63-500)
- Type II Faraday cage (AMETEK)
- MicroFil for glass pipette filling (28 gauge, 97 mm long; World Precision Instruments, cat. no. MF28G-5)
- Syringe for pressure monitoring (1 ml; B. Braun, cat. no. 9166017V)
- Stopcock for pressure monitoring (Discofix C; B. Braun, cat. no. 16494C)
- Polyethylene tubing (PE-160/10) for pressure monitoring (1 foot; 1.57 mm o.d. × 1.14 mm i.d.; Warner Instruments, cat. no. 64-0755)

Data analysis

- OriginPro v8.0 (OriginLab, <http://www.originlab.com/index.aspx?go=Products/Origin>)
- PatchMaster v2×90 (HEKA Instruments, http://www.heka.com/downloads/downloads_main.html)
- pClamp v10 (Molecular Devices, <https://www.moleculardevices.com/systems/conventional-patch-clamp/pclamp-10-software>)

Other

- 24-Well cell culture plate (Cellstar, cat. no. 662160)

- Microscope glass coverslip (12 mm; VWR, cat. no. 631-1577)
- Conical tube, 15 and 50 ml (Sarstedt, cat. nos. 62.554.001, 62.548.004)
- Eppendorf Research Plus pipette (1,000 µl; Eppendorf, cat. no. 3120000062)
- Eppendorf Research Plus pipette (200 µl; Eppendorf, cat. no. 3120000054)
- Eppendorf Research Plus pipette (20 µl; Eppendorf, cat. no. 3120000038)
- Eppendorf Research Plus pipette (2.5 µl; Eppendorf, cat. no. 3120000011)
- Needle (0.9 × 40 mm, 20 gauge; B. Braun, cat. no. 4657519)
- Cell culture flask, 25 cm² (50 ml; Greiner Bio-One, cat. no. 690160)
- Pipette tips (1,000 µl; Sarstedt, cat. no. 70.762)
- Pipette tips (200 µl; Sarstedt, cat. no. 70.760.001)
- Pipette tips (10 µl; Sarstedt, cat. no. 70.1130)
- Reaction tube (1.5 and 2.0 ml; Eppendorf Safe-Lock tubes; Eppendorf, cat. nos. 0030120086, 0030120094)
- Syringe filter, sterile (0.2 µm; VWR, cat. no. 10708S1G43BD)

REAGENT SETUP

Pipette solution (lysosome luminal) Prepare the solution with the following reagents (in mM): 140 Na-MSA, 5 K-MSA, 2 Ca-MSA, 1 CaCl₂, 10 HEPES and 10 MES. Adjust the pH to 4.6 with MSA. Adjust the osmolarity to 310 mosm/liter with glucose. Sterilize the solution by passing it through a 0.2-µm filter, prepare aliquots of 45 ml in 50-ml conical tubes and store them at 4 °C for up to 2–4 weeks.

! CAUTION Unless otherwise stated, for TPCs the recording pipette solution consists of high Na⁺ and Ca²⁺ to mimic physiological luminal conditions of the lysosome.

▲ CRITICAL To isolate lysosomal cation currents, MSA or gluconate variants of chemicals are used instead of chloride salts as impermeable anions.

▲ CRITICAL MES, which is characterized by a midrange pK_a (pH ~5 to 6), is applied to buffer the pH range between 2.5 and 5.

Bath solution (cytosolic) Prepare the bath solution with the following reagents (in mM): 140 K-MSA, 5 KOH, 4 NaCl, 0.39 CaCl₂, 1 EGTA and 10 HEPES. Adjust the pH to 7.2 with KOH. Adjust the osmolarity to 300 mosm/l with glucose. Sterilize the solution by passing it through a 0.2-µm filter, prepare aliquots of 45 ml in 50-ml conical tubes and store them at 4 °C for up to 2–4 weeks.

Poly-L-lysine coating solution Poly-L-lysine coating solution is 0.1 mg/ml of poly-L-lysine in 80 mM boric acid and 10 mM borate, sterilized by passing it through a 0.2-µm filter. Freshly prepare the solution before use.

Supplemented DMEM Supplement DMEM with 10% (vol/vol) FBS and 100 U of penicillin–streptomycin per ml. Store it at 4 °C for up to 2–4 weeks; warm it to 37 °C in a water bath before use.

PBS Buffer Prepare PBS buffer with the following reagents (in mM): 137 NaCl, 2.7 KCl, 10 Na₂HPO₄ and 2 KH₂PO₄. Adjust the pH to 7.4 with HCl. Prepare 500-ml aliquots, heat-sterilize them and store them at room temperature (21–23 °C) for up to 6 months.

0.05% (vol/vol) Trypsin Dilute 0.5% (vol/vol) trypsin at a 1:10 ratio with distilled sterile H₂O, prepare 10-ml aliquots in 15-ml conical tubes and store them at –20 °C for up to 2–4 months; warm the aliquots to 37 °C in a water bath before use.

Preparation of coated coverslips Microscope glass coverslips are autoclaved and exposed to poly-L-lysine coating solution for at least 24 h. Aspirate off the poly-L-lysine solution, rinse the coverslips five times with dH₂O and store them in dH₂O at room temperature for up to one month. Before plating cells, place one coverslip into each well of a 24-well plate. Spread 0.5–1 ml of PBS on each coverslip and aspirate. Allow the coverslips to dry completely under a laminar flow hood for at least 15 min.

PROCEDURE

Preparation of HEK293 cells for endolysosomal recordings ● TIMING 2–4 d

- 1| Maintain HEK293 cells (passages 1–16) in supplemented DMEM and keep them at 37 °C in a humidified atmosphere of 10% CO₂-containing air.
- 2| Treat HEK293 cells cultured in a 25-cm² flask with 0.5 ml of 0.05% (vol/vol) trypsin for 5 min in a 37 °C incubator (10% CO₂).
- 3| Typically, after 5 min cells are detached; otherwise, incubate for another 5 min.

- 4| Add 4.5 ml of supplemented DMEM to dilute the trypsin.
- 5| Pipette the cell suspension up and down several times.
- 6| Add 0.5 ml of cell suspension to a new cell culture flask (8×10^5 per flask), add 4.5 ml of supplemented DMEM and incubate at 37 °C in a humidified atmosphere of 10% CO₂-containing air for 2–3 d, then split the cells again.
- 7| Add 400 µl of cell suspension ($2\text{--}4 \times 10^5$ cells) to 8 ml of supplemented DMEM in a 15-ml conical tube.
- 8| Gently turn the tube upside down 2–3 times. Next, add 1 ml of supplemented DMEM with cells to eight wells of a 24-well plate containing poly-L-lysine-coated 12-mm glass coverslips.
- 9| One or two days before patch-clamp experiments, transfect the cells with Turbofect according to the manufacturer's protocol to generate cells transiently expressing TPC2 or TRPML1.
 ▲ **CRITICAL STEP** Fluorophore-tagged endolysosomal channel proteins are very helpful in identifying channel-protein-expressing endolysosomes used for whole-endolysosome patch-clamp recordings.
- 10| Grow the cells until they are 40–70% confluent ($1\text{--}5 \times 10^5$ cells per well).

Enlargement of endolysosomal vesicles ● TIMING 1–48 h, depending on the option followed

11| Add the precise concentration of pharmacological tool(s) to cell culture dishes or wells and incubate at 37 °C until enlarged vesicles begin to form. The size of enlarged endolysosomes can reach up to 1–10 µm depending on the tool compound, incubation time and cell type.

12| If you are proceeding to enlarge unspecific endolysosomes for electrophysiological studies, follow option A. If you are preparing for specific electrophysiological measurements of late endosomes/lysosomes, follow option B.

(A) Unspecific endolysosome enlargement using vacuolin-1 ● TIMING at least 1 h

- (i) Add vacuolin-1 to the culture medium and incubate at 37 °C and 10% CO₂.
 ▲ **CRITICAL STEP** Different cell types can be treated with 1–5 µM vacuolin-1 for 1 h to multiple days in culture^{4,34,35}. The optimal concentration and time of treatment should be determined experimentally. For example, we have treated macrophages with 1 µM vacuolin-1 for 1 h; COS-1, HEK293 and fibroblasts have been treated overnight with 1 µM vacuolin-1. Cardiomyocytes and skeletal muscle cells were treated with 5 µM vacuolin-1 for 24–48 h.
 ▲ **CRITICAL STEP** Perform Step 12A(i) within 1–2 h of performing Step 11.

(B) Late endosome/lysosome enlargement using YM201636 ● TIMING at least 1 h

- (i) Add YM201636 to the culture medium and incubate at 37 °C and 10% CO₂.
 ▲ **CRITICAL STEP** For HEK293 cells, use 0.4 µM YM201636 overnight or 0.8 µM YM201636 for 2 h. For macrophages, use 0.4 µM YM201636 for 1–3 h.
 ▲ **CRITICAL STEP** Perform Step 12B(i) within 1–2 h of performing Step 11.
 ▲ **CRITICAL STEP** YM201636 specifically enlarges Rab7- and LAMP-1-positive late endosomes and lysosomes, not Rab5-positive early endosomes (Fig. 2). Note, however, that on average YM201636-enlarged vesicles are slightly smaller than vacuolin-1-enlarged vesicles (3–8 µm).
 ▲ **CRITICAL STEP** Most cells are detached after prolonged treatment (>24 h for HEK293/ >4 h for macrophages) with a high concentration of YM201636 (>800 nM). YM201636-enlarged vacuoles shrink and vanish after 6–12 h when treated with a low concentration (<400 nM).

Pulling glass pipettes ● TIMING 1–5 min per pipette

▲ **CRITICAL** Pipette production is critical because the intracellular organelle membranes of the endolysosomes are fragile. The 6-cycle pulling procedure is validated for the Sutter Instrument P-97 puller with trough filament in combination with the Sutter Instrument BF150-75-10 glass pipette. Pulling procedures using other pullers and different glass pipettes will require individual optimization (for the critical procedure of pipette fabrication, see Steps 19–26).

13| Mount the glass capillary onto the puller for the fabrication of the patch pipette as described in the manufacturer's protocol.

14| Run a RAMP test with the puller to determine a heat value (HEAT) that will melt the glass capillaries under your experimental conditions (e.g., room temperature, filament, glass) without burning out the heater filament.

▲ **CRITICAL STEP** Parameters may need to be varied to produce desired pipettes if the filament of the puller is aged. Refer to the Sutter Instrument Pipette Cookbook (<https://www.sutter.com/MICROPIPETTE/p-97.html>).

PROTOCOL

15| Design a new pulling program for the Sutter Instrument puller with six individual pulling cycles using the HEAT, velocity (VEL) and time (TIME) parameters given in **Table 1**. Set the HEAT to the value determined in Step 14.

! **CAUTION** The parameters in **Table 1** may require individual optimization.

16| Press the green 'Pull' key on the keypad.

▲ **CRITICAL STEP** The capillary should be separated during the sixth cycle to produce two patch pipettes. Separation during earlier cycles will produce pipettes tips that are too sharp for seal formation (**Fig. 3d**, upper panel).

17| Loosen the clamping knobs and remove the pipettes from the puller.

18| Inspect the pipette tips with the eyepiece of a microforge and determine the opening diameter, sharpness and geometry. The tip opening should be 0.5–0.9 μm in diameter (**Fig. 4a**, left).

If the tip of the pipette is too wide ($>1 \mu\text{m}$) or too thick (**Fig. 3d**, lower panel; **Fig. 4a**, left), increase HEAT parameter of the sixth pull by 5 units or increase the VEL parameter by 1 unit for the fabrication of the next pipette. If the tip is too narrow and thin, decrease the parameters accordingly.

▲ **CRITICAL STEP** Optimal HEAT and VEL parameters for the sixth cycle must be determined after each pulling process. The VEL parameter for the fifth cycle is used to further adjust, if required.

19| Discard pipettes that are too sharp, too wide or too thin. Also discard pipettes with dust or protruding pieces of glass and pipettes with rough and unbalanced ends (**Fig. 3d**).

Pipettes with suboptimal geometry can be used to produce dissection pipettes in Steps 28–38.

▲ **CRITICAL STEP** At this stage, ~50% of the generated pipettes are not suitable for use in whole-endolysosomal patch-clamp experimentation.

▲ **CRITICAL STEP** Immediately polish pipettes with the correct tip size with a microforge (**Fig. 4b**).

Fire polishing patch-clamp pipettes using a microforge ● **TIMING 1–3 min per pipette**

20| Place the patch pipette in the pipette holder of the microforge according to the manufacturer's protocol.

21| Use the 35 \times objective lens to inspect the pipette tip (in combination with the 15 \times eyepiece lens, this results in a 525-fold magnification).

22| Move the patch pipette close to the filament with the micromanipulator.

! **CAUTION** The filament will expand during the process of heating.

▲ **CRITICAL STEP** Always place the pipette tip in the same area of the vision field of the microforge. 3/4 to 9/10 of the heat filament should be at a lower position and in the bottom of the vision field. Place the tip slightly higher than the center of the scale.

23| Set the temperature wheel to graduation level 80.

▲ **CRITICAL STEP** Adjust the temperature level according to your experimental conditions (e.g., room temperature, glass type, distance to pipette tip).

24| Turn the heater on with the foot switch and apply a brief heat pulse (1–2 s).

25| Monitor the polishing process through the eyepiece of the microforge.

▲ **CRITICAL STEP** The aim is to briefly melt the tip so that the glass can flow, resulting in a final tip geometry that is not too sharp, so that the pipette does not penetrate the membrane of the vesicle against which it is pressed and can efficiently promote seal formation. After final polishing, the inner path of the pipette tip should be very narrow, straight and linear (**Fig. 4a**; **Supplementary Video 4**). A steep taper, which corresponds to a blunt tip, leads to lower pipette resistance for the same opening diameter. The final resistance also depends on recording solutions in the different experimental designs. The optimal recording pipettes usually had resistances of 5–8 M Ω after fire polishing. The tip opening diameter should be $<0.3 \mu\text{m}$, and the parallel inner pipette should be $>2 \mu\text{m}$ (**Fig. 4a,c** and **d**).

26| Place the finished pipette in a closed box to protect it from dust.

27| Repeat Steps 13–26 until the desired number of pipettes have been fabricated.

▲ **CRITICAL STEP** Recording pipettes should be used within 6 h after polishing. Pipettes not used within 6 h or with tips that are too narrow can be used as isolation or dissection pipettes.

? **TROUBLESHOOTING**

Dissection and release of endolysosomal vesicles ● **TIMING** ~1–10 min

28| Remove one coverslip from the 24-well plate that contains cells with enlarged vesicles from Step 12 and transfer it to the microscope chamber (**Supplementary Videos 2 and 3**).

29| Add 1 ml of bath solution.

Cells can be stored in bath solution for ~1 h for whole-endolysosomal patch-clamp experimentation, which includes endolysosome isolation, sealing and recording steps. After 1 h, HEK293 cells tend to detach from the coverslip during endolysosome extraction and enlarged endolysosomes will become smaller, adhesive (i.e., sticking to the pipette) and difficult to isolate.

30| Using a MicroFil or a self-made plastic filling needle, fill an isolation pipette with luminal solution and mount the pipette onto the headstage of the patch-clamp setup.

31| Set the angle of the diagonal mode movement of the micromanipulator. The angle should be close to 30° (factory default).

32| Inspect the cells under the microscope (40× objective lens and 10× eyepiece) and search for cells with endosomes or lysosomes that are sufficiently enlarged and close to the edge of the cell membrane for isolation.

! **CAUTION** The size of the endolysosome should not be larger than 1/2 the size of the cell. If it is too large, it will be floating around. If it is too small, it will be hard to seal.

▲ **CRITICAL STEP** Vesicles close to cell edges are easier to isolate. Vesicles on the left side are usually difficult to control (assuming the pipette is approaching from the right side); in particular, dissecting the vesicle out of the cell is more difficult and vesicles break more easily under the pressure of the isolation pipette.

33| Set the MODE selector of micromanipulator to 0. Bring the isolation pipette into close proximity to the selected cell.

▲ **CRITICAL STEP** A MODE selector setting of 0 to 9 is used for very fast to very slow movements. A setting of 0 brings the isolation pipette to the selected cell. A setting of 4–5 is used to isolate the endolysosomal vesicle (Steps 33–36). A setting of 5–6 is used for gigaseal formation (Steps 44–46).

34| Set the MODE selector of the micromanipulator to 5. Move the isolation pipette downward until it touches the edge of the plasma membrane (**Figs. 5 and 7**).

35| Rapidly move the isolation pipette away horizontally. This will pull out a piece of plasma membrane (**Fig. 7a**).

36| Use the same pipette to push the endolysosome from the opposite side of the cell and press the cytoplasmic body to squeeze the endosome/lysosome out through the incision (**Figs. 5 and 7b**).

37| Using the isolation pipette, move the endolysosome away from the cell (**Fig. 7c**).

▲ **CRITICAL STEP** Parts of the plasma membrane or other materials might cover or contaminate the endosome/lysosome and lead to failure of sealing. This can be avoided by moving the endolysosome away from the cell.

? **TROUBLESHOOTING**

38| Inspect the isolated endolysosome under a microscope (**Fig. 7d**).

▲ **CRITICAL STEP** The membrane of endolysosomal vesicles is brighter and much thinner than the plasma membrane. Endolysosomal membranes are weak and almost transparent under a microscope.

? **TROUBLESHOOTING**

Gigaseal formation ● **TIMING** 1–2 min

39| Use a freshly polished recording pipette and fill it with the appropriate luminal solution.

40| Mount the pipette to the headstage of the amplifier.

PROTOCOL

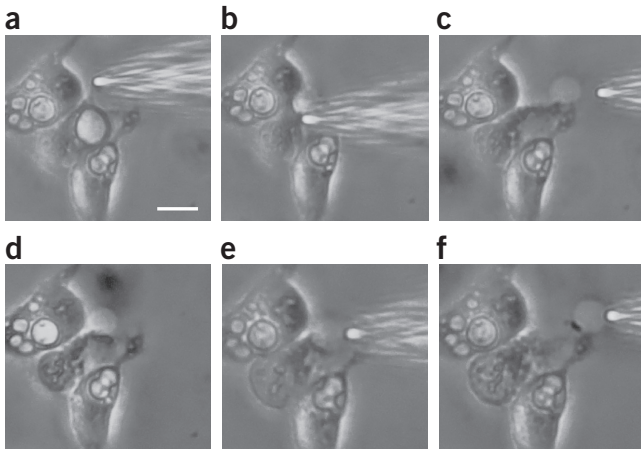


Figure 7 | Series of images illustrating the continuous process of isolation of a vacuolin-1-enlarged endolysosomal vesicle in a HEK293 cell (2-h treatment) with an ‘isolation pipette’ and gigaseal formation with the ‘recording pipette’. (a–c) First, an isolation pipette is used to cut open the plasma membrane and to push the endolysosomal vesicle out of the cell. (a) The targeted enlarged endolysosome, located on the right side of the cell in the center of the image, is shown. The cell membrane is cut open with an ‘isolation pipette’ at a position close to the endolysosome (Step 34). (b) The vesicle is pushed out through the opening in the membrane in the same ‘isolation pipette’ (Step 35). (c) The intact vesicle is located outside of the cell but is still connected by a small part to the cytoskeleton of the cell (Step 37). (d–f) A second pipette (‘recording pipette’) is used to form a gigaseal and to perform whole-endolysosome recording. (d) The isolated endolysosome sometimes moves back to the host cell within a few seconds. Unexpected movements of the isolated endolysosome should be considered before starting the patching step (Step 41). (e) Slight positive pressure from the tip of the recording pipette should be applied (this can be seen when the vesicle is moving forward (1–5 μm) slightly because of the liquid flow). An appropriate positive pressure (0.03–0.05 ml) keeps the pipette tip clean and increases the success rate for the experiment (Step 45). (f) Release of the positive pressure; a small backward flow helps to patch the vesicle membrane within 1 s (Step 47). After gigaseal formation for 10–30 s, the pipette with the intact vesicle on its tip can be moved away or up 1–20 μm , which stabilizes the configuration of the whole-endolysosome recording. Scale bar, 10 μm (applies to all the panels).

41 | Apply 20–50 mbar positive pressure to the pipette (or 0.03–0.05 ml of a 1-ml syringe for pressure control) and hold this pressure (lock the valve).

42 | Set the MODE selector of the micromanipulator to 0.

43 | Move the pipette tip into the bath solution and place it in the middle of the visual field. The pressure should be strong enough to see the liquid flow into the bath solution.

▲ CRITICAL STEP It is necessary to give positive pressure to avoid dust clogging the pipette tip. With pressure exceeding 50 mbar, it is easier to form a seal with the endolysosomal membrane, but it is not possible to break into the endolysosome to establish whole-endolysosome mode.

44 | Apply repetitive current pulses (+5 mV; 5 ms) to determine pipette resistance, seal resistance and series resistance to monitor the size of the pipette tip, seal formation and establishment of whole-endolysosome configuration, respectively (**Fig. 8**).

45 | Set the MODE selector of the micromanipulator to 6. Quickly move the pipette close to the top of the target vesicle (<30 s) (**Fig. 7e**).

46 | Move the pipette close to the vesicle until you see movement of the vesicle, which is caused by liquid flow out of the pipette.

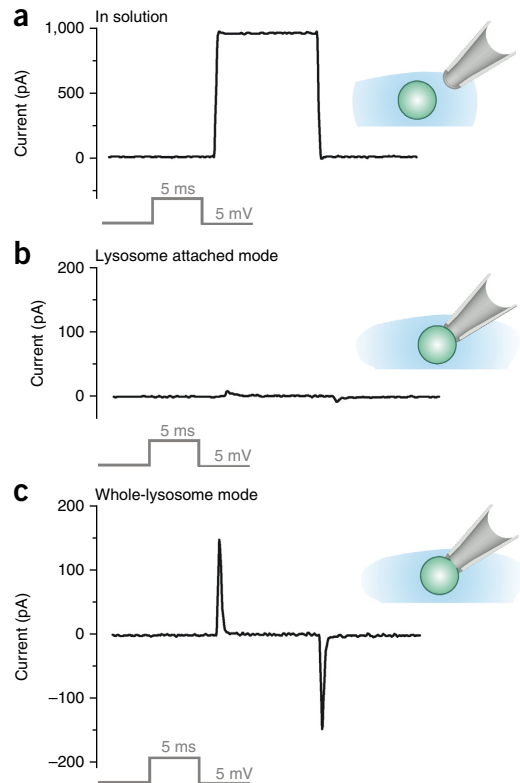


Figure 8 | Currents for calculation of pipette resistance, seal resistance, series resistance and cell capacitance. (a) The recording pipette is located in the bath solution. The rectangular voltage pulse (step: 5 ms; 5 mV; vacuolin-1-enlarged endolysosomal vesicle isolated from a HEK293 cell 2 h after treatment) causes a virtually rectangular current response. The pipette resistance can be calculated by dividing the command voltage by the current response. (b) During establishment of lysosome-attached mode (gigaseal formation), the current response diminishes rapidly. The seal resistance can be calculated by dividing the command voltage by the very small remaining current. (c) Application of the ZAP pulse causes an immediate membrane breakdown and an increase of the capacitive currents that indicate the successful formation of the whole-endolysosomal mode. For a spherical endolysosome, this current is described by a single exponential function of time. Series resistance can be calculated by dividing the amplitude of the capacitive currents by the command voltage. The capacity of the cell can be calculated by dividing the time constant of the capacitive currents by the series resistance.

47| Adjust the offset voltage of the pipette to 0 mV (Fig. 8a).

48| Release the positive pressure immediately. Under optimal conditions, the vesicle will be sucked in the direction of the pipette and attach to the membrane, and a gigaseal (1–20 GΩ) will form within 1 s (Figs. 7f and 8b).

? TROUBLESHOOTING

49| Monitor gigaseal formation by inspecting the current during the repetitive current pulses. It should diminish very quickly to 0 mV (Fig. 8b).

? TROUBLESHOOTING

50| If you are proceeding with single-channel recordings in endolysosome-attached mode, continue with option A. If you are proceeding with single-channel recordings in lumen-out mode, continue with option B. If you are proceeding with whole-endolysosome recordings in voltage-clamp and current-clamp mode or single-channel recordings in cytosol-out mode, continue with option C.

(A) Single-channel recordings in lysosome-attached mode

● TIMING 1–5 min, depending on the patch protocol

- (i) Form a gigaseal to establish lysosome-attached mode (Fig. 9).
- (ii) Change the feedback resistor of the headstage to 50 GΩ in the PatchMaster software (or Multiclamp 700B Commander). For an Axopatch 200B amplifier, switch the 'CONFIG' setting to 'PATCH' on the front panel and turn on the 'HEADSTAGE COOLING' switch on the rear panel. These settings provide the best signal-to-noise ratio, which is important for the recording of small single-channel currents.
 - ▲ CRITICAL STEP Turn on headstage cooling at least 1 h before experimentation so that the amplifier can equilibrate. If this is not done, the current offset will be changing throughout the course of the experiment.
- (iii) Acquire current traces using step potentials in software such as PatchMaster (or Clampex, for Axon amplifiers) and check whether single-channel events were detected (Fig. 10). If not, abandon this recording and try a new one.

▲ CRITICAL STEP In lysosome-attached mode, the voltage across the attached membrane patch (V_{patch}) is determined by the resting membrane potential of the endolysosome (V_{RMP}) and the voltage applied through the amplifier (V_{amp}). As the V_{RMP} is not known, the voltage dependence calculated from V_{amp} does not represent the true voltage dependence of the channel. The direction of currents in lysosome-attached recordings is opposite to those in whole-endolysosomal recordings.

(B) Single-channel recordings in lumen-out mode ● TIMING 1–5 min, depending on the patch protocol

- (i) After forming a gigaseal, pull off a membrane patch by moving the pipette away from the endolysosome quickly (>3 μm/s) with the manipulator (Fig. 9).
 - ▲ CRITICAL STEP After pulling off the membrane patch, the membrane surrounding the pipette tip often seals up to form a vesicle. In this case, the lumen-out mode can be achieved by taking the pipette tip out of the bath solution briefly to break the outer face of the vesicle.
- (ii) Change the feedback resistor of the headstage to 50 GΩ in the PatchMaster software (or Multiclamp 700B Commander). For an Axopatch 200B amplifier, switch the 'CONFIG' setting to 'PATCH' on the front panel and turn on the 'HEADSTAGE COOLING' switch on the rear panel.
 - ▲ CRITICAL STEP Turn on headstage cooling at least 1 h before experimentation so that the amplifier can equilibrate. If this is not done, the current offset will change throughout the course of the experiment.
- (iii) Acquire current traces using step potentials in software such as PatchMaster (or Clampex, for Axon amplifiers) and check whether single-channel events were detected. Keep in mind that the directions of current and voltage in lumen-out recordings are opposite to those of whole-endolysosomal recordings.
- (iv) Change the bath solution or add channel opener/blocker, if necessary.

(C) Establishment of whole-endolysosome mode ● TIMING 1 min

- (i) Set the ZAP command (fast voltage pulse) from the PatchMaster control to an initial value of -750 mV/0.5 ms.
- (ii) Use ZAP to break into the vesicle and to establish whole-endolysosomal mode.

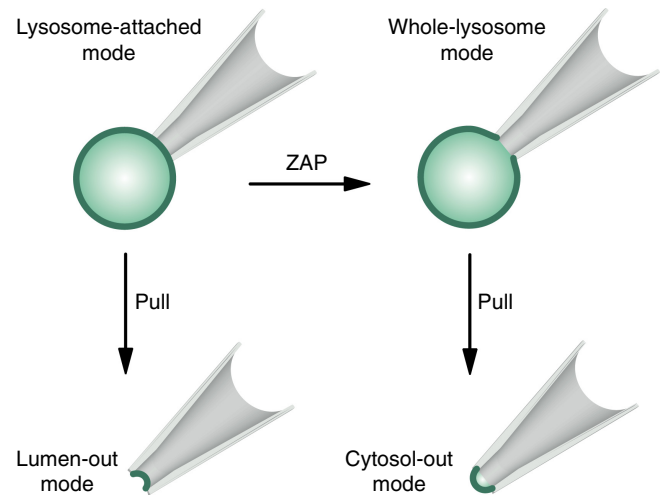


Figure 9 | Patch-clamp configurations for single-lysosome recordings. Single-lysosome recordings can be performed in three different modes: endolysosome-attached, lumen-out and cytosol-out.

PROTOCOL

- (iii) Observe a rapid increase of the transient currents during the repetitive voltage steps (**Fig. 8c**).
▲ CRITICAL STEP If break-in fails, increase the zapping time 2- to 10-fold step by step until break-in. If break-in still fails, apply a larger voltage, up to $-1,000$ mV.

? TROUBLESHOOTING

Recordings in whole-endolysosome mode ● TIMING 1–5 min, depending on the patch protocol

51| Cancel capacity transients by applying capacitance compensation circuitry until series resistance is <100 M Ω and/or capacitance remains in a reasonable range (from 0.1 ± 0.05 to 5 ± 0.5 pF).

! CAUTION If capacitance compensation fails (i.e., the capacitance value does not appear on the display and the small box in the ‘auto’ button (*E*) is darkened (indicating an error after autocompensation)), recording should not be continued.

? TROUBLESHOOTING

52| If you are proceeding with whole-endolysosome recordings in voltage-clamp mode, continue with option A. If you are proceeding with whole-endolysosome recordings in current-clamp mode, continue with option B.

(A) Voltage-clamp recordings in whole-endolysosomal mode ● TIMING 1–5 min, depending on the patch protocol

- (i) Apply a suitable holding potential, depending on your channel of interest or the cell type used.
- (ii) Acquire current traces by applying a protocol containing the desired voltage pulses with the PatchMaster software (Axon amplifiers) and record currents at room temperature.

(B) Current-clamp recordings in whole-endolysosomal mode ● TIMING 1–5 min, depending on the patch protocol

- (i) Switch the recording mode to $I = 0$ by clicking the ‘ $I = 0$ ’ button on the panel of the Multiclamp 700B Commander software. This will disconnect all external inputs.
- (ii) Open or set up an appropriate protocol for the current-clamp recording in the Clampex software.
! CAUTION Make sure that the holding current in the protocol is set to 0 before proceeding to the next step. The holding current will be injected into the endolysosome immediately after switching to IC (current-clamp) mode. This may cause a large change in membrane potential and may disrupt the gigaseal.
- (iii) Switch to current-clamp mode by clicking the ‘IC’ button on the panel of the Multiclamp 700B Commander software.
- (iv) Check the ‘Tuning’ checkbox and monitor the ‘Primary Output: Membrane Potential’ in the ‘Scope’ window of the Clampex software. Adjust the amplitude and frequency tuning parameters to generate a sawtooth pattern of voltage traces with ~ 10 mV amplitude.
- (v) Go to ‘Options/Auto’ menu, check the ‘Reduce Rs Compensation...’ button and close this menu. Check the ‘D Reduce if oscillation detected’ checkbox.
- (vi) Check the ‘Pipette Capacitance Neutralization’ checkbox and carefully increase the capacitance value until overshoot starts to show up in the voltage traces.
! CAUTION Overneutralizing the pipette capacitance will generate oscillations that may be harmful to the endolysosomes. Therefore, it is better to keep the checkbox ‘Reduce if oscillation detected’ checked and reduce the pipette capacitance neutralizing value slightly (e.g., to 0.5 pF) from optimal to prevent oscillation caused by capacitance changes during the recordings.

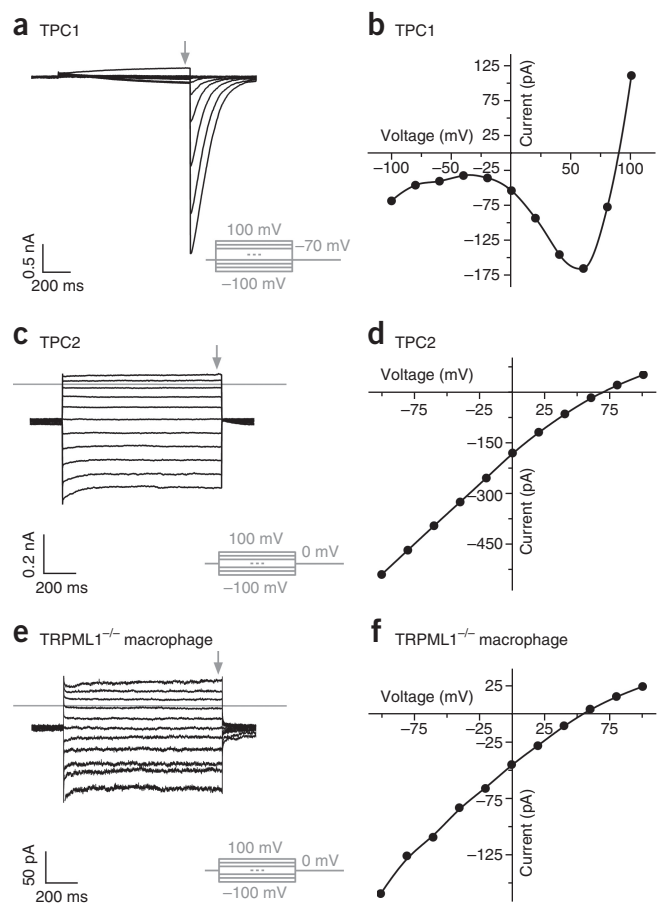


Figure 10 | Representative whole-endolysosome recordings. (a) Current traces were recorded from a vacuolin-1-enlarged endolysosome isolated from a HEK293 cell expressing TPC1 in the presence of $1 \mu\text{M}$ PI(3,5)P₂. (b) Current–voltage relationship for experiment shown in a. (c) Current traces were recorded from a vacuolin-1-enlarged endolysosome isolated from a HEK293 cell expressing TPC2 in the presence of $1 \mu\text{M}$ PI(3,5)P₂. (d) Current–voltage relationship for experiment shown in c. (e) Currents recorded from a vacuolin-1-enlarged endolysosome isolated from a TRPML1^{-/-} macrophage. (f) Current–voltage relationship for experiment shown in e. Panels a, c and e show current amplitudes obtained using a step protocol. Panels b, d and f show current–voltage relationships reconstructed from the currents in a, c and e (indicated by arrows), respectively.

- (vii) Automatically compensate for the series resistance by clicking the 'Auto' button in the 'Bridge balance' box. This should prevent the fast voltage step from appearing at the start and finish of the current tuning step. In some cases, you may have to manually adjust the value to reach optimal balance.
- (viii) Acquire voltage traces using the protocols of the data acquisition software.

Single-channel recordings in cytosol-out mode ● TIMING 1–5 min, depending on the patch protocol

53| Pull the pipette slowly (~0.5–1 μm/s) away from the endolysosome with manipulator to establish cytosol-out mode (Fig. 9).

▲ CRITICAL STEP The membrane fragments attached to the pipette tip should reseal to form a membrane patch whose cytosolic side is in contact with the bath solution.

54| In the PatchMaster (or MultiClamp 700B Commander) software, change the feedback resistor of the headstage to 50 GΩ. For an Axopatch 200B amplifier, switch the 'CONFIG' switch to 'PATCH' on the front panel and turn on the 'HEADSTAGE COOLING' switch on the rear panel to minimize the noise.

55| Acquire traces using step potentials in the PatchMaster (or Clampex, for Axon amplifiers) software and check whether single-channel events were detected. If not, abandon this recording and try a new one.

? TROUBLESHOOTING

Troubleshooting advice can be found in **Table 4**.

TABLE 4 | Troubleshooting table.

Step	Problem	Possible reason	Solution
27	Parallel path of the pipette is too short (<2 μm)	(a) Too-wide opening of the pipette tip (>1 μm) (b) Imbalance of the pipette tip (c) Tip is over-polished	(a) Increase the HEAT +5 on the sixth cycle of the pulling program on the P-97 puller and pull a new pipette (b) Check that the pipette position is right in the middle of the trough filament on the P-97 puller. If not, realign the filament according to the Sutter Instrument Pipette Cookbook and pull a new pipette (c) Pull a new pipette
37	Isolation of lysosome failed	(a) Cell was not well attached to the dish (b) Pipette was broken during isolation (c) Plasma membrane sticks to the pipette tip	(a) Optimize cell culture. Determine the optimal time window after harvesting the cells. Coat the coverslip with poly-L-lysine coating solution for a longer time period, or use fresh cells (b) Move down the pipette when the pipette tip touches the bottom of the coverslip in Step 36. Watch the tip move slightly toward the left. Once you notice this movement, stop moving down (c) Move the tip faster horizontally or toward the 2 or 4 o'clock position, or apply positive pressure to blow the membrane away
38	Isolated lysosome vanished	(a) Lysosome burst (b) Lysosome shrunk (c) Lysosome floated away	(a,b) Adjust the osmolality of the bath solution (c) Do not move the lysosome too far away from the cell with the isolation pipette
48	No automatic gigaseal formation after release of pressure	(a) Pressure was too low or there was a pressure leak (b) Pipette tip was blocked by air or contamination (c) Isolated was lysosome still covered by plasma membrane	(a) If the lysosome does not move onto the tip of the pipette right after release of the positive pressure, quickly move the patch pipette close to the lysosome (within 3 s) (b) Check that pipette resistance was not higher than 20 MΩ in the bath solution. Use a new recording pipette (c) To prevent the plasma membrane from covering the isolated lysosome, Steps 33–36 of the isolation protocol are critical. Try to repeat. Steps 34 and 35 a few times, until the damaged edge is large enough to release the lysosome easily, before proceeding to Step 36

(continued)

PROTOCOL

TABLE 4 | Troubleshooting table (continued).

Step	Problem	Possible reason	Solution
49	Still no gigaseal when the pipette tip is attached to the lysosomal membrane	(a) Pressure leak (b) No good connection between the lysosomal membrane and the pipette tip	(a) If no gigaseal is formed within 1 s, apply an additional 0.01–0.05 ml of negative pressure (usually not more than 0.05 ml) and hold the potential at -30 mV; this will help cause sealing within 5 min. When the gigaseal is established, release the pressure If no gigaseal forms within 5 min and the lysosome is still intact, try to patch again (b) Apply fast voltage ramp (-80 mV to $+80$ mV, 20 ms; repeat 10–100 times) for 1–3 min
50C(iii)	Loss of seal or lysosome during zapping	(a) Geometry of the pipette tip is not optimal (b) Pressure between the pipette and the bath was unbalanced	(a) Prepare new patch pipette (b) After gigaseal, slowly move the pipette with the lysosome vertically and horizontally away from the host cell until the host cell is outside the field of view. Then wait 60 s before zapping
51	Compensation failure	(a) Did not achieve a whole-endolysosome configuration (b) Capacitance value of the vesicle is smaller than 0.1 pF	(a) Go back to Step 49C(i–iii) (b) Remove the pipette and go back to Step 29

● TIMING

Steps 1–10, preparation of HEK293 cells for endolysosomal recordings: 2–4 d

Steps 11 and 12, enlargement of endolysosomal vesicles: 1–48 h

Steps 13–27, preparation of recording glass pipettes: 1–10 min per pipette

Steps 28–38, isolation of endolysosome from the cell: 1–10 min

Steps 39–55, formation of whole-endolysosomal recording: 3–12 min

ANTICIPATED RESULTS

Typical current traces obtained after the patch pipette crosses the surface of the recording solution are shown in **Figure 8**. Optimally shaped pipettes used for lysosomal patch-clamp are characterized by a pipette resistance of 5–8 M Ω . After seal formation, the seal resistance typically increases to a range of 8–10 G Ω . Finally, after breaking into the endolysosomal vesicle, slow transients appear, indicating optimal access to the lumen of the endolysosome. From the transients, series resistance and endolysosomal capacitance are calculated (**Table 2**). Typically, the series resistance ranges from 20 to 100 M Ω and the capacitance ranges from 0.1 to 5 pF.

Once whole-endolysosome conformation is achieved, specific currents can be recorded. In late endosomes and lysosomes TPCs can be readily recorded. Families of current traces obtained by applying a voltage step protocol (-100 mV to $+100$ mV, 20-mV increments, 2 s) side by side with the corresponding current–voltage relationships are shown in **Figure 10**. TPC1 and TPC2 currents are activated by applying PI(3,5)P₂. As PI(3,5)P₂ is a nonspecific agonist of TPCs and TRPML1 in late endolysosomes, TPC2-like currents are recorded from TRPML1^{-/-} peritoneal macrophages (**Fig. 10e,f**). TMEM175 channels are constitutively active and therefore the activation of these channels does not require the application of an activator (data not shown).

It is also possible to record dynamical time-dependent changes in lysosomal membrane potential in

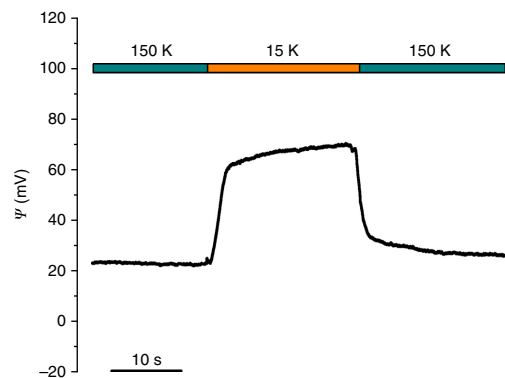
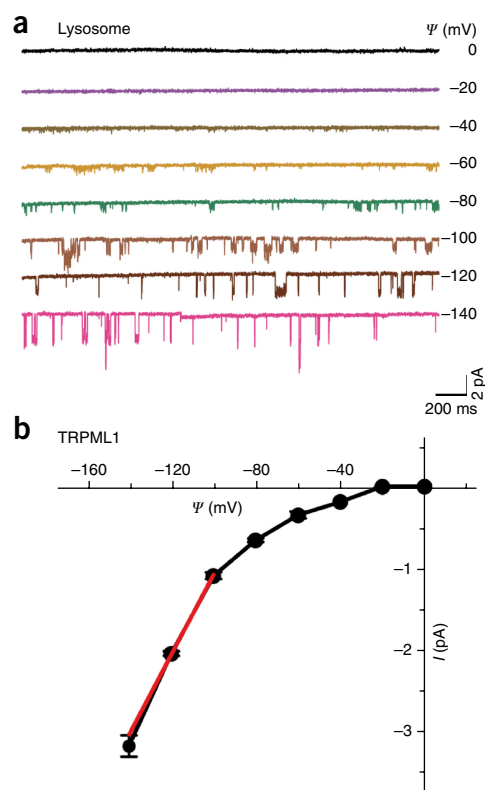


Figure 11 | Representative current-clamp recording from a vacuolin-1 (5 μ M overnight)-enlarged endolysosome isolated from a cortical astrocyte showing steady-state value and dynamic changes of lysosomal membrane potential. Pipette solution consists of 150 mM K-methanesulfonate, 1 mM HCl, 10 mM HEPES and 10 mM MES, pH 5.5. Bath solution consists of 150 mM K-MSA (or 15 mM K-MSA + 135 mM NMDG-MSA), 1 mM HCl and 10 mM HEPES, pH 7.2. Ψ , membrane voltage.

Figure 12 | Single-channel recordings. (a) Current recordings from isolated endolysosomes prepared from HEK293 cells overexpressing TRPML1 channels ($n = 1$). Shown are mean current amplitudes of all single-channel events at a given voltage. Pipette solution consists of 145 mM K-MSA, 5 mM KCl, 10 mM HEPES and 1 μ M PI(3,5)P₂, pH 7.2. Bath solution consists of 145 mM K-MSA, 5 mM KCl, 10 mM HEPES and 5 μ M PI(3,5)P₂, pH 7.2. (b) Current–voltage relationship for TRPML1 channels from a. The red line represents linear fitting of the three data points (–140, –120 and –100 mV). Ψ , membrane voltage.



current-clamp mode. **Figure 11** shows the time course of lysosomal membrane voltage, starting with a cytosolic solution containing 150 mM potassium, followed by a change to a solution containing 15 mM potassium and finally by an exchange back to a solution containing 150 mM potassium. The experiment demonstrates that reduction of potassium from 150 to 15 mM induces a depolarization of the lysosomal membrane potential by 50 mV. Given the composition of the solutions, the result suggests that potassium conductance is present in the lysosomal membrane.

Finally, single-channel activities can be recorded from endolysosomal membranes (**Fig. 12**). Using specific solutions, single-channel events can be recorded in cells expressing TRPML1 channels. For the experiment shown in **Figure 12**, a series of voltage pulses ranging from 0 mV to –140 mV (20-mV increments, step duration: 3 s; interstep interval: 2 s) was applied from a holding potential of 0 mV. The patch was recorded in endolysosome-attached mode and contained two single channels. From the experiment, a current–voltage relation was determined by plotting current amplitude of single-channel activities versus voltage. From this relation, the slope conductance was determined to be 49 pS.

Note: Any Supplementary Information and Source Data files are available in the online version of the paper.

ACKNOWLEDGMENTS This work was supported, in part, by funding from the German Research Foundation (SFB/TRR152 TP04 to C.G., TP06 to C.W.-S., and TP10 and TP12 to M.B., as well as SFB870 TP05 to C.W.-S. and M.B., and TP15 to C.W.-S.).

AUTHOR CONTRIBUTIONS C.-C.C. and C.C. developed and performed endolysosomal patch-clamp experiments. C.-C.C., C.C., E.B. and Y.-K.C. designed, collected and/or analyzed data. C.-C.C., C.C., S.F., D.R., C.G., C.W.-S. and M.B. designed the study and edited the manuscript. All the authors discussed the results and commented on the manuscript.

COMPETING FINANCIAL INTERESTS The authors declare no competing financial interests.

Reprints and permissions information is available online at <http://www.nature.com/reprints/index.html>. Publisher's note: Springer Nature remains neutral with regard to jurisdictional claims in published maps and institutional affiliations.

- Cang, C. *et al.* mTOR regulates lysosomal ATP-sensitive two-pore Na(+) channels to adapt to metabolic state. *Cell* **4**, 778–790 (2013).
- Dong, X.P. *et al.* The type IV mucopolipidosis-associated protein TRPML1 is an endolysosomal iron release channel. *Nature* **455**, 992–996 (2008).
- Cang, C. *et al.* TMEM175 is an organelle K(+) channel regulating lysosomal function. *Cell* **5**, 1101–1112 (2015).
- Dong, X.P. *et al.* PI(3,5)P(2) controls membrane trafficking by direct activation of mucolipin Ca(2+) release channels in the endolysosome. *Nat. Commun.* **1**, 38 (2010).
- Jentsch, T.J. *et al.* CLC chloride channels and transporters. *Curr. Opin. Neurobiol.* **3**, 319–325 (2005).

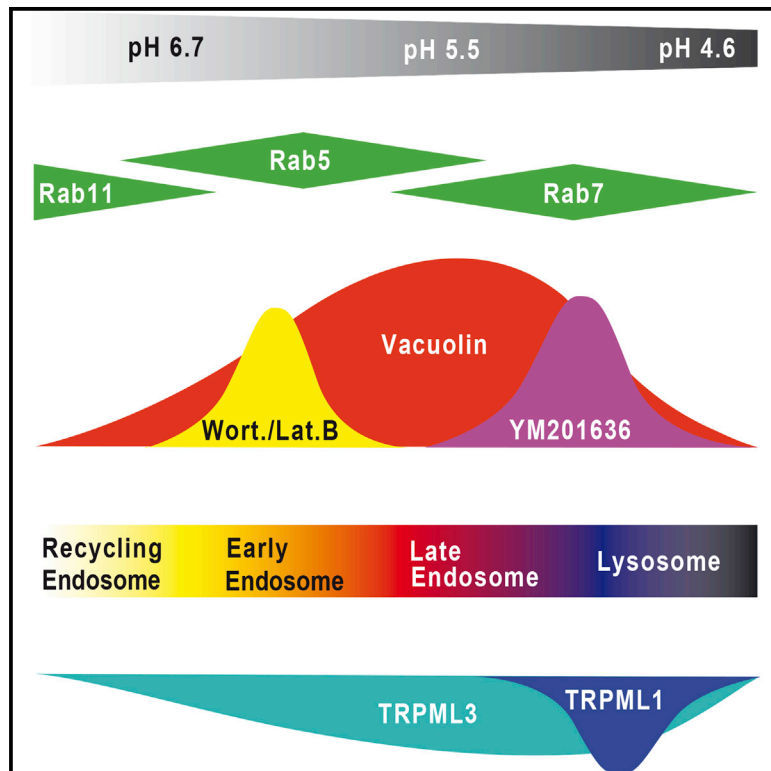
- Grimm, C. *et al.* Role of TRPML and two-pore channels in endolysosomal cation homeostasis. *J. Pharmacol. Exp. Ther.* **2**, 236–244 (2012).
- Grimm, C. *et al.* High susceptibility to fatty liver disease in two-pore channel 2-deficient mice. *Nat. Commun.* **5**, 4699 (2014).
- Sakurai, Y. *et al.* Two-pore channels control Ebola virus host cell entry and are drug targets for disease treatment. *Science* **6225**, 995–998 (2015).
- Chen, C.C. *et al.* A small molecule restores function to TRPML1 mutant isoforms responsible for mucopolipidosis type IV. *Nat. Commun.* **5**, 4681 (2014).
- Xu, H. & Ren, D. Lysosomal physiology. *Annu. Rev. Physiol.* **77**, 57–80 (2015).
- Hockey, L.N. *et al.* Dysregulation of lysosomal morphology by pathogenic LRRK2 is corrected by TPC2 inhibition. *J. Cell Sci.* **128**, 232–238 (2015).
- Schwake, M. *et al.* Lysosomal membrane proteins and their central role in physiology. *Traffic* **7**, 739–748 (2013).
- Chapel, A. *et al.* An extended proteome map of the lysosomal membrane reveals novel potential transporters. *Mol. Cell Proteomics.* **6**, 1572–1588 (2013).
- Zhang, F. & Li, P.-L. Reconstitution and characterization of a nicotinic acid adenine dinucleotide phosphate (NAADP)-sensitive Ca²⁺ release channel from liver lysosomes of rats. *J. Biol. Chem.* **282**, 25259–25269 (2007).
- Zhang, F. *et al.* TRP-ML1 functions as a lysosomal NAADP-sensitive Ca²⁺ release channel in coronary arterial myocytes. *J. Cell. Mol. Med.* **13**, 3174–3185 (2009).
- Pitt, S.J. *et al.* TPC2 is a novel NAADP-sensitive Ca²⁺ release channel, operating as a dual sensor of luminal pH and Ca²⁺. *J. Biol. Chem.* **285**, 35039–35046 (2010).
- Pitt, S.J. *et al.* Reconstituted human TPC1 is a proton-permeable ion channel and is activated by NAADP or Ca²⁺. *Sci. Signal.* **7**, ra46 (2014).

18. Patel, S. Function and dysfunction of two-pore channels. *Sci. Signal.* **8**, re7 (2015).
19. Feijóo-Bandín, S. *et al.* Two-pore channels (TPCs): novel voltage-gated ion channels with pleiotropic functions. *Channels* **20**, 1–14 (2016).
20. Grimm, C. *et al.* Role of TRPML and two-pore channels in endolysosomal cation homeostasis. *J. Pharmacol. Exp. Ther.* **342**, 236–244 (2012).
21. Venkatachalam, K. *et al.* The role of TRPMLs in endolysosomal trafficking and function. *Cell Calcium* **58**, 48–56 (2015).
22. Cheng, X. *et al.* Mucolipins: intracellular TRPML1-3 channels. *FEBS Lett.* **584**, 2013–2021 (2010).
23. Schieder, M. *et al.* Planar patch clamp approach to characterize ionic currents from intact lysosomes. *Sci. Signal.* **151**, 13 (2010).
24. Jha, A. *et al.* Convergent regulation of the lysosomal two-pore channel-2 by Mg²⁺, NAADP, PI(3,5)P₂ and multiple protein kinases. *EMBO J.* **33**, 501–511 (2014).
25. Samie, M. *et al.* A TRP channel in the lysosome regulates large particle phagocytosis via focal exocytosis. *Dev Cell.* **26**, 511–524 (2013).
26. Bellono, N.W. *et al.* A melanosomal two-pore sodium channel regulates pigmentation. *Sci. Rep.* **6**, 26570 (2016).
27. Shen, J. *et al.* SNARE bundle and syntaxin N-peptide constitute a minimal complement for Munc18-1 activation of membrane fusion. *J. Cell Biol.* **190**, 55–63 (2010).
28. Brailoiu, E. *et al.* An NAADP-gated two-pore channel targeted to the plasma membrane uncouples triggering from amplifying Ca²⁺ signals. *J. Biol. Chem.* **285**, 38511–38516 (2010).
29. Cerny, J. *et al.* The small chemical vacuolin-1 inhibits Ca(2+)-dependent lysosomal exocytosis but not cell resealing. *EMBO Rep.* **5**, 883–888 (2004).
30. Axon Instruments *The Axon Guide for Electrophysiology & Biophysics Laboratory Techniques* http://www.psychiatry.wustl.edu/zorumski/Axon_Guide.PDF (1993).
31. Cummins, T.R. *et al.* Voltage-clamp and current-clamp recordings from mammalian DRG neurons. *Nat. Protoc.* **4**, 1103–1112 (2009).
32. Guo, H. *et al.* Role of TRPM in melanocytes and melanoma. *Exp. Dermatol.* **21**, 650–654 (2012).
33. Lange, I. *et al.* TRPM2 functions as a lysosomal Ca²⁺-release channel in beta cells. *Sci. Signal.* **2**, ra23 (2009).
34. Nilius, B. *et al.* Transient receptor potential cation channels in disease. *Physiol. Rev.* **87**, 165–217 (2006).
35. Miao, Y. *et al.* A TRP channel senses lysosome neutralization by pathogens to trigger their expulsion. *Cell* **6**, 1306–1319 (2015).
36. Gu, M. & Xu, H. A painful TR(i)P to lysosomes. *J. Cell Biol.* **215**, 309–312 (2016).
37. Dong, X.P. *et al.* TRP channels of intracellular membranes. *J. Neurochem.* **113**, 313–328 (2010).
38. Cang, C. *et al.* The voltage-gated sodium channel TPC1 confers endolysosomal excitability. *Nat. Chem. Biol.* **10**, 463–469 (2014).
39. Melchionda, M. *et al.* Ca²⁺/H⁺ exchange by acidic organelles regulates cell migration *in vivo*. *J. Cell Biol.* **212**, 803–813 (2016).
40. Wang, X. *et al.* TPC proteins are phosphoinositide-activated sodium-selective ion channels in endosomes and lysosomes. *Cell* **2**, 372–383 (2012).
41. Novarino, G. *et al.* Endosomal chloride-proton exchange rather than chloride conductance is crucial for renal endocytosis. *Science* **5984**, 1398–1401 (2010).
42. Huang, P. *et al.* P2X₄ forms functional ATP-activated cation channels on lysosomal membranes regulated by luminal pH. *J. Biol. Chem.* **289**, 17658–17667 (2014).
43. Cao, Q. *et al.* BK channels alleviate lysosomal storage diseases by providing positive feedback regulation of lysosomal Ca²⁺ release. *Dev. Cell* **4**, 427–441 (2015).
44. Bertl, A. *et al.* Electrical measurements on endomembranes. *Science* **258**, 873–874 (1992).

Cell Chemical Biology

Small Molecules for Early Endosome-Specific Patch Clamping

Graphical Abstract



Authors

Cheng-Chang Chen, Elisabeth S. Butz, Yu-Kai Chao, ..., Martin Biel, Christian Wahl-Schott, Christian Grimm

Correspondence

christian.wahl@cup.uni-muenchen.de (C.W.-S.), christian.grimm@cup.uni-muenchen.de (C.G.)

In Brief

To functionally characterize ion channels in endolysosomal membranes with the patch-clamp technique, it is important to develop techniques to selectively enlarge organelles. Chen et al. found here that wortmannin and latrunculin B specifically enlarge Rab5-positive early endosomes.

Highlights

- A novel approach for early-endosome-selective patch clamping is provided
- Wortmannin and latrunculin B enable selective EE patch-clamp experimentation
- TRPML channels are characterized in EE and LE/LY
- TRPML3 is shown to be functionally active in both EE and LE/LY



Small Molecules for Early Endosome-Specific Patch Clamping

Cheng-Chang Chen,^{1,4} Elisabeth S. Butz,^{1,4} Yu-Kai Chao,¹ Yulia Grishchuk,² Lars Becker,³ Stefan Heller,³ Susan A. Slaugenhaupt,² Martin Biel,¹ Christian Wahl-Schott,^{1,*} and Christian Grimm^{1,5,*}

¹Department of Pharmacy, Center for Drug Research and Center for Integrated Protein Science Munich (CIPSM), Ludwig-Maximilians-Universität München, 81377 Munich, Germany

²Department of Neurology, Center for Human Genetic Research, Massachusetts General Hospital, Harvard University, Boston, MA 02114, USA

³Departments of Otolaryngology – HNS and Molecular & Cellular Physiology, Stanford University School of Medicine, Palo Alto, CA 94304, USA

⁴These authors contributed equally

⁵Lead Contact

*Correspondence: christian.wahl@cup.uni-muenchen.de (C.W.-S.), christian.grimm@cup.uni-muenchen.de (C.G.)

<http://dx.doi.org/10.1016/j.chembiol.2017.05.025>

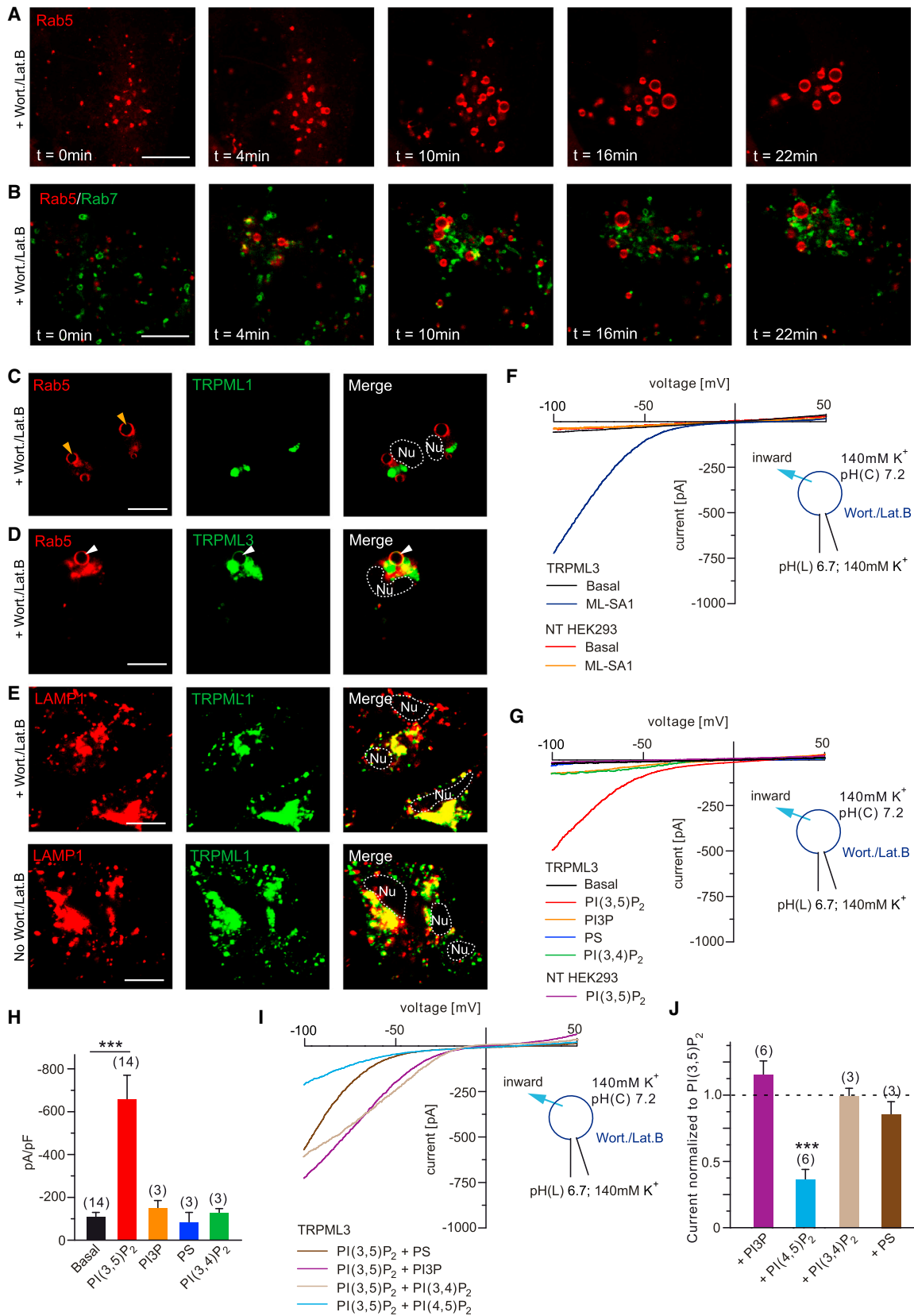
SUMMARY

To resolve the subcellular distribution of endolysosomal ion channels, we have established a novel experimental approach to selectively patch clamp Rab5 positive early endosomes (EE) versus Rab7/LAMP1-positive late endosomes/lysosomes (LE/LY). To functionally characterize ion channels in endolysosomal membranes with the patch-clamp technique, it is important to develop techniques to selectively enlarge the respective organelles. We found here that two small molecules, wortmannin and latrunculin B, enlarge Rab5-positive EE when combined but not Rab7-, LAMP1-, or Rab11 (RE)-positive vesicles. The two compounds act rapidly, specifically, and are readily applicable in contrast to genetic approaches or previously used compounds such as vacuolin, which enlarges EE, RE, and LE/LY. We apply this approach here to measure currents mediated by TRPML channels, in particular TRPML3, which we found to be functionally active in both EE and LE/LY in overexpressing cells as well as in endogenously expressing CD11b+ lung-tissue macrophages.

INTRODUCTION

For many years the best studied and characterized membrane proteins in eukaryotic cells were those located in the plasma membrane. Proteins in intracellular membranes, in particular ion channels and transporters, were much less well characterized, and their function and physiological roles were less well understood. In recent years, however, with the emerging technical capability to patch clamp endolysosomal organelles, a number of ion channels in endolysosomal membranes can be studied in more detail, e.g., TRPML channels (mucopolipins 1–3 or TRPML1–3), TPCs (two-pore channels, TPC1–2), P2X4, TMEM175, or BK (Ca²⁺-activated potassium channel) (Cang

et al., 2013, 2014, 2015; Chen et al., 2014; Dong et al., 2008; Grimm et al., 2014; Huang et al., 2014; Wang et al., 2015; Zhong et al., 2016). Endolysosomal ion channels and transport proteins are increasingly recognized as important regulators of endolysosomal function and human health. They are highly critical for the regulation of proton and other ionic concentrations within endolysosomal vesicles and participate in the regulation of the numerous endolysosomal vesicle trafficking as well as exo-, endo-, and phagocytic processes (Cheng et al., 2010; Grimm et al., 2012a; Samie et al., 2013; Patel, 2015; Venkatachalam et al., 2015; Grimm et al., 2017). Endolysosomal dysfunction can cause multiple storage disorders such as mucopolipidoses, sphingolipidoses, or neuronal ceroid lipofuscinoses, which typically go along with fatal neurodegenerative processes. Dysfunction of the endolysosomal and autophagic system has also been implicated in the development of neurodegenerative diseases such as Parkinson's or Alzheimer's disease, metabolic, retinal and pigmentation disorders, infectious diseases, and cancer (Fraldi et al., 2016; Kondratskiy et al., 2013; Medina and Ballabio, 2015; Mole and Cotman, 2015; Saftig and Sandhoff, 2013; Sakurai et al., 2015; Venkatachalam et al., 2015; Zhang et al., 2009). Development and progression of diseases, including those mentioned above, have recently been found to be often associated with dysfunction of endolysosomal ion channels or transporters such as TRPML channels, two-pore channels, CLC transport proteins, or the BK channel (Zhang et al., 2009; Jentsch et al., 2010; Weinert et al., 2010; Stauber et al., 2012; Bae et al., 2014; Calcrafft et al., 2009; Ruas et al., 2010; Chen et al., 2014; Grimm et al., 2014; Weinert et al., 2014; Hockey et al., 2015; Jentsch, 2015; Medina et al., 2015; Sakurai et al., 2015; Venkatachalam et al., 2015; De Leo et al., 2016; Favia et al., 2016; Kilpatrick et al., 2016; Zhong et al., 2016, 2017; Nguyen et al., 2017). In this context, it is also important to understand where the channels are functionally expressed, i.e., in early endosomes (EE) or late endosomes (LE), in lysosomes (LY), recycling endosomes (RE), autophagosomes, or lysosome-related organelles. Depending on the subcellular location, ion channels are likely to affect different trafficking pathways, resulting in different physiological and pathophysiological consequences when the channel is mutated, lost, or therapeutically targeted. Until now, one



(legend on next page)

compound, a small molecule called vacuolin, has been widely used to enlarge the size of endolysosomal vesicles, a step that is required to enable successful endolysosomal patch-clamp experimentation (Dong et al., 2008). However, vacuolin is not very selective in its ability to enlarge endolysosomal organelles as it enlarges different kinds of endolysosomal vesicles (Cerny et al., 2004; Lu et al., 2014). Hence, novel tools that enable selective patch-clamp experimentation on distinct endolysosomal organelles are urgently needed. Currently, only limited biochemical evidence is available to determine in which organelle a certain channel protein is expressed (Kim et al., 2009; Martina et al., 2009; Sun et al., 2015). We exemplarily confirm here the subcellular location(s) of TRPML channels, in particular TRPML1 and TRPML3. TRPML3 had been suggested previously to be present in both EE and LE/LY based on biochemical analyses (Kim et al., 2009; Martina et al., 2009). However, direct functional evidence that TRPML3 is found in different endolysosomal organelles, i.e., from patch-clamp analyses, was missing. Here, we use different small molecules, i.e., wortmannin (Wort.) and latrunculin B (Lat.B), for EE and YM201636 (Chen et al., 2014) for LE/LY instead of vacuolin or genetic tools such as Rab5Q79L (for EE; Stenmark et al., 1994; Cang et al., 2015) to selectively patch clamp EE versus LE/LY.

RESULTS

Wortmannin and Latrunculin B Specifically Enlarge EE when Combined

As reported previously, vacuolin-enlarged vesicles represent a rather non-homogeneous population of endolysosomal organelles as they comprise LE/LY (Rab7/LAMP1-positive vesicles) as well as EE (Rab5-positive vesicles) and RE (Rab11-positive vesicles) (Figure S1; Cerny et al., 2004). To identify more selective pharmacological tools for the enlargement of endolysosomal vesicles for patch-clamp experimentation, we tested several small molecules known or suggested previously in the literature to have an effect on intracellular vesicle trafficking, movement, or fusion/fission (Li et al., 1995; Jones et al., 1998;

Sheff et al., 2002; Greene and Gao, 2009). We eventually discovered that Wort. (200 nM) and Lat.B (10 nM) specifically and robustly enlarge EE (Rab5- or EEA1-positive vesicles) to a degree suitable for patch-clamp experimentation (i.e., >3–4 μm in diameter), but only when combined, while leaving LE/LY (Rab7/LAMP1-positive vesicles) or RE (Rab11-positive vesicles) unaffected (Figures 1A–1E, S1, and S2A, and Movies S1 and S2). When applied alone, neither drug resulted in sufficiently enlarged vesicular structures (Figure S3A and S3B). Importantly, Wort./Lat.B-enlarged vesicles were generally LAMP1/Rab7/TRPML1 or Rab11 negative (Figures 1E and S1; Movies S1 and S2).

TRPML3 Currents in EE Isolated from Overexpressing HEK293 Cells

In a first set of experiments, we demonstrate that in Wort./Lat.B-enlarged Rab5/TRPML3-positive organelles, large inwardly rectifying currents could be elicited with the TRPML channel agonist ML-SA1 (Figure 1F) (Shen et al., 2012; Wang et al., 2015) or with PI(3,5)P₂, an endolysosome-specific phosphoinositide previously shown to activate TRPML channels (Figures 1G–1J; Shen et al., 2012; Chen et al., 2014; Zhang et al., 2012). In EE isolated from non-transfected (NT) HEK293 cells, no ML-SA1 or PI(3,4)P₂ currents were detectable (Figures 1F and 1G). Phosphoinositides or phospholipids other than PI(3,5)P₂ did not result in significant channel activation nor did they significantly enhance PI(3,5)P₂-mediated channel activation (Figures 1G–1J). Zhang et al. (2012) have shown recently that PI(4,5)P₂ and PI(3,4)P₂ suppress PI(3,5)P₂-induced TRPML1 channel activity by 60%–70%. For TRPML3, we found that only PI(4,5)P₂ caused significant inhibition of PI(3,5)P₂-mediated activation, but not PI(3,4)P₂ (Figures 1I and 1J).

TRPML3 Currents in LE/LY Isolated from Overexpressing HEK293 Cells

To selectively measure TRPML channel activity in LE/LY, we performed patch-clamp experiments by using the PIKfyve inhibitor YM201636 to increase the size of LE/LY (Chen et al., 2014). Treatment with YM201636 resulted in enlarged

Figure 1. Effect of Wort./Lat.B on Organelles Expressing TRPML Channels and Endolysosomal Markers, and Early Endosomal Patch-Clamp Experiments in TRPML3 Channel Overexpressing Cells

(A and B) Representative confocal images (time series) showing the effect of 200 nM Wort. and 10 nM Lat.B on Rab5-mKate-positive vesicle enlargement (A), while Rab7-GFP positive vesicles remained unaffected (B). Experiments were performed in HEK293 cells. Images are taken from Movies S1 and S2. Scale bar, 10 μm .

(C–E) Representative confocal images of Rab5-mCherry and TRPML1-YFP (C), Rab5-mCherry and TRPML3-YFP (D), or LAMP1-mKate and TRPML1-YFP (E), transfected into HEK293 cells and treated for 20–30 min with 200 nM wortmannin (Wort.) and 10 nM latrunculin B (Lat.B). Significantly enlarged vesicles were observed only in combination. In (C), orange arrowheads point to Rab5-positive/TRPML1-negative enlarged vesicles (Rab5-positive vesicles were always TRPML1 negative); vesicle marked with white arrowheads in (D) is positive for Rab5 and TRPML3; in (E), it is shown that the size of the vesicles (LAMP1/TRPML1 positive) is unaffected by Wort./Lat.B treatment and comparable with untreated vesicles (No Wort./Lat.B). Scale bars, 10 μm .

(F) Representative currents from Wort./Lat.B-enlarged EE isolated from non-transfected (NT) HEK293 cells or from HEK293 cells expressing TRPML3-YFP, elicited by applying 10 μM ML-SA1.

(G) Representative currents from Wort./Lat.B-enlarged EE isolated from non-transfected (NT) HEK293 cells or from HEK293 cells expressing TRPML3-YFP, elicited by applying 1 μM PI(3,5)P₂ or 10 μM PI3P, 10 μM phosphatidylserine, 10 μM PI(4,5)P₂, or 10 μM PI(3,4)P₂.

(H) Statistical summary of data as shown in (G). Shown are average current densities at –100 mV (mean \pm SEM).

(I) Representative currents from Wort./Lat.B-enlarged EE isolated from HEK293 cells expressing TRPML3-YFP, elicited by applying 10 μM PI3P, 10 μM phosphatidylserine, 10 μM PI(4,5)P₂, or 10 μM PI(3,4)P₂ in combination with 1 μM PI(3,5)P₂.

(J) Statistical summary of data as shown in (I). Shown are average current densities at –100 mV (mean \pm SEM).

In all experiments, luminal pH was set to 6.7 and intracellular pH was set to 7.2 to mimic EE conditions. Luminal solution contained high potassium to detect maximal TRPML3 currents. Voltage ramps of 500 ms from –100 to +100 mV were applied every 5 s. In all statistical analyses, mean values of *n* independent experiments are shown as indicated. ****p* < 0.001, Student's *t* test, unpaired.

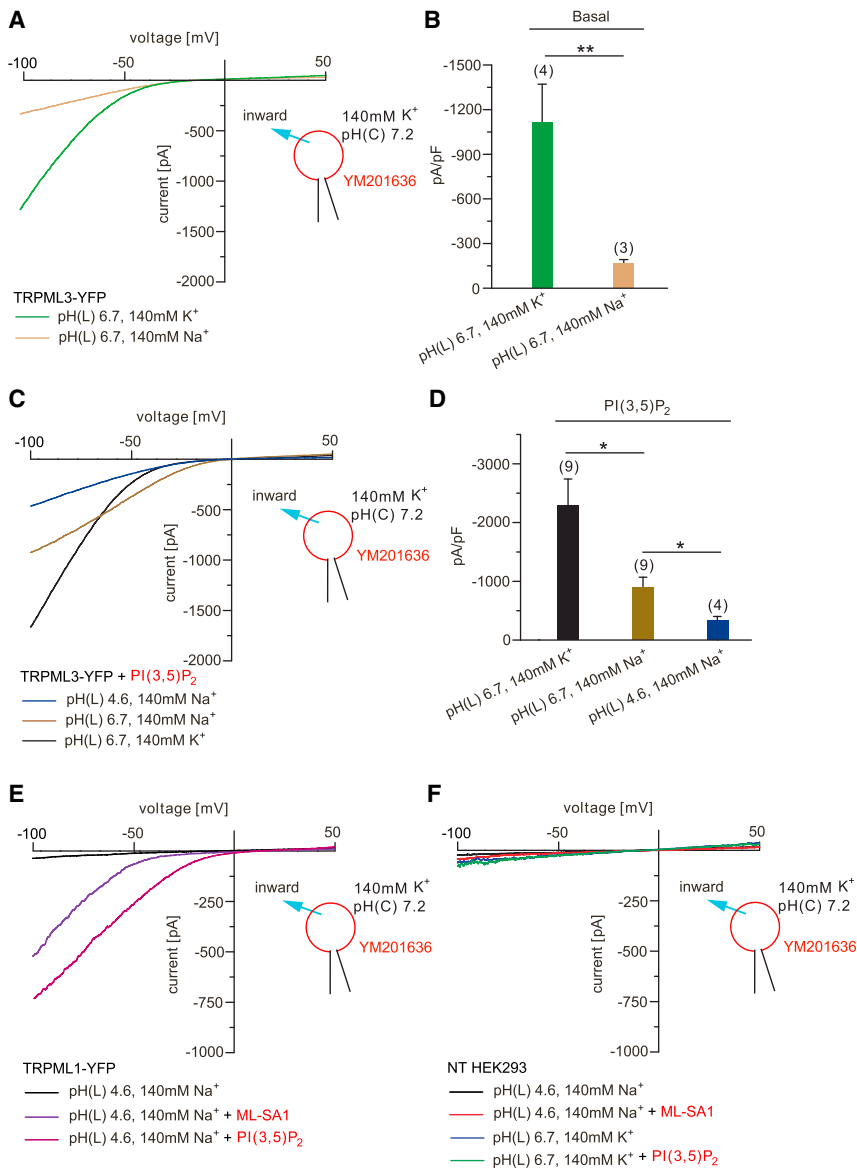


Figure 2. TRPML1 and TRPML3 Currents in YM201636-Enlarged LE/LY

(A) Representative basal currents from YM201636-enlarged LE/LY isolated from HEK293 cells expressing TRPML3-YFP. High luminal sodium decreased the average basal TRPML3 activity.

(B) Statistical summary of data as shown in (A). Shown are average current densities at -100 mV (mean \pm SEM).

(C) Representative TRPML3 currents from YM201636-enlarged LE/LY in the presence of PI(3,5)P2 ($1 \mu\text{M}$). High luminal sodium as well as low luminal pH decreased TRPML3 channel activity.

(D) Statistical summary of data as shown in (C). Shown are average current densities at -100 mV (mean \pm SEM).

(E) Representative ML-SA1 elicited currents from YM201636-enlarged LE/LY isolated from HEK293 cells expressing TRPML1-YFP.

(F) Representative ML-SA1 elicited currents from YM201636-enlarged LE/LY isolated from non-transfected (NT) HEK293 cells.

In all statistical analyses, the mean values of n independent experiments are shown as indicated. ** $p < 0.01$, * $p < 0.05$, Student's t test, unpaired.

sodium. A decrease in pH from 6.7 to 4.6 further reduced channel activity (Figures 2C and 2D). These findings are in agreement with previously described features of overexpressed TRPML3 measured using the whole-cell patch-clamp technique (Kim et al., 2008; Grimm et al., 2010, 2012b). In YM201636-enlarged LE/LY isolated from NT HEK293 or HEK293 cells overexpressing TRPML1, no basal currents were detectable (Figures 2E and 2F). ML-SA1 elicited currents in YM201636-enlarged vesicles overexpressing TRPML1 but not in YM201636-enlarged vesicles isolated from NT HEK293 cells (Figures 2E and 2F).

In summary, these data directly demonstrate the functional presence of TRPML3 in both EE and LE/LY, thus corroborating previously obtained data from immunofluorescence studies.

TRPML Currents in EE and LE/LY Isolated from Peritoneal Macrophages

We focused on macrophages to detect and characterize endogenous TRPML channel currents in intracellular organelles with this approach. We started with peritoneal macrophages (PM Φ) isolated from wild-type (WT), *Trpml1*^{-/-}, and *Trpml3*^{-/-} mice (Figure 3). RT-qPCR analyses revealed the presence of TRPML1 but the absence or very low level expression of TRPML2 and TRPML3 in PM Φ (Figure 3A). Like in HEK293 cells, Wort./Lat.B-enlarged vesicles were negative for LAMP1 but positive for EEA1 in PM Φ (Figure S2A), and YM201636-enlarged vesicles were LAMP1 positive but EEA1 or Rab11 negative (Figures S2B and S2C). The TRPML channel agonists ML-SA1 and PI(3,5)P₂

LAMP1/TRPML1-positive vesicles but did not enlarge Rab5- or Rab11-positive vesicles, confirming a dominant effect of YM201636 on LE/LY (Figure S3C). Likewise, TRPML3-expressing vesicles positive for LAMP1 were enlarged by YM201636 (Figure S3D). TRPML3-positive YM201636-enlarged vesicles were consistently negative for Rab5 (Figure S3D). In contrast to Wort./Lat.B-enlarged TRPML3-expressing vesicles, large basal currents were detectable in YM201636-enlarged TRPML3-expressing vesicles, possibly due to the presence of higher levels of PI(3,5)P₂ in LE/LY compared with EE and/or due to a higher expression level in LE/LY (Figures 2A and 2B). This basal activity of TRPML3 in LE/LY was strongly reduced when the luminal fluid contained high sodium (140 mM) instead of high potassium (140 mM) (Figures 2A and 2B). Basal activity was further enhanced by PI(3,5)P₂ (Figures 2C and 2D). Like basal currents, PI(3,5)P₂-enhanced currents were strongly reduced by replacing high luminal potassium with high luminal

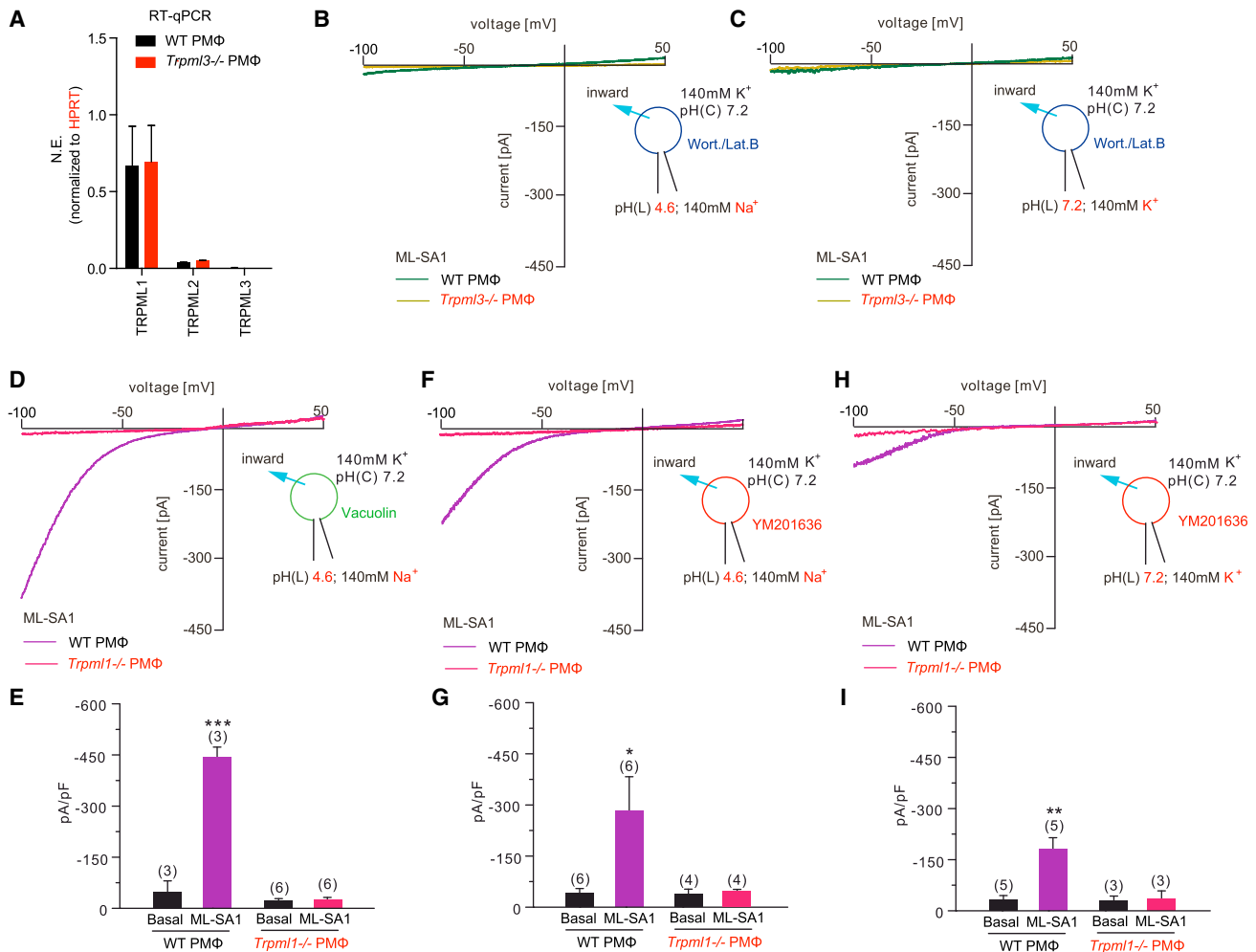


Figure 3. Functional Expression of Endogenous TRPML Channels in Peritoneal Macrophage Organelles

(A) RT-qPCR results for TRPML1, TRPML2, and TRPML3 in PMΦ normalized to HPRT (N.E., normalized expression). (B and C) Representative currents from Wort./Lat.B-enlarged EE isolated from PMΦ (WT and *Trpml3*^{-/-}), elicited by an application of 10 μM ML-SA1 under different pH and cationic conditions (conditions were set to evoke either maximal TRPML1 current activity [low luminal pH, high sodium, B] or maximal TRPML3 current activity [neutral pH, low sodium/high potassium, C]). (D) Representative currents from vacuolin-enlarged vesicles isolated from mouse (WT or *Trpml1*^{-/-}) primary peritoneal macrophages (PMΦ), elicited by an application of 10 μM ML-SA1. (E) Statistical summary of data as shown in (D). Shown are average current densities at -100 mV (mean ± SEM). (F) Representative currents from YM201636-enlarged LE/LY isolated from mouse (WT or *Trpml1*^{-/-}) primary peritoneal macrophages (PMΦ), elicited by an application of 10 μM ML-SA1. (G) Statistical summary of data as shown in (F). Shown are average current densities at -100 mV (mean ± SEM). (H) Representative currents from YM201636-enlarged LE/LY isolated from mouse (WT or *Trpml1*^{-/-}) primary peritoneal macrophages (PMΦ), elicited by an application of 10 μM ML-SA1 under pH 7.2 and high luminal potassium conditions. (I) Statistical summary of data as shown in (H). Shown are average current densities at -100 mV (mean ± SEM). In all statistical analyses, mean values of n independent experiments are shown as indicated. ***p < 0.001, **p < 0.01, *p < 0.05, Student's t test, unpaired.

were applied to elicit currents in Wort./Lat.B, YM201636, as well as vacuolin-enlarged vesicles. While neither TRPML1- nor TRPML3-like currents were detectable in Wort./Lat.B-enlarged vesicles (Figures 3B and 3C), TRPML1-like currents could be detected in vacuolin-enlarged PMΦ vesicles (Figures 3D and 3E) as reported previously (Samie et al., 2013). Likewise, TRPML1-like currents were detectable in YM201636-enlarged vesicles (Figures 3F and 3G). In WT, PMΦ currents of comparable size were measured in the vacuolin- as well as the

YM201636-enlarged vesicle groups when stimulated with ML-SA1 under pH 4.6 and high luminal sodium conditions (Figures 3D–3G). Both vacuolin- and YM201636-enlarged vesicles isolated from *Trpml1*^{-/-} PMΦ showed no more TRPML-like current activity (Figures 3D–3G). TRPML3-like channel activity was not detectable in any vesicle population isolated from PMΦ. Even replacing high luminal sodium with potassium and measuring at neutral pH (7.2), conditions that should favor detection of TRPML3 currents, did not reveal significant TRPML3-like

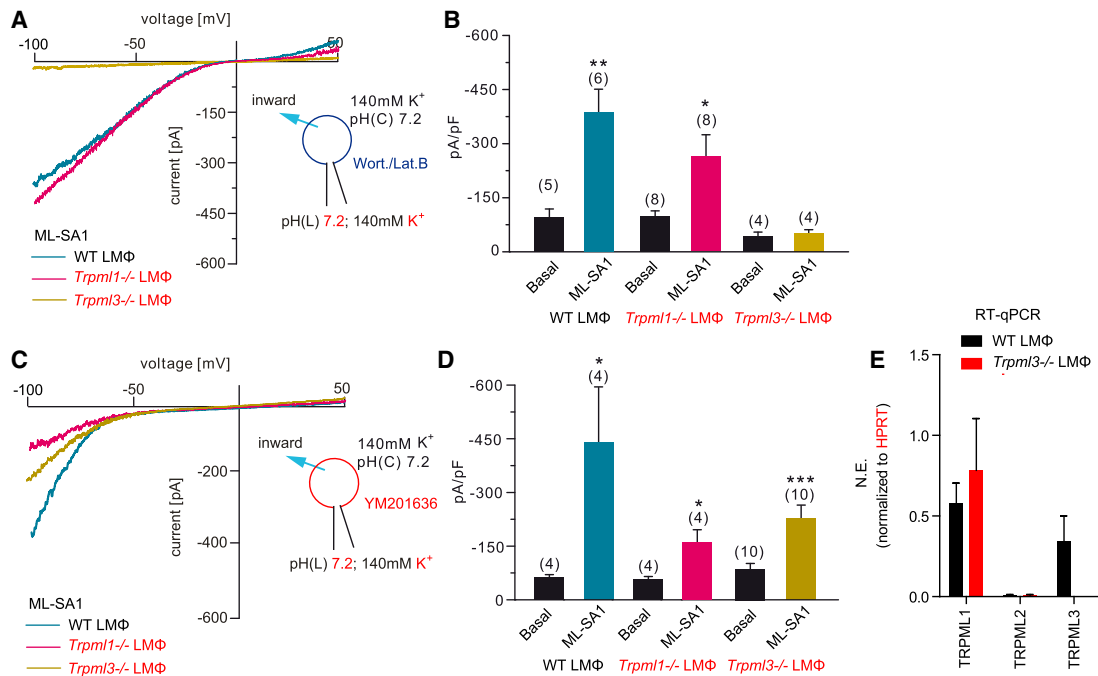


Figure 4. Functional Expression of Endogenous TRPML Channels in CD11b⁺ Lung-Tissue Macrophage Organelles

(A) Representative currents from Wort./Lat.B-enlarged EE isolated from *Trpml1*^{-/-} or *Trpml3*^{-/-} LMΦ, elicited by application of 10 μM ML-SA1.

(B) Statistical summary of data shown in (A). Shown are average current densities at -100 mV (mean ± SEM).

(C) Representative currents from YM201636-enlarged LE/LY isolated from murine (WT, *Trpml1*^{-/-} or *Trpml3*^{-/-}) CD11b⁺ primary lung-tissue macrophages (LMΦ), elicited by application of 10 μM ML-SA1.

(D) Statistical summary of data shown in (C). Shown are average current densities at -100 mV (mean ± SEM). In all experiments, conditions were set to evoke maximal TRPML3 current activity (neutral pH, low sodium).

(E) Shown are RT-qPCR results for TRPML1, TRPML2, and TRPML3 in LMΦ normalized to HPRT.

In all statistical analyses mean values of n independent experiments are shown as indicated. ***p < 0.001, **p < 0.01, *p < 0.05, Student's t test, unpaired.

channel activity, either in LE/LY or in EE (Figures 3C, 3H, and 3I). The remaining TRPML channel activity in LE/LY detectable under these conditions completely disappeared in *Trpml1*^{-/-} PMΦ (Figures 3H and 3I). These data support previous reports on ML-SA1 effects in WT and *Trpml1*^{-/-} PMΦ (Samie et al., 2013; Wang et al., 2015) and demonstrate the absence of TRPML-like currents other than TRPML1 from PMΦ LE/LY as well as the complete absence of TRPML-like currents from PMΦ EE.

TRPML Currents in EE and LE/LY Isolated from CD11b⁺ Lung-Tissue Macrophages

We next focused on different tissue macrophages and thus were able to identify endogenous TRPML3 expression and channel activity in CD11b⁺ lung-tissue macrophages (LMΦ). In patch-clamp experiments, TRPML3-like currents were detected in both EE and LE/LY isolated from LMΦ (Figures 4A–4D). In EE isolated from *Trpml3*^{-/-} LMΦ, ML-SA1-induced currents were completely absent (independent of the pH and ionic conditions applied; Figures 4A, 4B, S4A, and S4B), while in EE isolated from *Trpml1*^{-/-} or WT LMΦ, strong TRPML3-like channel activity elicited by applying ML-SA1 was detectable (Figures 4A and 4B). In LE/LY, TRPML3-like currents were also detectable under neutral pH and high luminal potassium conditions (Figures 4C and 4D). In contrast to EE, we found also ML-SA1-induced cur-

rents in LE/LY isolated from *Trpml3*^{-/-} LMΦ (Figures 4C and 4D). Under highly acidic conditions in the lumen and with high luminal sodium (140 mM), ML-SA1-induced currents in LE/LY isolated from *Trpml3*^{-/-} LMΦ were not significantly different from those measured in LE/LY isolated from WT (Figures S4C–S4F). These data suggest the presence of TRPML3 in EE and the presence of both TRPML1 and TRPML3 in LE/LY of LMΦ. This is in accordance with RT-qPCR analyses of LMΦ, confirming the presence of TRPML1 and TRPML3 but not TRPML2 in normal, non-stimulated LMΦ (Figure 4E).

DISCUSSION

Our data demonstrate that the simple and short-term (<20–30 min at 37°C) combined application of two pharmacological tools, Wort. and Lat.B, can be used to specifically enlarge EE (Figure 5A) to a degree suitable for patch-clamp experimentation (>3–4 μm). We further demonstrate here that the PIKfyve inhibitor YM201636 is a suitable pharmacological tool to selectively enlarge LE/LY (Figure 5A), while vacuolin enlarges EE, RE, as well as LE/LY. We have validated our technique by studying the subcellular expression of TRPML channels, in particular TRPML3, in endogenously expressing macrophages isolated from WT and TRPML knockout mice, respectively, as well as in overexpressing HEK293 cells. Our data

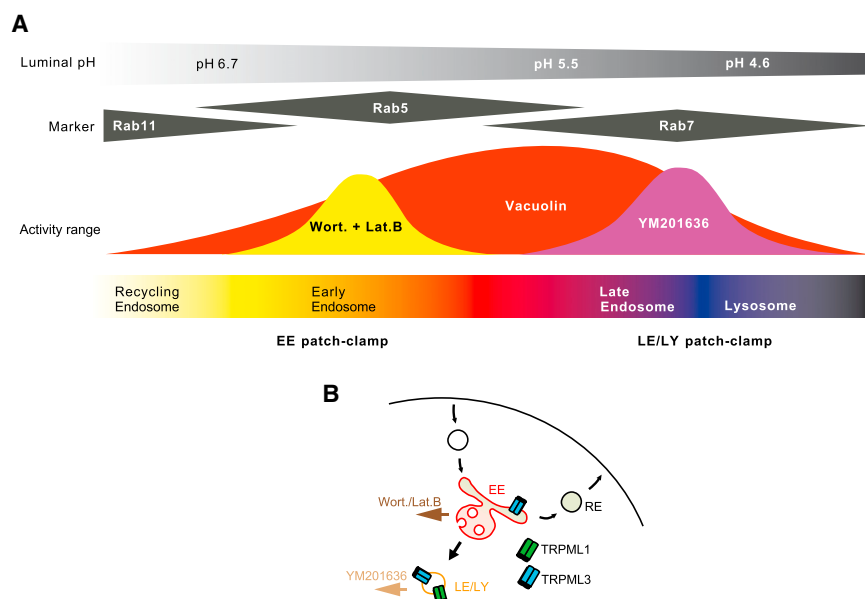


Figure 5. Characteristics of Available Pharmacological Tools for Endolysosomal Patch-Clamp Analysis

(A) Cartoon showing schematically the activity ranges of the different pharmacological tools used for the enlargement of endolysosomal vesicles for patch clamp. The combination of Wort. and Lat.B is highly specific for early endosomes (EE) excluding recycling endosomes (RE). YM201636 is selectively enlarging LE/LY. Vacuolin enlarges EE, RE, as well as LE/LY alike.

(B) Cartoon showing schematically the subcellular location(s) of TRPML1 and TRPML3.

suggest that within the endolysosomal system, TRPML3 shows a less selective expression pattern than TRPML1 (Figure 5B). Expression of TRPML3 in EE as well as LE/LY had been claimed before based on biochemical analyses (Kim et al., 2009; Martina et al., 2009). The organelle-selective patch-clamp experiments presented here essentially confirm these findings by directly proving the functional activity of TRPML3 in both EE and LE/LY, while TRPML1 activity was found only in LE/LY.

The fact that Wort. and Lat.B act, when combined, so specifically and rapidly on the enlargement of EE (up to $>5 \mu\text{m}$) is a novel and surprising finding. Latrunculins are produced by sponges such as the red sea sponge *Latrunculia magnifica* (Kashman et al., 1980). Latrunculins were originally shown to disrupt microfilament organization and to interfere with actin polymerization (Spector et al., 1983). However, it was also found that they disrupt endosomal sorting of transferrin (Sheff et al., 2002), and more recently Greene and Gao (2009) postulated an important role for actin dynamics in the internalization and endosomal sorting/trafficking of clathrin-mediated endocytosis. Wort. is a fungal metabolite that was first isolated from *Penicillium wortmanni*. It is a non-specific inhibitor of phosphoinositide 3-kinases (PI3K) (Wymann et al., 1996; Walker et al., 2000; Kong and Yamori, 2008). In addition to Wort., we tested a range of other available kinase/PI3K inhibitors (Figure S5) such as staurosporine, quercetin, LY294002, ZSTK474, or AS605240 (Walker et al., 2000; Kong and Yamori, 2008). Staurosporine has a range of affinities for different kinases. The plant-derived bioflavonoid quercetin [2-(3,4-dihydroxyphenyl)-3,5,7-trihydroxy-4H-1-benzopyran-4-one] is also a broad-spectrum protein kinase inhibitor. Compared with quercetin, LY294002 inhibits PI3K more selectively than protein kinases. LY294002 was the first synthetic PI3K inhibitor, and its chemical structure is based on the model compound quercetin, which was previously shown to inhibit PI3K as well as various other protein kinases. In addition, both Wort. and LY294002 inhibit mTOR and DNA-PK (Kong and Yamori, 2008). While Wort. also inhibits MLCK, LY294002 in-

hibits CK2. ZSTK474 is a specific pan-PI3K inhibitor and shows no inhibition against mTOR and DNA-PK (Kong and Yamori, 2008). AS-605240 was reported as a PI3K γ -selective inhibitor that showed more than 30-fold selectivity for PI3K γ over PI3K δ and PI3K β , and 7.5-fold selectivity over PI3K α . Furthermore, AS-605240 was shown to be ineffective in inhibiting a panel of protein kinases (Kong and Yamori, 2008). We tested these compounds alone or in combination with Lat.B (in different concentrations and at different time points) and found that neither staurosporine, quercetin, LY294002, ZSTK474, nor AS605240 had an effect on Rab5-positive EE comparable with Wort. (Figure S5). From these data, we conclude that the observed effect is specific to Wort. and unlikely to be mediated by PI3K inhibition. This conclusion is supported by the fact that compounds that are selective PI3K inhibitors had no effect (Figure S5).

We further demonstrate here that TRPML channels are differentially expressed in different populations of macrophages. While TRPML1 (but no other TRPML channel) is found in peritoneal macrophages under basal conditions, TRPML3 is only found in specific tissue macrophages such as CD11b+ lung-tissue macrophages. Increasing evidence suggests that TRPML channels are expressed in different macrophages (Samie et al., 2013; Sun et al., 2015). Macrophages are quite diverse in function and genetic composition (Davies et al., 2013; Gautier et al., 2012). They are found in organs and tissues throughout the human body and contribute to a rather diverse range of physiological processes, such as clearance of cellular debris and effete erythrocytes, iron processing, immune surveillance, response to infection, initiation of inflammatory responses and wound healing (Davies et al., 2013). Samie et al. (2013) have recently shown that TRPML1 regulates red blood cell phagocytosis in macrophages. Sun et al. (2015) reported an upregulation of TRPML2 in activated macrophages such as bone marrow-derived macrophages and alveolar macrophages and claimed predominant expression in RE, and Remis et al. (2014) suggested, based on in situ hybridization experiments, that TRPML3 is expressed in alveolar macrophages. That ion channels such as TRPML channels are differentially expressed in macrophages is further supported by recent evidence provided by Gautier et al. (2012) who found TRPML3 (Mcoln3) expressed in lung but not peritoneal macrophages or microglia based on their analyses of gene expression profiles, essentially corroborating our findings.

The complex regulation of phagocytic and endocytic as well as intracellular trafficking and degradation processes in different types of tissue macrophages will become more comprehensive if the expression of key regulators of these processes, such as distinct ion channels, pumps, and transporters, can be resolved down to the specific organellar level. Given the huge diversity in function and the overall heterogeneity of tissue macrophages, this knowledge may help to better understand how macrophages are able to fulfill their specialized roles in such diverse tissues as spleen, lung, liver, skin, or bone.

Taken together, selective EE patch clamping with simple pharmacological tools is an important step forward for the functional characterization of endogenously expressed endolysosomal ion channels. In the future, more specific tools will hopefully be found to perform similar experiments, e.g., with RE, lysosome-related organelles, or perhaps even synaptic vesicles or secretory organelles. Substantial progress in the selectivity of endolysosomal patch clamping will further facilitate strategies to exploit endolysosomal ion channels as novel therapeutic targets and will help us to understand how the differential expression of key components in the endolysosomal system, such as ion channels and transporters, contributes to the regulation of different trafficking pathways in healthy and diseased cells.

SIGNIFICANCE

We show here that we can selectively patch clamp subpopulations of endolysosomal organelles by using distinct small molecules for specific vesicle enlargement. Thus, we can demonstrate where exactly ion channels such as TRPML channels are functionally expressed within the complex endolysosomal trafficking network. The endolysosomal trafficking and transport machinery relies heavily on the correct function of the specific sets of proteins, in particular ion channels, transporters, and pumps that are expressed in the membranes of the multiple different vesicles that contribute to this machinery. Endolysosomal dysfunction can cause lysosomal storage disorders such as mucopolysaccharidoses, sphingolipidoses, or neuronal ceroid lipofuscinoses, which typically go along with fatal neurodegenerative processes. Dysfunction of the endolysosomal system has also been implicated in the development of many other diseases, ranging from metabolic diseases, retinal and pigmentation disorders to infectious diseases and even cancer. One important prerequisite for a successful investigation of endolysosomal ion channels is the availability of tools and techniques to study them in the organellar membranes where they are endogenously expressed. The widely used compound vacuolin is relatively unspecific in enlarging endolysosomal organelles. Here, we describe here novel tools to more specifically enlarge early versus late endolysosomal vesicles for patch clamping. Wortmannin in combination with latrunculin B specifically enlarges EE, while YM201636 specifically enlarges LE/LY. To validate this approach, we applied these tools to measure TRPML channels, in particular TRPML1 and TRPML3, in EE versus LE/LY and demonstrate that in contrast to TRPML1, TRPML3 is functionally active in both EE and LE/LY in overexpressing HEK293 as well as in endogenously expressing cells.

STAR★METHODS

Detailed methods are provided in the online version of this paper and include the following:

- **KEY RESOURCES TABLE**
- **CONTACT FOR REAGENT AND RESOURCE SHARING**
- **EXPERIMENTAL MODEL AND SUBJECT DETAILS**
 - Mice
 - Cell Lines and Primary Cell Culture
- **METHOD DETAILS**
 - Transfection and Compound Treatment of Cells
 - Confocal Imaging and Antibody Staining
 - Whole-EE and Whole-LE/LY Manual Patch-Clamp Experiments
 - RT-qPCR
- **QUANTIFICATION AND STATISTICAL ANALYSIS**

SUPPLEMENTAL INFORMATION

Supplemental Information includes five figures and two movies and can be found with this article online at <http://dx.doi.org/10.1016/j.chembiol.2017.05.025>.

AUTHOR CONTRIBUTIONS

C.G. designed the study, collected and analyzed data, and wrote the manuscript. C.-C.C. designed and performed all endolysosomal patch-clamp experiments. E.B., Y.-K.C., Y.G., and L.B. designed, collected, and/or analyzed data. S.S., S.H., C.W.-S., and M.B. edited the manuscript. S.S. and Y.G. generated and provided *Trpm1*^{-/-} mice. All the authors discussed the results and commented on the manuscript.

ACKNOWLEDGMENTS

We thank Berit Noack for technical support. DsRed-rab11 WT was a gift from Richard Pagano (Addgene plasmid no. 12679). This work was supported, in part, by funding from the German Research Foundation (SFB/TRR152 TP04 to C.G., TP06 to C.W.-S., and TP12 to M.B.).

Received: January 25, 2017

Revised: March 30, 2017

Accepted: May 26, 2017

Published: July 20, 2017

REFERENCES

- Bae, M., Patel, N., Xu, H., Lee, M., Tominaga-Yamanaka, K., Nath, A., Geiger, J., Gorospe, M., Mattson, M.P., and Haughey, N.J. (2014). Activation of TRPML1 clears intraneuronal A β in preclinical models of HIV infection. *J. Neurosci.* *34*, 11485–11503.
- Calcraft, P.J., Ruas, M., Pan, Z., Cheng, X., Arredouani, A., Hao, X., Tang, J., Rietdorf, K., Teboul, L., Chuang, K.T., et al. (2009). NAADP mobilizes calcium from acidic organelles through two-pore channels. *Nature* *459*, 596–600.
- Cang, C., Zhou, Y., Navarro, B., Seo, Y.J., Aranda, K., Shi, L., Battaglia-Hsu, S., Nissim, I., Clapham, D.E., and Ren, D. (2013). mTOR regulates lysosomal ATP-sensitive two-pore Na⁽⁺⁾ channels to adapt to metabolic state. *Cell* *152*, 778–790.
- Cang, C., Bekele, B., and Ren, D. (2014). The voltage-gated sodium channel TPC1 confers endolysosomal excitability. *Nat. Chem. Biol.* *10*, 463–469.
- Cang, C., Aranda, K., Seo, Y.J., Gasnier, B., and Ren, D. (2015). TMEM175 is an organelle K⁽⁺⁾ channel regulating lysosomal function. *Cell* *162*, 1101–1112.
- Choudhury, A., Dominguez, M., Puri, V., Sharma, D.K., Narita, K., Wheatley, C.L., Marks, D.L., and Pagano, R.E. (2002). Rab proteins mediate Golgi

- transport of caveola-internalized glycosphingolipids and correct lipid trafficking in Niemann-Pick C cells. *J. Clin. Invest.* **109**, 1541–1550.
- Chen, C.C., Keller, M., Hess, M., Schiffmann, R., Urban, N., Wolfgang, A., Schaefer, M., Bracher, F., Biel, M., and Wahl-Schott, C. (2014). A small molecule restores function to TRPML1 mutant isoforms responsible for mucopolidosis type IV. *Nat. Commun.* **5**, 4681.
- Cheng, X., Shen, D., Samie, M., and Xu, H. (2010). Mucolipins: intracellular TRPML1-3 channels. *FEBS Lett.* **584**, 2013–2021.
- Cerny, J., Feng, Y., Yu, A., Miyake, K., Borghonovo, B., Klumperman, J., Meldolesi, J., McNeil, P.L., and Kirchhausen, T. (2004). The small chemical vacuolin-1 inhibits Ca(2+)-dependent lysosomal exocytosis but not cell resealing. *EMBO Rep.* **5**, 883–888.
- Davies, L.C., Jenkins, S.J., Allen, J.E., and Taylor, P.R. (2013). Tissue-resident macrophages. *Nat. Immunol.* **14**, 986–995.
- De Leo, M.G., Staianom, L., Vicinanza, M., Luciani, A., Carissimo, A., Mutarelli, M., Di Campli, A., Polishchuk, E., Di Tullio, G., Morra, V., et al. (2016). Autophagosome-lysosome fusion triggers a lysosomal response mediated by TLR9 and controlled by OCRL. *Nat. Cell Biol.* **18**, 839–850.
- Dong, X.P., Cheng, X., Mills, E., Dellling, M., Wang, F., Kurz, T., and Xu, H. (2008). The type IV mucopolidosis-associated protein TRPML1 is an endolysosomal iron release channel. *Nature* **455**, 992–996.
- Favia, A., Pafumi, I., Desideri, M., Padula, F., Montesano, C., Passeri, D., Nicoletti, C., Orlandi, A., Del Bufalo, D., Sergi, M., et al. (2016). NAADP-dependent Ca(2+) signaling controls melanoma progression, metastatic dissemination and neoangiogenesis. *Sci. Rep.* **6**, 18925.
- Fraldi, A., Klein, A.D., Medina, D.L., and Settembre, C. (2016). Brain disorders due to lysosomal dysfunction. *Annu. Rev. Neurosci.* **39**, 277–295.
- Gautier, E.L., Shay, T., Miller, J., Greter, M., Jakubzick, C., Ivanov, S., Helft, J., Chow, A., Elpek, K.G., Gordonov, S., et al. (2012). Gene-expression profiles and transcriptional regulatory pathways that underlie the identity and diversity of mouse tissue macrophages. *Nat. Immunol.* **13**, 1118–1128.
- Greene, W., and Gao, S.J. (2009). Actin dynamics regulate multiple endosomal steps during Kaposi's sarcoma-associated herpesvirus entry and trafficking in endothelial cells. *PLoS Pathog.* **5**, e1000512.
- Grimm, C., Jörs, S., Saldanha, S.A., Obukhov, A.G., Pan, B., Oshima, K., Cuajungco, M.P., Chase, P., Hodder, P., and Heller, S. (2010). Small molecule activators of TRPML3. *Chem. Biol.* **17**, 135–148.
- Grimm, C., Hassan, S., Wahl-Schott, C., and Biel, M. (2012a). Role of TRPML and two-pore channels in endolysosomal cation homeostasis. *J. Pharmacol. Exp. Ther.* **342**, 236–244.
- Grimm, C., Jörs, S., Guo, Z., Obukhov, A.G., and Heller, S. (2012b). Constitutive activity of TRPML2 and TRPML3 channels versus activation by low extracellular sodium and small molecules. *J. Biol. Chem.* **287**, 22701–22708.
- Grimm, C., Holdt, L.M., Chen, C.C., Hassan, S., Müller, C., Jörs, S., Cuny, H., Kissing, S., Schröder, B., Butz, E., et al. (2014). High susceptibility to fatty liver disease in two-pore channel 2-deficient mice. *Nat. Commun.* **5**, 4699.
- Grimm, C., Chen, C.C., Wahl-Schott, C., and Biel, M. (2017). Two-pore channels: catalyzers of endolysosomal transport and function. *Front. Pharmacol.* **8**, 45.
- Hockey, L.N., Kilpatrick, B.S., Eden, E.R., Lin-Moshier, Y., Brailoiu, G.C., Brailoiu, E., Futter, C.E., Schapira, A.H., Marchant, J.S., and Patel, S. (2015). Dysregulation of lysosomal morphology by pathogenic LRRK2 is corrected by TPC2 inhibition. *J. Cell Sci.* **128**, 232–238.
- Hruz, T., Wyss, M., Docquier, M., Pfaffli, M.W., Masanetz, S., Borghi, L., Verbrugghe, P., Kalaydjieva, L., Bleuler, S., Laule, O., et al. (2011). RefGenes: identification of reliable and condition specific reference genes for RT-qPCR data normalization. *BMC Genomics* **12**, 156.
- Huang, P., Zou, Y., Zhong, X.Z., Cao, Q., Zhao, K., Zhu, M.X., Murrell-Lagnado, R., and Dong, X.P. (2014). P2X4 forms functional ATP-activated cation channels on lysosomal membranes regulated by luminal pH. *J. Biol. Chem.* **289**, 17658–17667.
- Jentsch, T.J. (2015). Discovery of CLC transport proteins: cloning, structure, function and pathophysiology. *J. Physiol.* **593**, 4091–4109.
- Jentsch, T.J., Maritzen, T., Keating, D.J., Zdebik, A.A., and Thévenod, F. (2010). CIC-3—a granular anion transporter involved in insulin secretion? *Cell Metab.* **12**, 307–308.
- Jörs, S., Grimm, C., Becker, L., and Heller, S. (2010). Genetic inactivation of Trpml3 does not lead to hearing and vestibular impairment in mice. *PLoS One* **5**, e14317.
- Jones, A.T., Mills, I.G., Scheidig, A.J., Alexandrov, K., and Clague, M.J. (1998). Inhibition of endosome fusion by wortmannin persists in the presence of activated Rab5. *Mol. Biol. Cell* **9**, 323–332.
- Kashman, Y., Groweiss, A., and Shmueli, U. (1980). Latrunculin, a new 2-thiazolidinone macrolide from the marine sponge *Latrunculia magnifica*. *Tetrahedron Lett.* **21**, 3629–3632.
- Kilpatrick, B.S., Magalhaes, J., Beavan, M.S., McNeill, A., Gegg, M.E., Cleeter, M.W., Bloor-Young, D., Churchill, G.C., Duchon, M.R., Schapira, A.H., and Patel, S. (2016). Endoplasmic reticulum and lysosomal Ca²⁺ stores are remodelled in GBA1-linked Parkinson disease patient fibroblasts. *Cell Calcium* **59**, 12–20.
- Kim, H.J., Li, Q., Tjon-Kon-Sang, S., So, I., Kiselyov, K., Soyombo, A.A., and Muallem, S. (2008). A novel mode of TRPML3 regulation by extracytosolic pH absent in the varitint-waddler phenotype. *EMBO J.* **27**, 1197–1205.
- Kim, H.J., Soyombo, A.A., Tjon-Kon-Sang, S., So, I., and Muallem, S. (2009). The Ca(2+) channel TRPML3 regulates membrane trafficking and autophagy. *Traffic* **10**, 1157–1167.
- Kondratskyi, A., Yassine, M., Kondratska, K., Skryma, R., Slomianny, C., and Prevarskaya, N. (2013). Calcium-permeable ion channels in control of autophagy and cancer. *Front. Physiol.* **4**, 272.
- Kong, D., and Yamori, T. (2008). Phosphatidylinositol 3-kinase inhibitors: promising drug candidates for cancer therapy. *Cancer Sci.* **9**, 1734–1740.
- Li, G., D'Souza-Schorey, C., Barbieri, M.A., Roberts, R.L., Klippel, A., Williams, L.T., and Stahl, P.D. (1995). Evidence for phosphatidylinositol 3-kinase as a regulator of endocytosis via activation of Rab5. *Proc. Natl. Acad. Sci. USA* **92**, 10207–10211.
- Lu, Y., Dong, S., Hao, B., Li, C., Zhu, K., Guo, W., Wang, Q., Cheung, K.H., Wong, C.W., Wu, W.T., Markus, H., et al. (2014). Vacuolin-1 potently and reversibly inhibits autophagosome-lysosome fusion by activating RAB5A. *Autophagy* **10**, 1895–1905.
- Martina, J.A., Lelouvier, B., and Puertollano, R. (2009). The calcium channel mucolipin-3 is a novel regulator of trafficking along the endosomal pathway. *Traffic* **10**, 1143–1156.
- Medina, D.L., and Ballabio, A. (2015). Lysosomal calcium regulates autophagy. *Autophagy* **11**, 970–971.
- Medina, D.L., Di Paola, S., Peluso, I., Armani, A., De Stefani, D., Venditti, R., Montefusco, S., Scotto-Rosato, A., Prezioso, C., Forrester, A., et al. (2015). Lysosomal calcium signalling regulates autophagy through calcineurin and TFEB. *Nat. Cell Biol.* **17**, 288–299.
- Mole, S.E., and Cotman, S.L. (2015). Genetics of the neuronal ceroid lipofuscinoses (Batten disease). *Biochim. Biophys. Acta* **1852**, 2237–2241.
- Nguyen, O.N., Grimm, C., Schneider, L.S., Chao, Y.K., Atzberger, C., Bartel, K., Watermann, A., Ulrich, M., Mayr, D., Wahl-Schott, C., et al. (2017). Two-pore channel function is crucial for the migration of invasive cancer cells. *Cancer Res.* **77**, 1427–1438.
- Patel, S. (2015). Function and dysfunction of two-pore channels. *Sci. Signal.* **8**, re7.
- Remis, N.N., Wiwatpanit, T., Castiglioni, A.J., Flores, E.N., Cantú, J.A., and García-Añoveros, J. (2014). Mucolipin co-deficiency causes accelerated endolysosomal vacuolation of enterocytes and failure-to-thrive from birth to weaning. *PLoS Genet.* **10**, e1004833.
- Ruas, M., Rietdorf, K., Arredouani, A., Davis, L.C., Lloyd-Evans, E., Koegele, H., Funnell, T.M., Morgan, A.J., Ward, J.A., Watanabe, K., et al. (2010). Purified TPC isoforms form NAADP receptors with distinct roles for Ca(2+) signaling and endolysosomal trafficking. *Curr. Biol.* **20**, 703–709.
- Saftig, P., and Sandhoff, K. (2013). Cancer: killing from the inside. *Nature* **502**, 312–313.

- Sakurai, Y., Kolokoltsov, A.A., Chen, C.C., Tidwell, M.W., Bauta, W.E., Klugbauer, N., Grimm, C., Wahl-Schott, C., Biel, M., and Davey, R.A. (2015). Ebola virus. Two-pore channels control Ebola virus host cell entry and are drug targets for disease treatment. *Science* *347*, 995–998.
- Samie, M., Wang, X., Zhang, X., Goschka, A., Li, X., Cheng, X., Gregg, E., Azar, M., Zhuo, Y., Garrity, A.G., et al. (2013). A TRP channel in the lysosome regulates large particle phagocytosis via focal exocytosis. *Dev. Cell* *26*, 511–524.
- Sheff, D.R., Kroschewski, R., and Mellman, I. (2002). Actin dependence of polarized receptor recycling in Madin-Darby canine kidney cell endosomes. *Mol. Biol. Cell* *13*, 262–275.
- Shen, D., Wang, X., Li, X., Zhang, X., Yao, Z., Dibble, S., Dong, X.P., Yu, T., Lieberman, A.P., Showalter, H.D., et al. (2012). Lipid storage disorders block lysosomal trafficking by inhibiting a TRP channel and lysosomal calcium release. *Nat. Commun.* *3*, 731.
- Spector, I., Shochet, N.R., Kashman, Y., and Groweiss, A. (1983). Latrunculins: novel marine toxins that disrupt microfilament organization in cultured cells. *Science* *219*, 493–495.
- Stauber, T., Weinert, S., and Jentsch, T.J. (2012). Cell biology and physiology of CLC chloride channels and transporters. *Compr. Physiol.* *2*, 1701–1744.
- Stenmark, H., Parton, R.G., Steele-Mortimer, O., Lütcke, A., Gruenberg, J., and Zerial, M. (1994). Inhibition of rab5 GTPase activity stimulates membrane fusion in endocytosis. *EMBO J.* *13*, 1287–1296.
- Sun, L., Hua, Y., Vergarajauregui, S., Diab, H.I., and Puertollano, R. (2015). Novel role of TRPML2 in the regulation of the innate immune response. *J. Immunol.* *195*, 4922–4932.
- Venkatachalam, K., Wong, C.O., and Zhu, M.X. (2015). The role of TRPMLs in endolysosomal trafficking and function. *Cell Calcium* *58*, 48–56.
- Venugopal, B., Browning, M.F., Curcio-Morelli, C., Varro, A., Michaud, N., Nanthakumar, N., Walkley, S.U., Pickel, J., and Slaugenhaupt, S.A. (2007). Neurologic, gastric, and ophthalmologic pathologies in a murine model of mucopolipidosis type IV. *Am. J. Hum. Genet.* *81*, 1070–1083.
- Wang, W., Gao, Q., Yang, M., Zhang, X., Yu, L., Lawas, M., Li, X., Bryant-Genevier, M., Southall, N.T., Marugan, J., et al. (2015). Up-regulation of lysosomal TRPML1 channels is essential for lysosomal adaptation to nutrient starvation. *Proc. Natl. Acad. Sci. USA* *112*, 1373–1381.
- Wymann, M.P., Bulgarelli-Leva, G., Zvelebil, M.J., Pirola, L., Vanhaesebroeck, B., Waterfield, M.D., and Panayotou, G. (1996). Wortmannin inactivates phosphoinositide 3-kinase by covalent modification of Lys-802, a residue involved in the phosphate transfer reaction. *Mol. Cell Biol.* *16*, 1722–1733.
- Walker, E.H., Pacold, M.E., Perisic, O., Stephens, L., Hawkins, P.T., Wymann, M.P., and Williams, R.L. (2000). Structural determinants of phosphoinositide 3-kinase inhibition by wortmannin, LY294002, quercetin, myricetin, and staurosporine. *Mol. Cell.* *6*, 909–919.
- Weinert, S., Jabs, S., Supancharit, C., Schweizer, M., Gimber, N., Richter, M., Rademann, J., Stauber, T., Kornak, U., and Jentsch, T.J. (2010). Lysosomal pathology and osteopetrosis upon loss of H⁺-driven lysosomal Cl⁻ accumulation. *Science* *328*, 1401–1403.
- Weinert, S., Jabs, S., Hohensee, S., Chan, W.L., Kornak, U., and Jentsch, T.J. (2014). Transport activity and presence of ClC-7/Ostm1 complex account for different cellular functions. *EMBO Rep.* *15*, 784–791.
- Zhang, L., Sheng, R., and Qin, Z. (2009). The lysosome and neurodegenerative diseases. *Acta Biochim. Biophys. Sin.* *41*, 437–445.
- Zhang, X., Li, X., and Xu, H. (2012). Phosphoinositide isoforms determine compartment-specific ion channel activity. *Proc. Natl. Acad. Sci. USA* *109*, 11384–11389.
- Zhong, X.Z., Sun, X., Cao, Q., Dong, G., Schiffmann, R., and Dong, X.P. (2016). BK channel agonist represents a potential therapeutic approach for lysosomal storage diseases. *Sci. Rep.* *6*, 33684.
- Zhong, X.Z., Zou, Y., Sun, X., Dong, G., Cao, Q., Pandey, A., Rainey, J.K., Zhu, X., and Dong, X.P. (2017). Inhibition of transient receptor potential channel mucolipin-1 (TRPML1) by lysosomal adenosine involved in severe combined immunodeficiency diseases. *J. Biol. Chem.* *292*, 3445–3455.

STAR★METHODS

KEY RESOURCES TABLE

REAGENT or RESOURCE	SOURCE	IDENTIFIER
Antibodies		
Rabbit monoclonal anti-EEA1 (C45B10)	Cell Signaling Technology	Cat#3288S; RRID: AB_2096811
Rat monoclonal anti-lamp1 (1D4B)	Developmental Studies Hybridoma Bank	Cat#1D4B; RRID: AB_528127
Rabbit polyclonal anti-Rab11	Abcam	Cat#ab3612; RRID: AB_10861613
Anti-rat IgG (H+L) (Alexa Fluor 488 conjugate)	Cell Signaling Technology	Cat#4416S; RRID: AB_10693769
Anti-rabbit IgG Cy3-AffiniPure Donkey	Jackson ImmunoResearch Labs	Cat#711-165-152; RRID: AB_2307443
Chemicals, Peptides, and Recombinant Proteins		
Wortmannin	Sigma-Aldrich	W1628; CAS: 19545-26-7
Latrunculin B from <i>Latruncula magnifica</i>	Sigma-Aldrich	L5288; CAS: 76343-94-7
YM201636	Chemdea	Cat#CD0181; CAS: 371942-69-7
AS605240	Sigma-Aldrich	A0233; CAS: 648450-29-7
LY294,002 hydrochloride	Sigma-Aldrich	L9908; CAS: 934389-88-5
ZSTK474	Selleckchem	Cat#S1072; CAS: 475110-96-4
Quercetin	Sigma-Aldrich	Q4951; CAS: 117-39-5
Staurosporin (STS)	Sigma-Aldrich	S5921; CAS: 62996-74-1
MLSA-1	Sigma-Aldrich	SML0627; CAS: 332382-54-4
PI(3,5)P ₂	AG Scientific	P-1123; CAS: 299216-96-6
PI3P	AG Scientific	P-1131; CAS: 214068-76-5
PI(3,4)P ₂	AG Scientific	P-1119; CAS: 188885-38-3
PI(4,5)P ₂	AG Scientific	P-1115; CAS: 204858-53-7
PS	AG Scientific	P7769; CAS: 51446-62-9
Critical Commercial Assays		
Lung Dissociation Kit	Milentyi Biotech	130-095-927
RNeasy Plus Mini Kit	Qiagen	Cat# 74134
RevertAid first strand cDNA synthesis Kit	ThermoScientific	Cat# K1621
CD11b MicroBeads, human and mouse	Milentyi Biotech	130-049-601
Experimental Models: Cell Lines		
Human: HEK 293	DSMZ	ACC 305
Human: HEK 293 stable expressing TRPML3-YFP	Grimm et al., 2010	N/A
Human: HEK 293 stable expressing TRPML1-YFP	Chen et al., 2014	N/A

(Continued on next page)

Continued		
REAGENT or RESOURCE	SOURCE	IDENTIFIER
Experimental Models: Organisms/Strains		
Mouse: TRPML1, Mcoln1 ^{tm1Sasl}	Venugopal et al., 2007	N/A
Mouse: TRPML3 Mcoln3 ^{tm1.1Hels}	Jörs et al., 2010	N/A
Oligonucleotides		
qPCR Primer for TRPML1 (NM_053177); forward: GCCTTGGGCCAATGGATCA reverse: CCCTTGATCAATGTCAAAGGTA	www.pga.mgh.harvard.edu/primerbank	PrimerBank ID: 16716462c2
qPCR Primer for TRPML2 (NM_026656); forward: AATTTGGGGTCACGTCATGC reverse: AGAATCGAGAGACGCCATCG	this paper	N/A
qPCR Primer for TRPML3 (NM_134160); forward: GAGTTACCTGGTGTGGCTGT reverse: TGCTGGTAGTGCTTAATTGTTTCG	this paper	N/A
qPCR Primer for HPRT (NM_013556) forward: GCTCGAGATGTCATGAAGGAGAT reverse: AAAGAACTTATAGCCCCCTTGA	Hruz et al., 2011	N/A
Recombinant DNA		
Plasmid: GFP-Rab7	this paper	N/A
Plasmid: LAMP1-mKate	this paper	N/A
Plasmid: Rab5-mCherry	this paper	N/A
Plasmid: Rab5-mKate	this paper	N/A
Plasmid: DsRed-Rab11	Choudhury et al., 2002	Addgene Plasmid #12679
Plasmid: Rab11-Citrin	this paper	N/A
Plasmid: TRPML1-YFP	Grimm et al., 2010	N/A
Plasmid: TRPML3-YFP	Grimm et al., 2010	N/A
Software and Algorithms		
Origin8	OriginLab	http://www.originlab.com/origin
GraphPad Prism	GraphPad Software Inc.	https://www.graphpad.com/scientific-software/prism/

CONTACT FOR REAGENT AND RESOURCE SHARING

Further information and requests for resources and reagents should be directed to and will be fulfilled by Lead Contact, Christian Grimm (christian.grimm@cup.uni-muenchen.de)

EXPERIMENTAL MODEL AND SUBJECT DETAILS

Mice

Animals were used under approved animal protocols and University of Munich (LMU) Institutional Animal Care Guidelines.

Trpml1^{-/-} KO mice were obtained from Dr. Susan Slaughaupt (Harvard) and were generated as described in Venugopal et al. (2007). For genotyping of *Trpml1*^{-/-} KO mice the following forward and reverse primers were used: 5'-tgaggagagccaagctcatt-3' (sense), 5'-tcactctcctgcctcatct-3' (antisense) and 5'-tggctggacgtaaacctctc-3' (antisense), expected bands 400 bp (WT), 200 bp (KO); cycling conditions: annealing temperature 58°C, 35 cycles.

Trpml3^{-/-} KO mice were generated by deleting exon11 as described previously (Jörs et al., 2010). For genotyping of *Trpml3*^{-/-} KO and WT mice two primer pairs were used: 5'-gaacacactgactacccccaa-3' (sense) and 5'-tacagtttacagatgtgttgag-3' (antisense), expected bands: 309 bp (WT), no band (KO); 5'-gaacacactgactacccccaa-3' (sense) and 5'-agagttcactagaacgaagttcctattcc-3' (antisense), expected bands: no band (WT), 374 bp (KO); cycling conditions: 35 cycles, annealing temperature 65°C for both.

Cell Lines and Primary Cell Culture

All cell culture cells were cultured in a standard humidified 37°C incubator, with 5% CO₂. HEK293 cells were maintained in low glucose DMEM supplemented with 10% FBS, 100 U penicillin/mL and 100 µg streptomycin/mL. HEK293 cells stably expressing TRPML3-YFP (Grimm et al., 2010) were selected using G418 at a final concentration of 0.8 mg/mL.

Primary peritoneal and lung tissue macrophages were isolated from 6 to 10 weeks old TRPML1^{-/-}, TRPML3^{-/-} and wildtype mice of both gender.

For preparation of macrophages, mice were deeply anesthetized with isoflurane and killed by cervical dislocation. For harvesting peritoneal macrophages (PM Φ), the outer skin of the peritoneum was carefully opened and 10 mL phosphate buffer saline (PBS) were injected into the peritoneal cavity. After detaching macrophages by massaging the peritoneum, the cell suspension was collected using a syringe and a 20G needle. Cells were pelleted and subsequently cultured in F12/DMEM supplemented with 20% FBS, 100 U penicillin/mL, and 100 μ g streptomycin/mL. PM Φ were used for experiments within 2-10 days after isolation. Lung macrophages (LM Φ) were isolated from dissociated whole lung tissue by positive magnetic cell sorting (MACS) for CD11b-positive cells using the protocol for “CD11b MicroBeads, mouse” (130-049-601, Miltenyi Biotech) according to manufacturer’s instructions. Single-cell suspensions of the tissues were prepared employing the “Lung Dissociation Kit” (130-095-927; Miltenyi Biotech). Briefly, isolated tissue was rinsed in PBS, cut in 7-10 pieces and incubated in 2.4 mL 1x buffer S containing enzyme A and enzyme D for 45 min at 37 °C. Afterwards, cells were passed through a 100 μ m nylon mesh followed by one more separation through a 30 μ m nylon mesh. Following a centrifugation step, cells were recollected with MicroBeads conjugated to monoclonal rat anti-mouse CD11b antibody (130-049-601, Miltenyi Biotech) and incubated for 15 min at 4 °C. CD11b-positive cells were sorted with MS MiniMACS columns and the eluted fraction was seeded onto Poly-L-Lysine coated cover slips and maintained in F12/DMEM containing 20% FBS, 100 U penicillin/mL, and 100 μ g streptomycin/mL. LM Φ were used for experiments only one day after isolation.

METHOD DETAILS

Transfection and Compound Treatment of Cells

For patch clamp experiments and live cell imaging, cells were plated on 12 mm or 25 mm glass cover slips 24-72 hours before experiments. HEK293 cells were transiently transfected with Turbofect (Fermentas) according to the manufacturer’s protocol and used for experiments 24-48 hours after transfection. The following N- and C-terminally tagged plasmids were used: TRPML1-YFP, TRPML3-YFP, Rab5-mCherry, Rab5-mKate, GFP-Rab7, mKate-Rab7, Citrin-Rab11, DsRed-Rab11 and LAMP1-mKate.

For vesicle enlargement, transfected and untransfected cells were treated with either 1 μ M vacuolin (HEK293 cells: overnight (o/n); M Φ : 1 h), YM201636 (HEK293 cells: 800 nM / 2 h or 400 nM / 12 h; PM Φ : 400nM / 1-2 h; LM Φ : 400 nM / 1-3 h), or a combination of 200 nM wortmannin and 10 nM latrunculin B (HEK293 cells: 10-15 min; PM Φ : 20 min; LM Φ : 1 h) prior to experimentation. Cells were treated with compounds at 37 °C and 5% CO₂. YM201636 was obtained from Chemdea (CD0181), wortmannin and latrunculin B from Sigma-Aldrich (W1628 and L5288). Compounds were washout before patch-clamp experimentation.

For kinase inhibitor study, HEK293 cells were treated as indicated with Staurosporin (S5921), LY294002 (L9908), Quercetin (Q4951), AS605240 (A0233) (all from Sigma-Aldrich) or ZSTK474 (Selckchem).

Confocal Imaging and Antibody Staining

Confocal images were conducted using a Zeiss LSM510 or a Leica SP8 confocal microscope. For live cell imaging, medium was replaced by unsupplemented medium without phenol red. For videos, HEK293 cells were incubated in a climate chamber for temperature and humidity control (Okolabs, Burlingame, CA, USA) during imaging and compound treatment. For immunocytochemistry, peritoneal macrophages were stained using anti-LAMP1 (1D4B; Developmental Studies Hybridoma Bank, 1:250) and anti-EEA1 (C45B10) (3288; Cell Signaling Technology, 1:100) or anti-Rab11 (abcam ab3612, 1:200) antibodies, respectively. Briefly, cells were grown on coverslips and treated as indicated. Cells were then fixed with ice-cold methanol for 10 min at -20°C and permeabilised with 0.2% saponin. Alexa488 (Cell Signaling Technology) or Cy3 (Jackson ImmunoResearch Lab) were used as secondary antibodies for detection.

Whole-EE and Whole-LE/LY Manual Patch-Clamp Experiments

Mean capacitance value for EE of HEK293 stable cell lines was 1.0 ± 0.1 pF (n = 54). For EE of primary cells it was 0.4 ± 0.1 pF (n = 26). For LE/LY of HEK293 stable cell lines it was 1.1 ± 0.3 pF (n = 42). For LE/LY of primary cells it was 0.6 ± 0.1 pF (n = 56). Currents were recorded using an EPC-10 patch-clamp amplifier (HEKA, Lambrecht, Germany) and PatchMaster acquisition software (HEKA). Data were digitized at 40 kHz and filtered at 2.8 kHz. Fast and slow capacitive transients were cancelled by the compensation circuit of the EPC-10 amplifier. All recordings were obtained at room temperature and were analyzed using PatchMaster acquisition software (HEKA) and OriginPro 6.1 (OriginLab). Recording glass pipettes were polished and had a resistance of 4-8 M Ω . For all experiments, salt-agar bridges were used to connect the reference Ag-AgCl wire to the bath solution to minimize voltage offsets. Liquid junction potential was corrected. For the application of the lipids (A.G. Scientific) or small molecule agonists (ML-SA1), cytoplasmic solution was completely exchanged by cytoplasmic solution containing agonist. The current amplitudes at -100 mV were extracted from individual ramp current recordings. Unless otherwise stated, cytoplasmic solution contained 140 mM K-MSA, 5 mM KOH, 4 mM NaCl, 0.39 mM CaCl₂, 1 mM EGTA and 10 mM HEPES (pH was adjusted with KOH to 7.2). Luminal solution contained 140 mM Na-MSA, 5 mM K-MSA, 2 mM Ca-MSA 2 mM, 1 mM CaCl₂, 10 mM HEPES and 10 mM MES (pH was adjusted with methanesulfonic acid to 4.6). In all experiments, 500-ms voltage ramps from -100 to +100 mV were applied every 5 s. All statistical analysis was done using Origin8 or GraphPadPrism software.

RT-qPCR

Total RNA was prepared from cultured primary macrophages using RNeasy Plus Mini Kit (Qiagen) according to the manufacturer's protocol. cDNA was synthesized from total RNA with RevertAid First Strand cDNA Synthesis Kit (Thermo Scientific) utilizing both random hexamer primer and oligo(dT)₁₈-primer. qPCR was performed on a StepOne Plus Real-time PCR system (Applied Biosystems) using SYBR Select Master Mix (Applied Biosystems). Reactions were carried out in duplicate or triplicate under conditions according to manufacturer's recommendations. The following forward and reverse primers were used for TRPML1 (NM_053177), TRPML2 (NM_026656), TRPML3 (NM_134160), and HPRT (NM_013556): 5'-gcctgggccaatggatca-3' (sense), 5'-cccttggatcaatgtcaaaggta-3' (antisense) (TRPML1), 5'-aattgggggtcacgtcatgc-3' (sense), 5'-agaatcgagagacgccatcg-3' (antisense) (TRPML2), 5'-gagttacctgggtggctgt-3' (sense), 5'-tgctggtagtgcttaattgttcg-3' (antisense) (TRPML3), and 5'-gctcgagatgtcatgaaggagat-3' (sense), 5'-aaagaacttatagcccccttga-3' (antisense) (HPRT). Primer efficiencies were between 1.9 and 2.1. Non-template controls were included to ensure specificity of the primer pairs. Product specificity and amplicon size were controlled by sequencing and gel analysis of the qPCR products. Relative expression of target gene levels was determined by normalization against HPRT levels. Samples were run in duplicates using 3-5 biological replicates per group.

QUANTIFICATION AND STATISTICAL ANALYSIS

Details of statistical analyses and *n* values are provided in the figure legends. Statistical analyses were carried out using Origin 8 and GraphPad Prism 5. All error bars are depicted as mean ± SEM. Statistical significance was determined via Student's *t*-test, unless stated otherwise. Significance is denoted on figures as outlined in the legends. Statistics were derived from at least three independent experiments.

Two-Pore Channel Function Is Crucial for the Migration of Invasive Cancer Cells

Ong Nam Phuong Nguyen¹, Christian Grimm², Lina S. Schneider¹, Yu-Kai Chao², Carina Atzberger¹, Karin Bartel¹, Anna Watermann¹, Melanie Ulrich¹, Doris Mayr³, Christian Wahl-Schott², Martin Biel², and Angelika M. Vollmar¹

Abstract

Metastatic invasion is the major cause of cancer-related deaths. In this study, we introduce two-pore channels (TPC), a recently described class of NAADP- and PI(3,5)P₂-sensitive Ca²⁺-permeable cation channels in the endolysosomal system of cells, as candidate targets for the treatment of invasive cancers. Inhibition of the channel abrogated migration of metastatic cancer cells *in vitro*. Silencing or pharmacologic inhibition of the two-pore channel TPC2 reduced lung metas-

tasis of mammary mouse cancer cells. Disrupting TPC function halted trafficking of β 1-integrin, leading to its accumulation in EEA1-positive early endosomes. As a consequence, invasive cancer cells were no longer able to form leading edges, which are required for adequate migration. Our findings link TPC to cancer cell migration and provide a preclinical proof of concept for their candidacy as targets to treat metastatic cancers. *Cancer Res*; 77(6): 1427–38. ©2017 AACR.

Introduction

Metastasis is the major cause of cancer-related deaths. The formation of secondary, metastatic growth includes proliferation and extensive vascularization of the primary tumor, detachment and invasion of tumor cells, circulation of single tumor cells, arrest in distant sites, extravasation, and, finally, proliferation within the organ (1). Extensive studies in the last decades contributed to a better understanding of these processes. However, still about 90% of cancer-associated mortality is due to metastasis. Therefore, new strategies to prevent metastasis are urgently needed (1, 2).

To successfully colonize secondary sites, cancer cells gained the ability to migrate (2, 3). A crucial step in migration is the binding to ligands of the extracellular matrix (ECM), which is mediated by integrins. These cell surface receptors display a diverse family of glycoproteins consisting of 18 α -subunits and 8 β -subunits. Besides mediating cell attachment to the ECM, integrins are linked to the cytoskeleton through the formation of

clusters with actin-associated proteins such as vinculin. Furthermore, ligation of integrins induces a network of intracellular signaling pathways including the activation of focal adhesion kinase (FAK) and Src, altogether regulating cell migration (3).

To fulfill the function as migration-promoting receptors, integrins have to be trafficked to the front of the cell for assembly of focal adhesions. These adhesions act as traction sites for the movement and are afterwards disassembled at the rear of the cell for detachment. Hence, integrins need to be dynamically turned over, which is achieved by endocytic trafficking (4, 5). After endocytosis, integrins are carried to early endosomes where sorting into recycling and degradative pathways takes place. Under normal conditions, the larger portion recycles back to the plasma membrane. Disturbing this process can alter the composition of focal adhesions, thereby influencing cell migration (4).

There is increasing evidence that two-pore channels (TPC) are key players in the regulation of endocytic transport (6–8). It has been postulated that inhibiting these channels alters Ca²⁺ signaling during endolysosomal fusion events, resulting in defects in vesicle trafficking (9–11). TPCs are assigned to the superfamily of voltage-gated ion channels (8). There are two different TPC subtypes present in primates, TPC1 and TPC2. TPC1 is primarily expressed on endosomal membranes while TPC2 dominates on lysosomal membranes (8, 10, 12). Activation of these channels is presumably triggered by the second messenger nicotinic acid adenine dinucleotide phosphate (NAADP) and by phosphatidylinositol 3,5-bisphosphate [PI(3,5)P₂; refs. 8, 13–15]. Distinct experiments suggested TPCs as Ca²⁺-permeable channels indicating that TPCs might be involved in Ca²⁺ release from endo- and lysosomal stores (7–9, 13, 16).

This work unveils that TPCs play a crucial role in the formation of metastasis as silencing TPC1 and TPC2 reduced the adhesion and migration of invasive tumor cells *in vitro*. Similar results were achieved with Ned-19, an antagonist of NAADP (17), and tetrandrine, recently shown to inhibit TPC1 and TPC2 (18). Remarkably, both silencing of TPC2 with siRNA or by pharmacologic inhibition showed efficacy in a metastatic *in vivo* model.

¹Department of Pharmacy, Pharmaceutical Biology, Ludwig-Maximilians-University Munich, Munich, Germany. ²Department of Pharmacy, Center for Drug Research and Center for Integrated Protein Science Munich (CIPSM), Ludwig-Maximilians-University Munich, Munich, Germany. ³Pathological Institute, Ludwig-Maximilians-University Munich, Munich, Germany.

Note: Supplementary data for this article are available at Cancer Research Online (<http://cancerres.aacrjournals.org/>).

O.N.P. Nguyen and C. Grimm contributed equally to this article.

Corresponding Authors: Angelika M. Vollmar, Department of Pharmacy, Pharmaceutical Biology, Ludwig-Maximilians-University Munich, Butenandtstrasse 5-13, Munich 81377, Germany. Phone: 4989-2180-77172; Fax: 4989-2180-77170; E-mail: angelika.vollmar@cup.uni-muenchen.de; and Martin Biel, Department of Pharmacy, Center for Drug Research and Center for Integrated Protein Science Munich (CIPSM), Ludwig-Maximilians-University Munich, Butenandtstrasse 5-13, Munich 81377, Germany. Phone: 4989-2180-77328; E-mail: martin.biel@cup.uni-muenchen.de

doi: 10.1158/0008-5472.CAN-16-0852

©2017 American Association for Cancer Research.

Inhibition of TPCs led to the accumulation of integrins in endocytic vesicles and impaired formation of leading edges, indicating that TPCs are significantly involved in integrin recycling.

Materials and Methods

Cell lines and reagents

The cancer cell line T24 was obtained from Dr. B. Mayer (Surgical Clinic, LMU, Munich, Germany) and recently authenticated by the DSMZ. HUH7 were purchased from Japanese Collection of Research Bioresources and 4T1-Luc (4T1) from PerkinElmer. Method of cell authentication was short tandem repeat (STR) DNA typing by using 8 different and highly polymorphic STR loci. T24 cells were grown in McCoy, HUH7 cells in DMEM high glucose, and 4T1 cells in RPMI1640 medium. All media were supplemented with 10% FCS. *trans*-Ned-19 (Ned-19) was purchased from Tocris Bioscience, and tetrandrine from Santa Cruz Biotechnology.

qRT-PCR

qRT-PCR of TPC1 and TPC2 was performed as described previously (19). Following primers were used: TPC2 forward (fw): 5'-GTA CCC CTC TTG TGT GGA CG-3'; reverse (rv), 5'-GGC CCT GAC AGT GAC AAC TT-3'; TPC1 fw, 5'-GGA GCC CTT CTA TTT CAT CGT-3'; rv, 5'-CGG TAG CGC TCC TTC AAC T-3'; actin was used as housekeeping gene. The following primers were used: fw, 5'-CCA ACC GCG AGA AGA TGA-3'; rv, 5'-CCA GAG GCG TAC AGG GAT AG-3'.

Whole-endolysosomal patch clamp

Whole-endolysosomal patch-clamp recordings were performed by modified conventional patch-clamp. T24 cells were treated with 1 μ mol/L vacuolin-1 for at least 4 hours. Currents were recorded using an EPC-10 patch-clamp amplifier and PatchMaster acquisition software (HEKA). Data were digitized at 40 kHz and filtered at 2.8 kHz. Recording pipettes had a resistance of 8–10 M Ω . Liquid junction potential was corrected. Pipette solution (corresponding to luminal endolysosomal solution) contained 140 mmol/L sodium methanesulfonate, 5 mmol/L potassium methanesulfonate (KMSA), 2 mmol/L calcium methanesulfonate, 1 mmol/L CaCl₂, 10 mmol/L HEPES and 10 mmol/L MES, pH 4.6. Bath solution (corresponding to cytosolic solution) contained 140 mmol/L KMSA, 5 mmol/L KOH, 4 mmol/L NaCl, 0.39 mmol/L CaCl₂, 1 mmol/L EGTA, and 10 mmol/L HEPES, pH 7.2. PI(3,5)P₂ was used in a water-soluble diC8 form (A.G. Scientific). All compounds including PI(3,5)P₂ were prepared as high-concentration stock solutions, added to the bath solutions to match the final concentration indicated. pH of bath solution and pipette solution were adjusted with KOH and MSA, respectively. All recordings were obtained at 21°C–23°C and were analyzed using PatchMaster and Origin 6.1 (OriginLab) software.

Tissue staining

Two-micron thick tissue sections were used. Antigen retrieval was done with Target Retrieval Solution from Dako and the sections were heated for 30 minutes in the microwave. Blocking of endogenous peroxidase was done in 7.5% hydrogen peroxide for 10 minutes. Anti-TPC2 (atlas antibodies, diluted 1:60) was applied as primary antibody for 1 hour at room temperature. An unspecific control antibody (rabbit IgG isotype, diluted 1:60) was used under the same conditions as for anti-TPC2 to detect any background staining of the primary antibody. For antibody detec-

tion, ImmPress reagent anti-rabbit Ig was utilized according to the manual and DAB+ for 3 minutes at room temperature was used as a chromogen. Slides were counterstained with hematoxylin for 20 seconds and finally embedded in mounting medium and covered with glass coverslips.

Cell transfection

A total of 2×10^5 T24 cells were transfected using the ScreenFect A Transfection Kit (Genaxxon bioscience). TPC1 and TPC2 were silenced using siRNA from Santa Cruz Biotechnology. Nontargeting siRNA was used as a control.

Boyden chamber assay

A total of 1×10^5 treated or silenced cells were placed on top of the Transwell chamber (Corning) in media without FCS. Twenty-four-well plate was filled with medium with 10% FCS. Transwell chambers were placed in it and incubated for 16 hours. Migrated cells were fixed and stained with crystal violet/methanol. The top of the Transwell chamber was cleaned and pictures were taken. Migrated cells were counted with ImageJ (NIH, Bethesda, MD).

Endolysosomal preparation

Isolation of endolysosomal proteins was conducted as described before (20). In short, three 6-well plates of T24 cells transfected with siTPC1, siTPC2, or siNT were washed with PBS. Five-hundred microliters of homogenization buffer was added and the cells were detached with a cell scraper. Homogenization was performed with a Potter S Homogenizer (B. Braun) at 12 \times 900 rpm. Homogenized cells were collected into a microcentrifuge tube and were centrifuged at 14,000 \times g, 4°C for 15 minutes. Supernatant was collected into a 1.5-mL ultracentrifuge tube (Beckman), one volume of 16 mmol/L CaCl₂ was added and the preparation was mixed by shaking at 4°C for 5 minutes. Ultracentrifugation was performed at 18,000 \times g, 4°C for 15 minutes. Supernatant was removed and the formed pellet was resuspended in 250 μ L wash buffer. After ultracentrifugation at 25,000 \times g, 4°C for 15 minutes, supernatant was removed and pellet was resuspended in 50 μ L wash buffer. Protein concentration was determined and 20 μ g of endolysosomal preparation was used for Western blot analysis.

Adhesion assay

A total of 5×10^4 silenced or stimulated T24 cells were seeded onto μ -slides 8-well ibidiTreat and allowed to attach for 1 hour. Subsequently, cells were fixed with 4% paraformaldehyde (PFA) and stained with rhodamine-phalloidin (Molecular Probes) and Hoechst 33342 (Hoechst; Sigma) for 30 minutes. Cells were mounted with FluorSave Reagent mounting medium (Merck) and analyzed with a Zeiss LSM 510 Meta confocal microscope (Jena).

Chemotaxis

A total of 6×10^4 T24 cells were seeded on μ -Slide Chemotaxis^{3D} (IBIDI) and allowed to attach for 3 hours. Chemotaxis experiment (20 hours) was performed as described previously (21). Cell tracking was performed with ImageJ plugin Manual tracking (Fabrice Cordelières, Institut Curie, Orsay, France). Thirty cells were tracked per experiment. Data analysis was done with Chemotaxis and Migration Tool (IBIDI). Rayleigh test was used to

describe uniformity of distribution of cell endpoints. With $P > 0.05$, uniformity is rejected (22).

Measurement of cell death

Flow cytometry analysis was performed as described previously (19). Specific cell death was calculated as follows: specific cell death = $[(x - Co) / (100 - Co)] \times 100$

Membrane staining

A total of 2×10^4 HUH7 cells were seeded onto μ -slides 8-well ibidiTreat. For membrane labeling, the PKH 26 red fluorescent cell linker mini kit was used (Sigma). After silencing or pharmacologic treatment, cells were incubated with the dye according to the manufacturer's instructions for 2 minutes. After removal, cells were incubated with pure FCS for 1 minutes followed by an incubation of 2 hours in medium. Cells were then fixed with PFA and stained with Hoechst for 10 minutes. Washed cells were mounted in FluorSave Reagent mounting medium and the cells were analyzed by confocal microscopy.

Lysotracker staining

A total of 2×10^4 T24 cells were seeded onto μ -slides 8-well ibidiTreat and were silenced or stimulated. Thereafter, the cells were incubated for 30 minutes with $1 \mu\text{mol/L}$ Lysotracker Red DND-99 (Molecular Probes) and Hoechst in PBS. After removal, pictures were taken immediately with a Zeiss LSM 510 Meta confocal microscope.

β 1-integrin internalization

A total of 1×10^4 T24 cells were seeded onto μ -slides 8-well ibidiTreat and were silenced or stimulated. Cells were starved for 90 minutes and stained with β 1-integrin (TS2/16; Santa Cruz Biotechnology) in cold 0.01% BSA/DMEM without FCS for 45 minutes at 4°C . Washed cells were incubated with 0.01% BSA/DMEM with FCS for 1 hour at 37°C . Next, $1 \mu\text{mol/L}$ phorbol 12-myristate 13-acetate (Merck) in 0.01% BSA/DMEM with FCS was added for 30 minutes at 37°C . After washing and fixing cells with PFA, 0.1% Triton-X100 was added. Alexa Fluor 488-goat-anti-mouse (Molecular Probes) and Hoechst were used for 1 hour to stain cells. Washed cells were embedded in FluorSave Reagent mounting medium and analyzed by confocal microscopy.

Immunocytochemistry

A total of 1×10^4 T24 cells were seeded onto μ -slides 8-well ibidiTreat (IBIDI). Silenced or treated cells were fixed with PFA prior to permeabilization with 0.2% Triton X-100/PBS. Hereafter, unspecific binding sites were blocked with 1% BSA/PBS containing 0.1% Triton X-100. Antibodies were diluted in blocking solution. Used antibodies are given as follows: β 1-integrin (TS2/16), EEA1, LAMP3 (Santa Cruz Biotechnology). Nuclei were stained with Hoechst. Cells were embedded in FluorSave Reagent mounting medium and analyzed by confocal microscopy.

Staining of migrating cells

A confluent T24 cell layer was scratched with a pipette tip, after silencing or treatment. Cells were allowed to migrate for 5 hours and subsequently fixed with PFA. Samples were stained as described under the section "Immunocytochemistry." Antibodies given below were used: β 1-integrin (TS2/16), vinculin (Santa Cruz Biotechnology), pFAK^{S732}, pSrc^{Y418} (Invitrogen), Alexa Fluor 680-goat-anti-rabbit and Alexa Fluor 643-goat-anti-mouse

(Molecular Probes). Rhodamine-phalloidin was used to stain actin, Hoechst for nuclei.

Western blot analysis

Western blot analysis was performed as described previously (19). Following antibodies were used: TPC2 (Alomone), LAMP3, β 1-integrin (TS2/16), FAK (Santa Cruz Biotechnology), pFAK^{S732}, pSrc^{Y418} (Molecular Probes), Src (L4A1; Cell Signaling Technology), actin (Millipore), HRP-goat-anti-rabbit (Bio-Rad), and HRP-goat-anti-mouse (Santa Cruz Biotechnology).

In vivo mouse model

4T1-Luc cells were pretreated with $150 \mu\text{mol/L}$ Ned-19, $10 \mu\text{mol/L}$ tetrandrine or DMSO for 24 hours. Alternatively, cells were silenced with siTPC2 or siNT for 72 hours. Female BALB/cOlaHsd mice (Envigo) were inoculated with 1×10^5 4T1-Luc cells via the tail vein. After five days, imaging of the mice was performed using the IVIS Lumina system with Living Image software 4.4 (Caliper Life Sciences) immediately after intraperitoneal injection of 6 mg luciferin (potassium salt, PerkinElmer). The total signal per defined region of interest was calculated as photons/second/cm² (total flux/area). Animal experiments were approved by the District Government of Upper Bavaria in accordance with the German Animal Welfare and Institutional guidelines.

Statistical analysis

GraphPad Prism Software was used for all statistical analyses. In some experiments, data were normalized to control or as indicated.

Results

TPCs in cancer cells

TPCs have been described in different cell types (9, 18, 23); however, not in cancer cells so far. TPC2 mRNA is distinctly expressed in T24 (bladder cancer), Jurkat (leukemia), and HUH7 (HCC) cells (Fig. 1A). mRNA levels of TPC1 were particularly high in T24 and HUH7 cells (Fig. 1B). Tumor tissue sections of HCC patients showed a highly positive staining for TPC2 (Fig. 1C). Together, these data suggest the presence of TPCs in cancer cells. To verify TPC functionality in T24 cancer cells, we isolated lysosomes and performed endolysosomal patch-clamp experiments. The applied whole-endolysosomal patch-clamp method is illustrated in Fig. 1D. PI(3,5)P₂-elicited currents were strongly reduced after applying tetrandrine (Fig. 1E and F), recently shown to inhibit TPC1 and TPC2 (18).

TPCs affect cancer cell migration and adhesion

Previous studies in TPC2-deficient MEF cells showed defects in the endolysosomal degradation pathway (9, 11). As alterations in this pathway through inhibition of another endolysosome-associated protein, the vacuolar ATPase (V-ATPase), have been described to reduce the ability of invasive cancer cells to migrate (21), we hypothesized that TPCs affect cancer cell migration. Silencing TPC1 and TPC2 by siRNA in T24 cells resulted in significantly reduced migration through pores in Boyden chamber assays (Fig. 2A). Knockdown efficiency is shown in Fig. 2B and C. Moreover, these cells showed diminished adhesion after 1 hour of seeding (Fig. 2D). To get more information about the migratory defect, movement of the silenced cells exposed to a diffusive

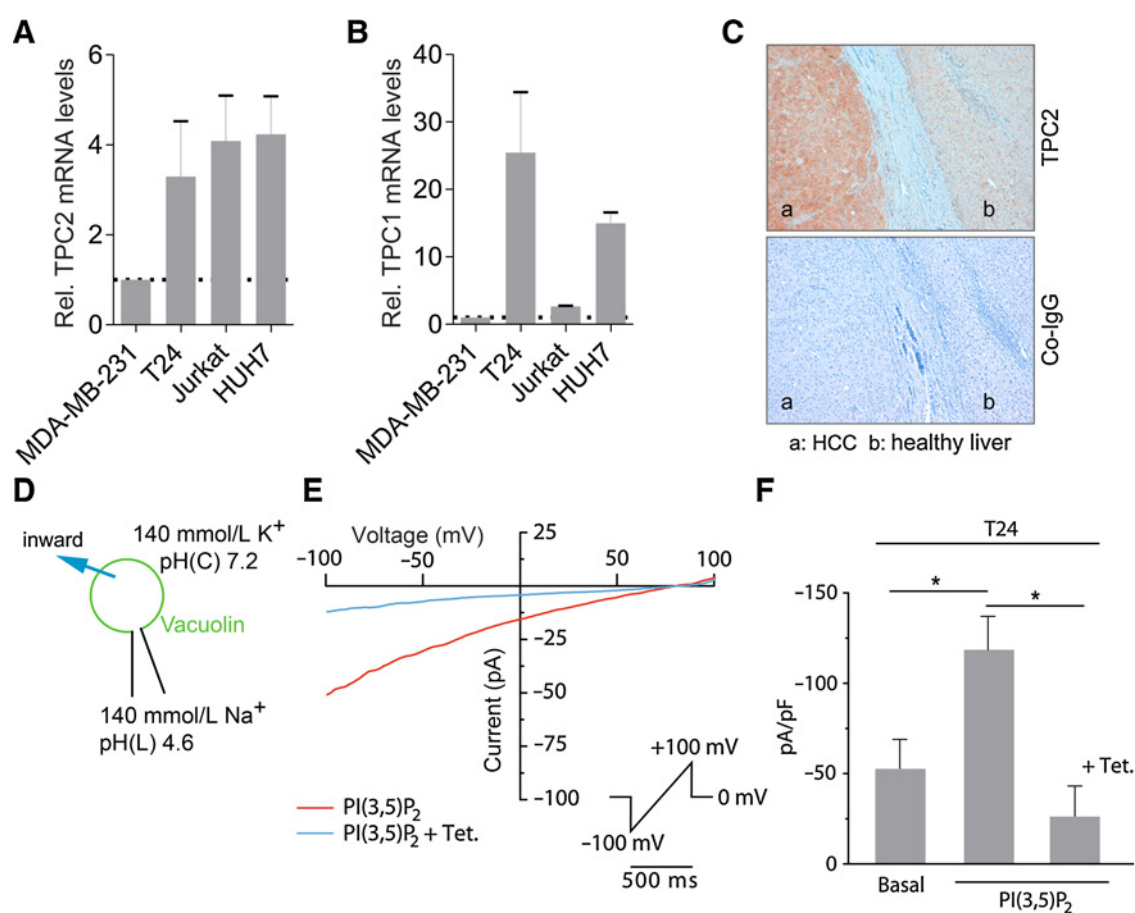


Figure 1.

TPCs in cancer cells. **A** and **B**, mRNA levels of TPC2 and TPC1 in different cancer cell lines were assessed by qRT-PCR using the SYBR Green PCR Master Mix. Expression level of MDA-MB-231 cells was set at 1. Bars, SEM of three independent experiments performed in duplicate. **C**, Human liver sections (HCC and surrounding tissue) were stained with an antibody against TPC2 or with an unspecific isotype control antibody (Co-IgG). Counterstaining was done with hematoxylin. One representative specimen is shown. **D**, Cartoon illustrating whole-endolysosomal patch-clamp method. **E**, Representative current-voltage relation recorded from a vacuolin-enlarged endolysosomal vesicle manually isolated from cultured T24 cells. Shown are the effect of $1 \mu\text{mol/L}$ PI(3,5)P₂ and the blocking effect of 500 nmol/L tetrandrine. **F**, Population data for current amplitudes at -100 mV obtained from experiments as shown in **E**. *, $P < 0.05$, Student *t* test; data are shown as mean \pm SEM.

gradient of FCS (0%–10%) was analyzed. Figure 2E shows control cells moving clearly toward the highest FCS concentrations, whereas knockdown cells displayed reduced directional migration, which is expressed as *P* value in the Rayleigh test. Not only directed migration but also cell mobility seems to be affected as velocity was significantly reduced in silenced cells. Thus, TPC1 and TPC2 seem to play a pivotal role in two major steps of metastasis formation: adhesion and migration.

Pharmacologic inhibition of TPC1 and TPC2 reduces cancer cell migration and adhesion

To further investigate the potential of TPCs as novel targets for cancer therapy, two pharmacologic inhibitors of TPC1 and TPC2 were used. The NAADP antagonist Ned-19 (17) showed significant reduction of migration through pores in T24 and HUH7 cells (Fig. 3A). Along this line, treatment with tetrandrine abrogated migration in Boyden chambers in T24, HUH7, and 4T1 cells (Fig. 3B). Both TPC inhibitors further impaired adhesion in T24 cells as displayed in Fig. 3C. Importantly, Ned-

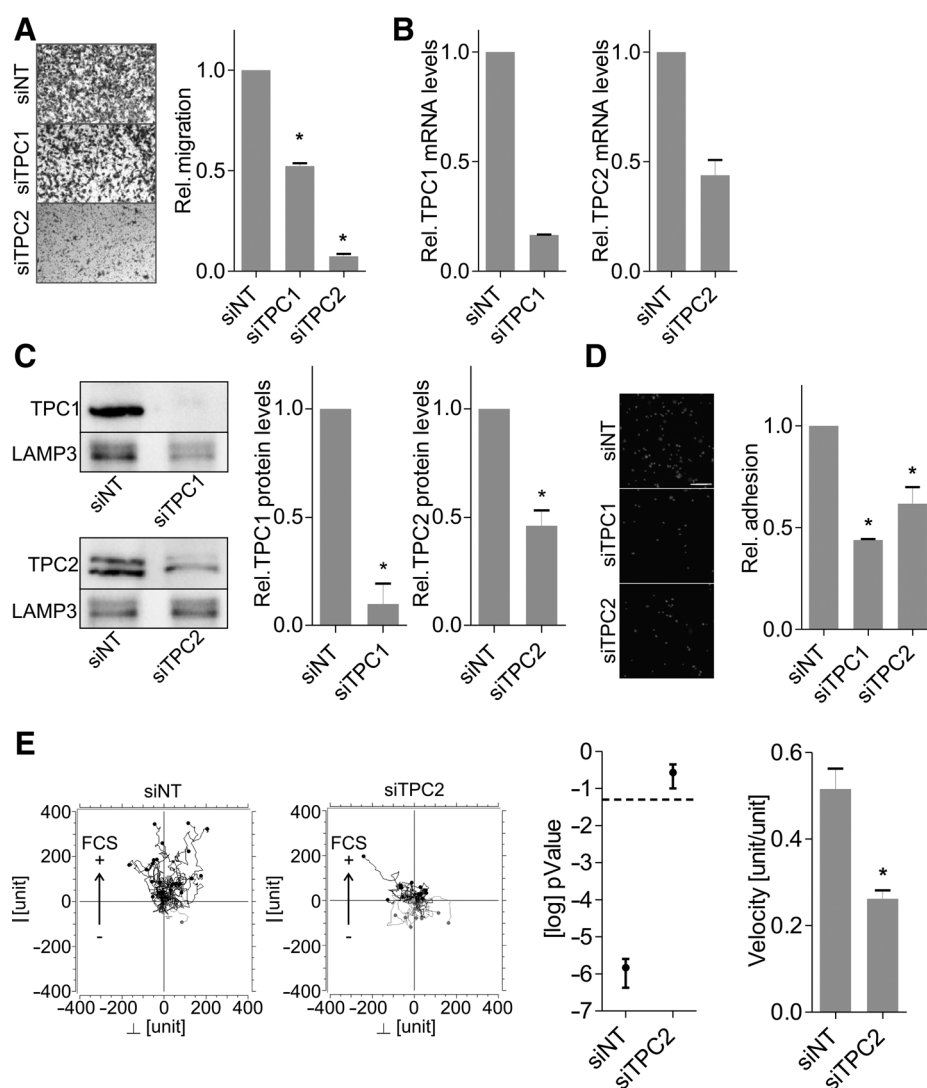
19 and tetrandrine had no effect on cell survival in all tested concentrations and at all tested time points (Fig. 3D). These results strengthen our finding that TPC1 and TPC2 are required for migration of cancer cells.

Accumulation of enlarged acidic vesicles after pharmacologic inhibition and TPC silencing

As TPC1 and TPC2 are located in the endolysosomal system (8, 10, 12) of cells, investigating this process after inhibition of TPCs seemed mandatory. First, membranes of cells were stained with PKH26 fluorescent dye and subsequently allowed to recycle. As Fig. 4A indicates, cells treated with Ned-19 and tetrandrine as well as cells silenced with siTPC1 and siTPC2 accumulated up to 2-fold enlarged vesicles compared with control cells, indicating that general recycling was impaired after TPC inhibition. Staining with LysoTracker Red DND-99 showed that the accumulated enlarged vesicles are acidic compartments. This experiment further indicates that the acidification of endocytic vesicles was neither affected after pharmacologic inhibition nor after siRNA

Figure 2.

Silencing of TPC1 and TPC2 leads to reduced migration and adhesion in cancer cells. For all experiments, T24 cells were silenced with siRNA against TPC1 and TPC2 for 72 hours. **A**, siRNA-treated cells were allowed to migrate in Transwell chambers for 16 hours. **B**, qPCR analysis of TPC1 and TPC2 mRNA levels were assessed with the SYBR Green PCR Master Mix. Bars, SEM of three independent experiments performed in duplicate. **C**, Western blot analysis of TPC1 and TPC2 protein levels in endolysosomal preparations. LAMP3 served as loading control and marker for lysosomes. Bars, SEM of three independent experiments, $^* P < 0.05$ (*t* test). **D**, After silencing, cells were allowed to adhere for 1 hour, fixed, and stained (rhodamine-phalloidin, Hoechst). Cells were analyzed by confocal microscopy. Scale bars, 150 μm . Bars in **A** and **D** are the SEM of three independent experiments, $^* P < 0.05$ (one-way ANOVA, Dunnett multiple comparison test). **E**, Movement of silenced T24 cells along a FCS gradient was monitored (20 hours) by live cell imaging and analyzed for directed migration (*P* value) and velocity (ImageJ, IBIDI software). Dashed line, $P = 0.05$. Bars are the SEM of three independent experiments, $^* P < 0.05$ (*t* test).



silencing (Fig. 4B). To elucidate the connection between disturbed recycling and inhibited cell migration, we selected key proteins of migration that are predominantly trafficked via the endolysosomal system, such as integrins.

Disturbed $\beta 1$ -integrin recycling through inhibition of TPCs

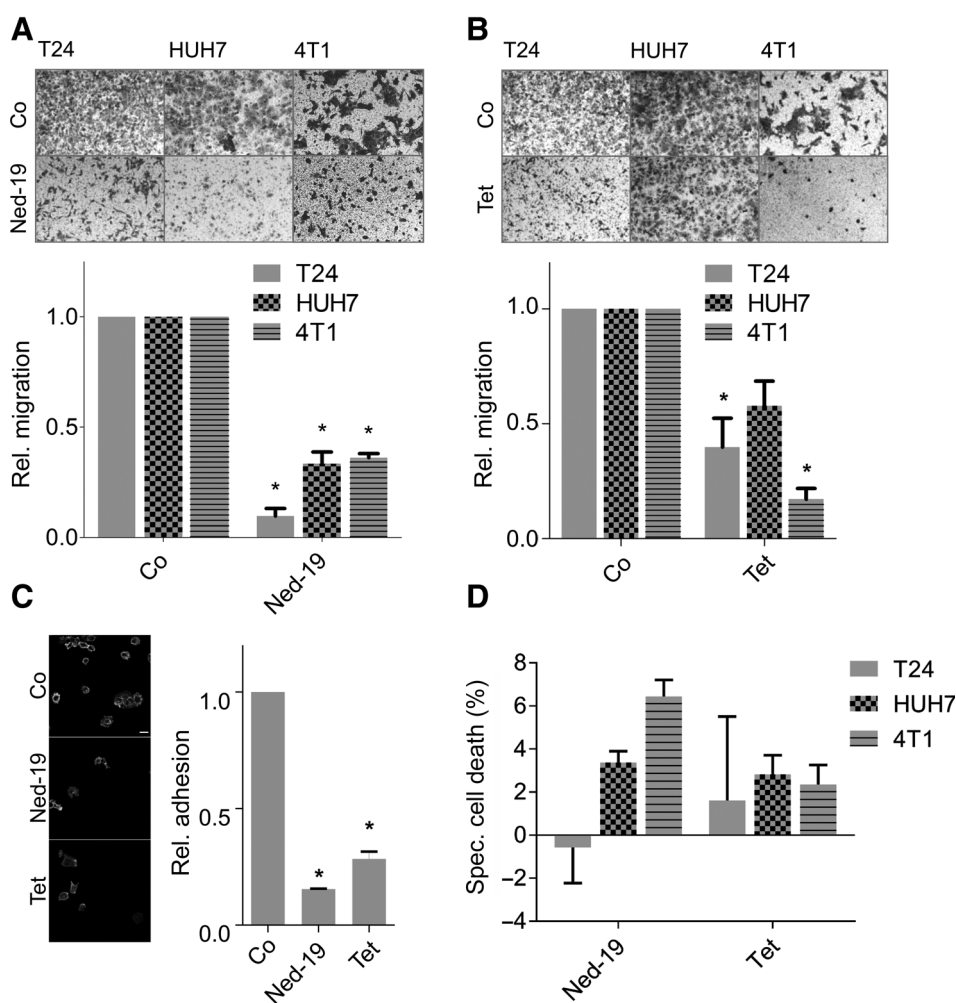
Integrins feature prominently in cancer cell adhesion and migration. Under normal conditions, these transmembrane receptors get rapidly recycled through the endolysosomal system (4). As inhibition of TPCs hampered endocytosis, we checked whether recycling of $\beta 1$ -integrin is hindered as well. Internalization assays of $\beta 1$ -integrin in T24 cells showed an up to 2-fold enlargement of $\beta 1$ -integrin-positive vesicles after treatment with Ned-19 or tetrandrine compared with control (Fig. 5A, left). As shown in the right panel of Fig. 5A, comparable results were achieved when TPC1 or TPC2 was silenced in the cells. Moreover, staining of $\beta 1$ -integrin-positive vesicles with EEA1 and LAMP3 displayed a higher overlap of $\beta 1$ -integrin vesicles with EEA1, indicating an accumulation in early endosomes rather than in lysosomes (Fig. 5B). In summary, these findings illustrate that TPC inhibition or silencing evokes disturbances in $\beta 1$ -integrin recycling.

Polarization and protrusion of the cell are essential for accurate cell migration. Protrusions in the direction of migration are stabilized through integrins linked to the actin cytoskeleton. Therefore, integrins have to be recycled to the leading edges of migrating cells (4, 5). To explore the ability to form leading edges, scratch assays were performed. Under these conditions, Ned-19 as well as tetrandrine inhibited the formation of wound-directed, $\beta 1$ -integrin-, pSrc-, pFAK-, and vinculin-positive polarized lamellipodia (Fig. 6A, top). Accordingly, silencing of TPC1 or TPC2 resulted in the same effects (Fig. 6A, bottom). These findings can be easily accounted for by disturbed $\beta 1$ -integrin trafficking to the front of the cell. Consistently, total protein levels of $\beta 1$ -integrin, FAK, pFAK, Src, and pSrc were not significantly altered after Ned-19 treatment (Fig. 6B), further corroborating an effect on $\beta 1$ -integrin recycling.

Reduced formation of lung metastasis *in vivo* by pharmacologic TPC inhibition and siRNA silencing of TPC2

To extend the relevance of TPC inhibition on chemotactic migration and invasion, we investigated whether tetrandrine was effective in abrogating cancer cell dissemination in a mouse model. The 4T1-Luc syngeneic metastatic mouse

Nguyen et al.

**Figure 3.**

Ned-19 and tetrandrine inhibit cancer cell migration and adhesion. **A** and **B**, T24, HUH7, and 4T1 cells were pretreated with Ned-19 and tetrandrine for 8 hours (T24: 250 $\mu\text{mol/L}$ Ned-19, 15 $\mu\text{mol/L}$ Tet; HUH7: 150 $\mu\text{mol/L}$ Ned-19, 2.5 $\mu\text{mol/L}$ Tet; 4T1: 150 $\mu\text{mol/L}$ Ned-19, 10 $\mu\text{mol/L}$ Tet). Cells were allowed to migrate in Transwell chambers for 16 hours in the presence of the inhibitor. **C**, After 24 hours of treatment with inhibitors used in **A** and **B**, T24 cells were allowed to adhere for 1 hour, fixed, and stained (rhodamine-phalloidin, Hoechst). Cells were analyzed by confocal microscopy. Scale bars, 150 μm . Bars in **A–C** are the SEM of three independent experiments, *, $P < 0.05$ (t test). **D**, Cell death was assessed after 24 hours of treatment with inhibitors used in **A** and **B** by flow cytometry analysis. Data represent means of three independent experiments performed in triplicates \pm SEM.

mammary cancer model was used for this purpose (24–26). 4T1-Luc cells express a luciferase reporter, which enables for live imaging. After intravenous injection, 4T1-Luc cells disseminate to distant organs homing preferably to lungs. Along this line, control animals showed easily detectable lung metastasis after five days of 4T1-Luc cell injection. Remarkably, both pretreatment with Ned-19 or tetrandrine significantly diminished formation of lung metastasis (Fig. 7A and B). The data were supported by a subsequent *in vivo* experiment using TPC2-silenced 4T1-Luc cells, which also formed significantly fewer lung tumors compared with control transfected cells (Fig. 7C). These findings strongly support the hypothesis that targeting TPCs might be a very promising and viable strategy for metastatic cancer therapy.

Discussion

This study designates TPCs as promising targets for the treatment of invasive cancers. Disruption of TPC function abrogates cancer cell migration *in vitro* and *in vivo*, resulting from disturbed integrin trafficking in the endolysosomal system.

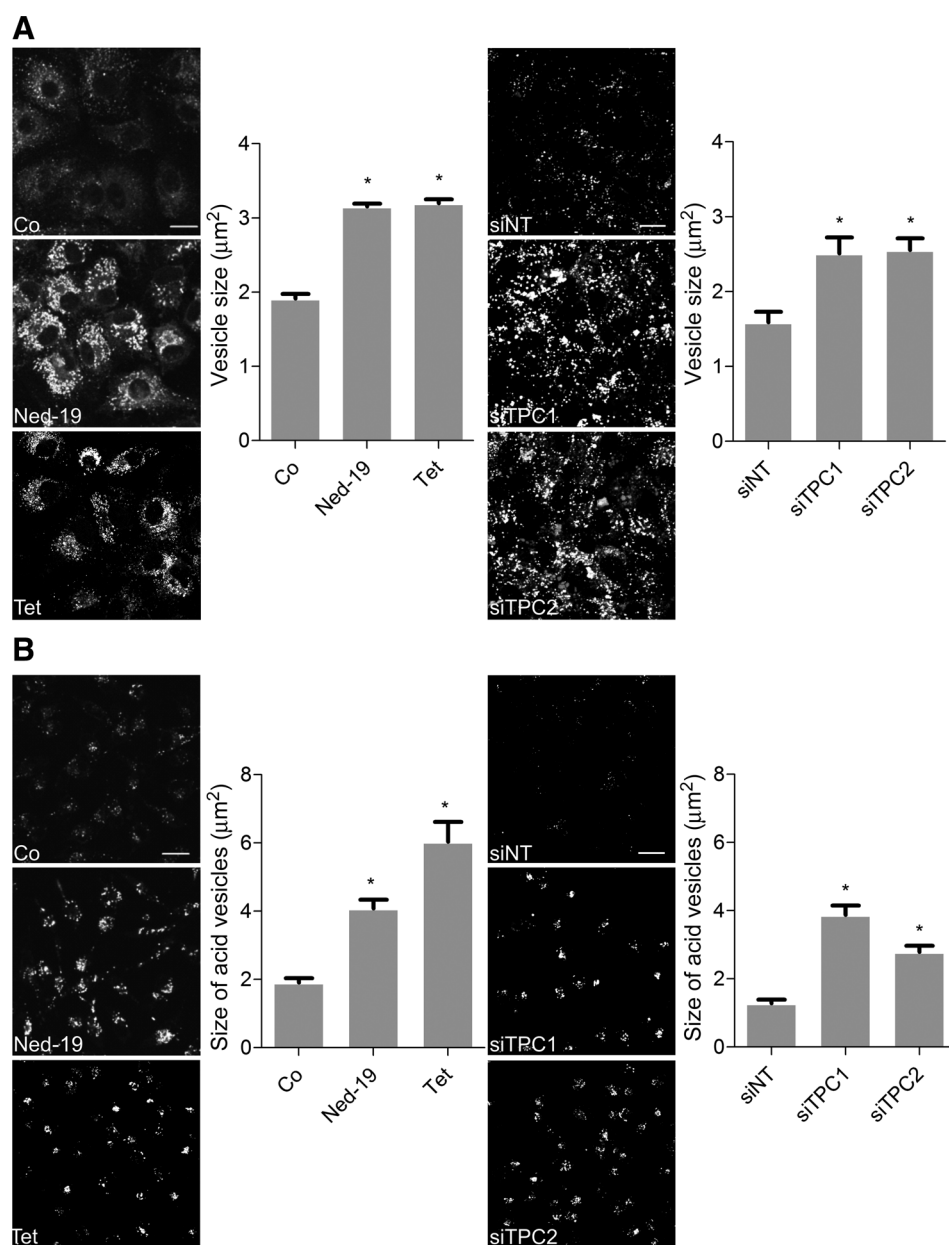
TPCs are Ca^{2+} -permeable cation channels located in the membrane of endosomes and lysosomes (7–10, 12, 13, 16). In recent years, evidence has accumulated that TPCs are substantially

implicated in the regulation of endolysosomal trafficking processes. Thus, a lack of TPC2 in mouse embryonic fibroblasts resulted in an accumulation of LDL and EGF/EGFR in intracellular vesicles (9) and led to delayed PDGFR β degradation (11). Pharmacologic inhibition of TPCs resulted in accumulation of cholera toxin within endolysosomes, which is normally delivered to the Golgi, and enlarged lysosomes dramatically (10). Disrupting TPC function also reduced Ebola virus trafficking through endosomal vesicles, preventing infection (18). Consistently, we observed an accumulation of integrins in early endosomes after TPC inhibition in invasive cancer cells.

When looking at general endocytic trafficking and receptor recycling, another protein located in the endolysosomal membrane of cells comes into focus, the V-ATPase. V-ATPases are multiunit proton pumps, which actively transport protons from the cytoplasm into intracellular compartments thereby regulating its pH (27). In several reports, it has been observed that altering pH by inhibition of V-ATPase results in impaired trafficking and recycling of signaling molecules. Hence, disturbed V-ATPase function led to the accumulation of Notch in the endolysosomal system (28) and of cholesterol in intracellular compartments (29). In cancer cells, inhibition of V-ATPase affected EGF receptor (21) and transferrin receptor internalization, the latter resulting in apoptosis (19).

Figure 4.

Inhibition of TPCs disrupts endocytic recycling. **A**, Membranes were stained with PKH 26 red in HUH7 cells after 24 hours of Ned-19 (150 $\mu\text{mol/L}$) and tetrandrine (2.5 $\mu\text{mol/L}$) treatment or after 72 hours of TPC1 and TPC2 silencing. Cells were allowed to recycle again for 2 hours. Fixed cells were analyzed by confocal microscopy. **B**, Ned-19 (250 $\mu\text{mol/L}$, 24 hours), tetrandrine (15 $\mu\text{mol/L}$, 24 hours)-treated or siRNA-silenced (72 hours) T24 cells were stained with LysoTracker Red DND-99 and analyzed by confocal microscopy. Nuclei in **A** and **B** were stained with Hoechst. Vesicles were analyzed with ImageJ. Bars, SEM of three independent experiments, *, $P < 0.05$ (t test). Scale bars, 20 μm .



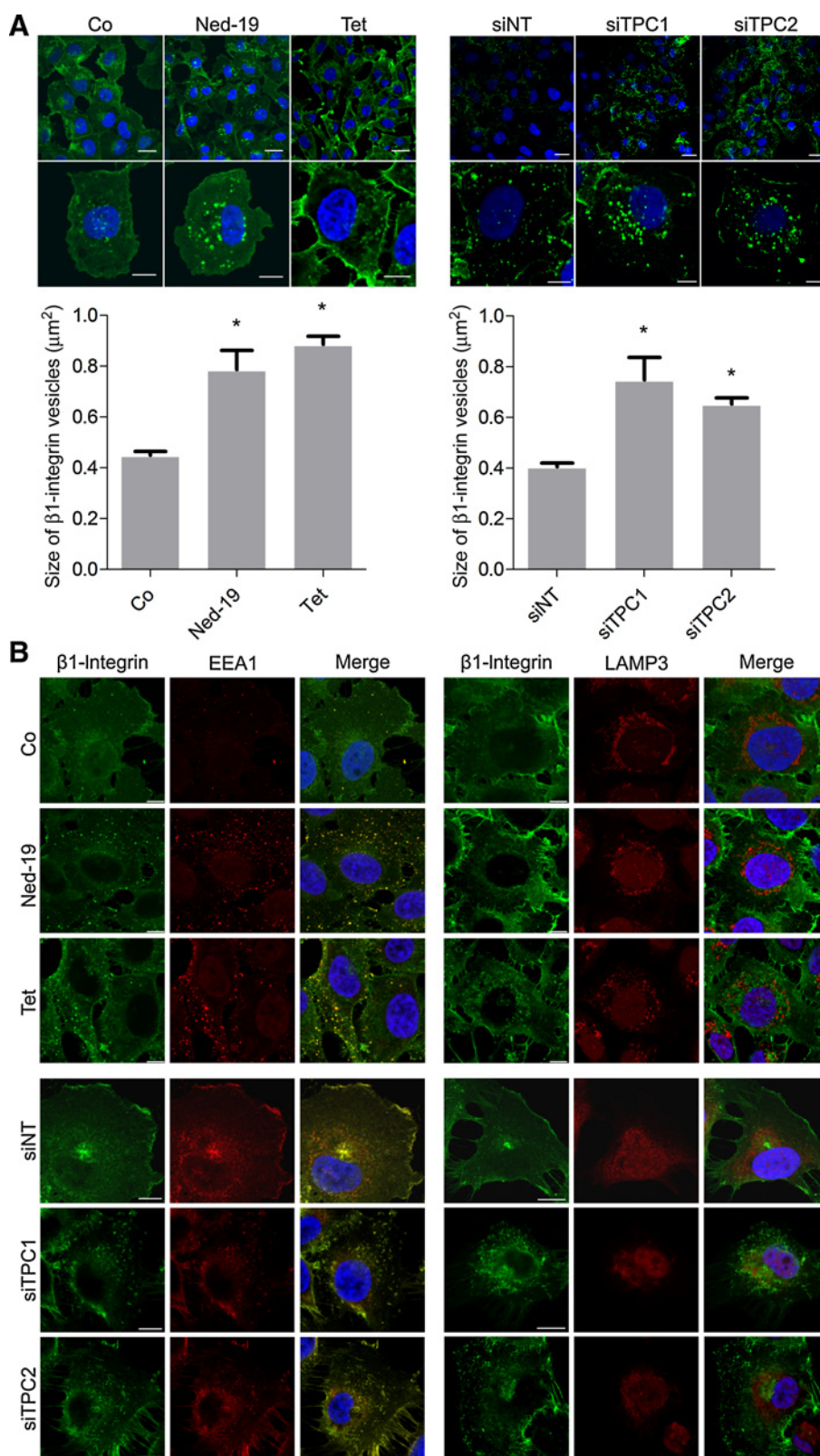
Taken together, targeting the endolysosomal system either by TPC or V-ATPase inhibition can apparently both impair adequate endocytic trafficking. As it is quite evident for V-ATPase inhibition that this is due to altered pH, there is still an ongoing discussion regarding TPCs. Impaired Ca^{2+} signaling may be one reason; however, it has also been postulated that alkalinizing of the lysosomal pH is responsible for the inhibition of autophagosomal-lysosomal fusion (30). In our study, we observed an accumulation of enlarged acidic vesicles after TPC inhibition, hence no alkalinizing of pH. Other recent publications have also found no evidence for changes in endolysosomal pH under basal conditions in TPC-deficient cells (9, 11, 31).

Alterations in Ca^{2+} signaling are widely accepted to lead to impaired trafficking and fusion of endocytic vesicles (9, 10). This

hypothesis is further supported by the finding that Ca^{2+} chelators, BAPTA and EGTA-AM, are able to inhibit fusion of late endosomes and lysosomes (32). In this context, it is interesting to note that another Ca^{2+} -permeable endolysosomal channel, TRPML1, has been proposed to be required for fusion between late endosomes and lysosomes in *Drosophila* (33). In humans, loss or mutation of this channel leads to the lysosomal storage disorder mucopolipidosis type IV (34–36), further supporting the importance of Ca^{2+} signaling.

Regardless of what the main cause of this impairment is, inhibition of TPC function led to a clear accumulation of $\beta 1$ -integrins in early endosomes. Integrins link the cell to the ECM enabling adhesion and migration (37). To migrate, the cell must be polarized meaning that different molecular processes occur at the front and back of a moving cell (5).

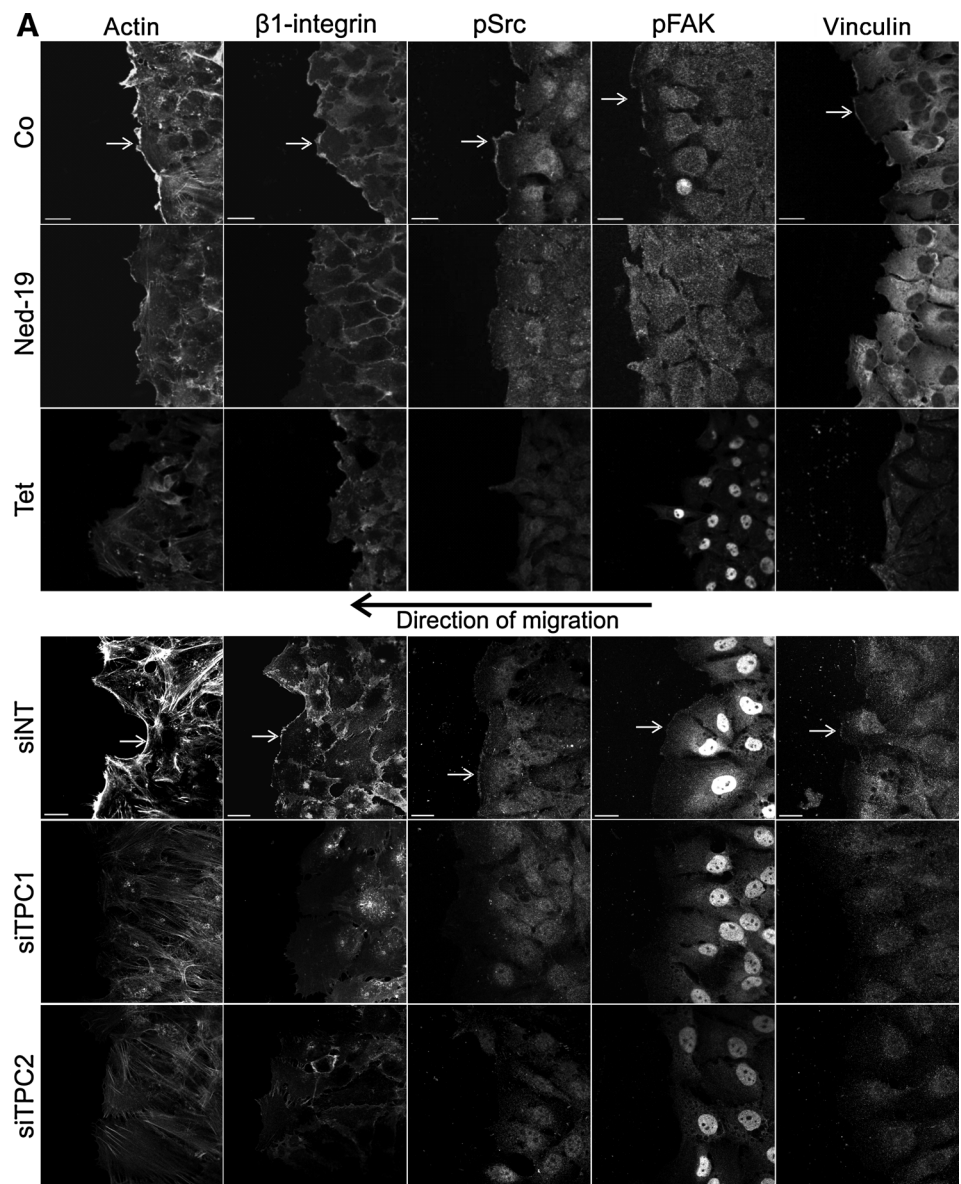
Nguyen et al.

**Figure 5.**

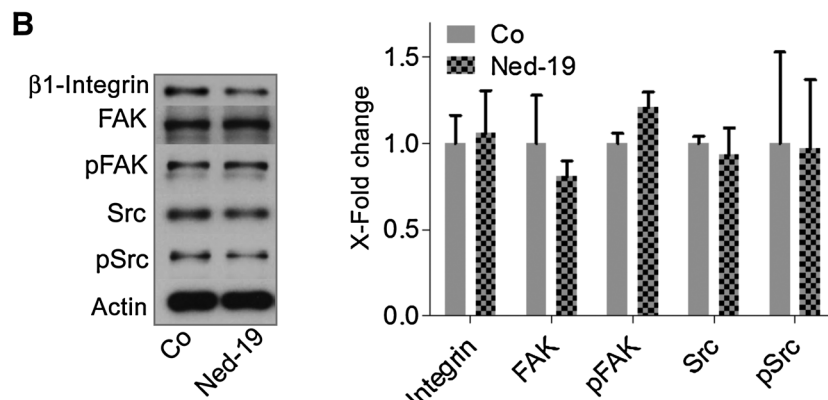
$\beta 1$ -Integrin recycling is hindered after TPC inhibition. **A**, Internalized $\beta 1$ -integrin was stained in T24 cells after 24 hours of Ned-19 (250 $\mu\text{mol/L}$) and tetrandrine (15 $\mu\text{mol/L}$) treatment or after 72 hours of siRNA silencing. Scale bars, 20 μm (top pictures) and 10 μm (bottom pictures). Vesicles were analyzed with ImageJ. Bars, SEM of three independent experiments, *, $P < 0.05$ (t test). **B**, Ned-19 (250 $\mu\text{mol/L}$, 24 hours) and tetrandrine (15 $\mu\text{mol/L}$, 24 hours)-treated or siRNA-silenced (72 hours) T24 cells were stained for $\beta 1$ -integrin (green), EEA1, LAMP3 (red), and nuclei with Hoechst (blue). Scale bars, 10 μm . Pictures of cells in **A** and **B** were taken with a confocal microscope.

Therefore, several proteins are trafficked towards the front of the cell. For example, growth factor receptors and chemokine receptors are recycled to specific sites of the leading edge to

mediate promigratory signals. Importantly, adhesive contacts are regulated by the recycling and degradation of integrins (4). Hence, the turnover of integrins is crucial for migration. We

**Figure 6.**

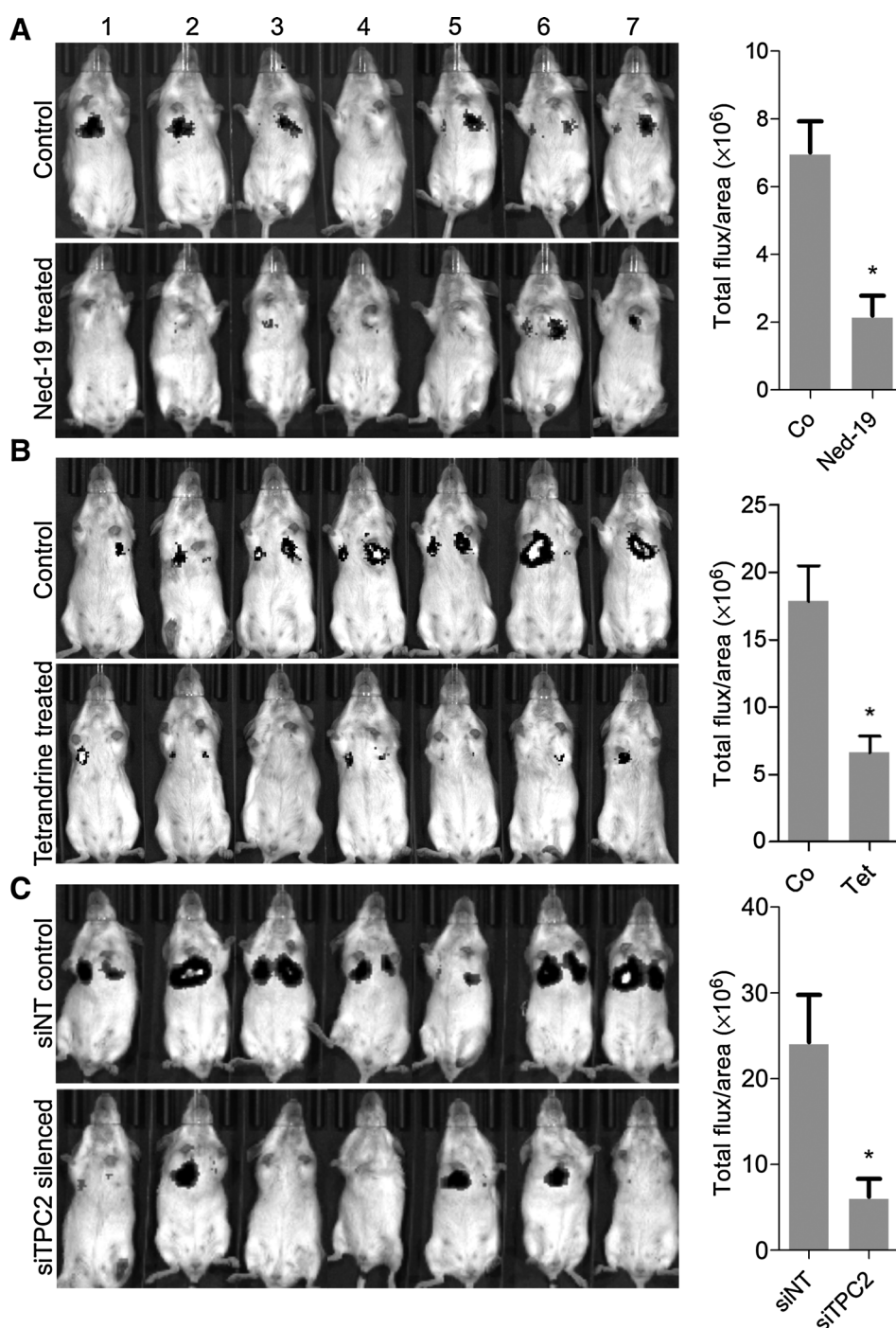
TPC function is required for the formation of leading edges. **A**, T24 cells were scratched and let migrate for 5 hours after a pretreatment with 250 $\mu\text{mol/L}$ Ned-19 and 15 $\mu\text{mol/L}$ tetrandrine for 16 hours or after siRNA silencing for 72 hours. Fixed cells were stained for actin, $\beta 1$ -integrin, pSrc, pFAK, and vinculin (white). Nuclei were stained with Hoechst. One representative picture out of three independent experiments is shown. Scale bars, 20 μm . White arrows, leading edges. **B**, Total protein amounts of $\beta 1$ -integrin, pSrc, Src, pFAK, and FAK were detected by Western blot analysis in T24 cells after treatment with 250 $\mu\text{mol/L}$ Ned-19 for 24 hours. One representative blot is shown. Quantification was done with ImageJ. Bars, SEM of three independent experiments.



could observe in our studies, in addition to an accumulation of $\beta 1$ -integrin in enlarged vesicles, reduced $\beta 1$ -integrin localization at the leading edge of migrating cells after TPC inhibition

or silencing. These findings suggest that disrupted TPC function alters $\beta 1$ -integrin trafficking, resulting in reduced adhesion to ECM and insufficient polarization of the cell.

Nguyen et al.

**Figure 7.**

Inhibition of TPC function in 4T1-Luc cells reduces the formation of lung metastasis *in vivo*. **A** and **B**, 4T1-Luc cells were pretreated with 150 $\mu\text{mol/L}$ Ned-19, 10 $\mu\text{mol/L}$ tetrandrine, or DMSO for 24 hours. **C**, 4T1-Luc cells were silenced with siTPC2 or siNT for 72 hours. **A-C**, 1×10^5 cells were injected intravenously into BALB/cOlaHsd mice. On day five after cell inoculation, bioluminescence signals were measured by imaging the mice in ventrodorsal position. The total signal per defined region of interest was calculated as photons/second/cm² (total flux/area). Bars, SEM of 7 animals. *, $P < 0.05$ (*t* test).

Besides mediating adhesion to ECM, integrins are also essential for cell migration as they regulate promigratory signaling pathways. Thus, integrin ligation induces clustering, resulting in the activation of FAK. Active FAK recruits Src family kinases to focal adhesions, altogether promoting cell migration and invasion. In addition, focal contacts contain different actin-associated proteins, such as vinculin, which links integrin to the cytoskeleton (3). In our study, inhibition of TPC function or expression clearly diminished the accumulation of integrin, pFAK, pSrc, and vinculin at the leading edge of migrating cells. This suggests that

adequate $\beta 1$ -integrin trafficking is crucial for the initiation of promigratory mechanisms.

To fulfill these functions, integrins form heterodimeric receptors. Pairing of α and β subunits decides for the specific binding of certain matrix ligands. Previous investigations on the $\beta 1$ -integrin subunit revealed a central role in adhesion, extravasation, and migration in T24 cancer cells (38). Moreover, reports show that $\beta 1$ -integrin and FAK signaling is implicated in the initial proliferation of cancer cells disseminated into the lungs (39). Our own experiments are consistent with these notions. Further research

over the last several years led to the development of integrin-targeted therapeutics, which are now tested in clinical studies against cancer and other diseases (3). The mAb volociximab is the first $\alpha 5\beta 1$ integrin antagonist in clinical trials against metastatic clear cell renal cell carcinoma, metastatic melanoma, non-small cell lung cancer, and peritoneal cancer among others (40, 41). In addition, several therapeutic antibodies targeting $\alpha v\beta 3$ integrin are under development or in clinical phases as antitumor agents such as *Vitaxin* and *CNTO 95* (40). Taken together, targeting integrins is a highly promising and viable strategy for the treatment of metastatic cancers.

In summary, our study reveals a potential novel role for TPCs in the formation of metastasis. Impaired TPC function reduced adhesion and migration of cancer cells *in vitro* and diminished formation of metastasis *in vivo*. Most likely, this is due to disturbed trafficking of integrins known to act promigratory. Here we link TPCs to fundamental processes in cancer cell migration, rendering them new and attractive targets for the treatment of invasive carcinomas.

Disclosure of Potential Conflicts of Interest

No potential conflicts of interest were disclosed.

Authors' Contributions

Conception and design: C. Grimm, L.S. Schneider, C. Wahl-Schott, M. Biel, A.M. Vollmar

Development of methodology: O.N.P. Nguyen, C. Grimm, L.S. Schneider, M. Ulrich, C. Wahl-Schott, M. Biel, A.M. Vollmar

Acquisition of data (provided animals, acquired and managed patients, provided facilities, etc.): C. Grimm, C. Atzberger, K. Bartel, A. Watermann, M. Ulrich, D. Mayr

Analysis and interpretation of data (e.g., statistical analysis, biostatistics, computational analysis): O.N.P. Nguyen, C. Grimm, L.S. Schneider, Y.-K. Chao, C. Atzberger, K. Bartel, D. Mayr, C. Wahl-Schott, M. Biel

Writing, review, and/or revision of the manuscript: O.N.P. Nguyen, C. Grimm, L.S. Schneider, C. Atzberger, C. Wahl-Schott, M. Biel, A.M. Vollmar

Administrative, technical, or material support (i.e., reporting or organizing data, constructing databases): Y.-K. Chao, K. Bartel

Study supervision: O.N.P. Nguyen, C. Grimm, C. Wahl-Schott, A.M. Vollmar

Acknowledgments

We thank Cheng-Chang Chen for the outstanding instructions and supervision of the lysosomal patch-clamp recordings. We also thank Kerstin Loske for the great support during the animal experiments.

Grant Support

This work was supported by funding from the German Research Foundation (SFB/TRR152 TP04 to C. Grimm, TP06 to C. Wahl-Schott, TP12 to M. Biel, and FOR1406 to A.M. Vollmar).

The costs of publication of this article were defrayed in part by the payment of page charges. This article must therefore be hereby marked *advertisement* in accordance with 18 U.S.C. Section 1734 solely to indicate this fact.

Received March 22, 2016; revised December 22, 2016; accepted December 22, 2016; published OnlineFirst January 20, 2017.

References

- Fidler IJ. Timeline: the pathogenesis of cancer metastasis: the 'seed and soil' hypothesis revisited. *Nat Rev Cancer* 2003;3:453–58.
- Chaffer CL, Weinberg RA. A perspective on cancer cell metastasis. *Science* 2011;331:1559–64.
- Hood JD, Cheresh DA. Role of integrins in cell invasion and migration. *Nat Rev Cancer* 2002;2:91–100.
- Maritzen T, Schachtner H, Legler DF. On the move: endocytic trafficking in cell migration. *Cell Mol Life Sci* 2015;72:2119–34.
- Ridley AJ. Cell migration: integrating signals from front to back. *Science* 2003;302:1704–09.
- Brailoiu E, Churamani D, Cai X, Schrlau MG, Brailoiu GC, Gao X, et al. Essential requirement for two-pore channel 1 in NAADP-mediated calcium signaling. *J Cell Biol* 2009;186:201–09.
- Zong X, Schieder M, Cuny H, Fenske S, Gruner C, Rötzer K, et al. The two-pore channel TPCN2 mediates NAADP-dependent Ca²⁺ release from lysosomal stores. *Pfluegers Arch/Eur J Physiol* 2009;458:891–99.
- Calcraft PJ, Ruas M, Pan Z, Cheng X, Arredouani A, Hao X, et al. NAADP mobilizes calcium from acidic organelles through two-pore channels. *Nature* 2009;459:596–600.
- Grimm C, Holdt LM, Chen C-C, Hassan S, Müller C, Jörs S, et al. High susceptibility to fatty liver disease in two-pore channel 2-deficient mice. *Nat Commun* 2014;5:4699.
- Ruas M, Rietdorf K, Arredouani A, Davis LC, Lloyd-Evans E, Koegel H, et al. Purified TPC isoforms form NAADP receptors with distinct roles for Ca²⁺ signaling and endolysosomal trafficking. *Curr Biol* 2010;20:703–09.
- Ruas M, Chuang KT, Davis LC, Al-Douri A, Tynan PW, Tunn R, et al. TPC1 has two variant isoforms, and their removal has different effects on endolysosomal functions compared to loss of TPC2. *Mol Cell Biol* 2014;34:3981–92.
- Rietdorf K, Funnell TM, Ruas M, Heinemann J, Parrington J, Galione A. Two-pore channels form homo- and heterodimers. *J Biol Chem* 2011;286:37058–62.
- Schieder M, Rotzer K, Bruggemann A, Biel M, Wahl-Schott CA. Characterization of two-pore channel 2 (TPCN2)-mediated Ca²⁺ currents in isolated lysosomes. *J Biol Chem* 2010;285:21219–22.
- Wang X, Zhang X, Dong X-p, Samie M, Li X, Cheng X, et al. TPC proteins are phosphoinositide-activated sodium-selective ion channels in endosomes and lysosomes. *Cell* 2012;151:372–83.
- Jha A, Ahuja M, Patel S, Brailoiu E, Muallem S. Convergent regulation of the lysosomal two-pore channel-2 by Mg²⁺, NAADP, PI(3,5)P₂ and multiple protein kinases. *EMBO J* 2014;33:501–11.
- Ruas M, Davis LC, Chen CC, Morgan AJ, Chuang KT, Walseth TF, et al. Expression of Ca²⁺-permeable two-pore channels rescues NAADP signalling in TPC-deficient cells. *EMBO J* 2015;34:1743–58.
- Naylor E, Arredouani A, Vasudevan SR, Lewis AM, Parkesh R, Mizote A, et al. Identification of a chemical probe for NAADP by virtual screening. *Nat Chem Biol* 2009;5:220–26.
- Sakurai Y, Kolokoltsov AA, Chen CC, Tidwell MW, Bauta WE, Klugbauer N, et al. Two-pore channels control Ebola virus host cell entry and are drug targets for disease treatment. *Science* 2015;347:995–98.
- Schneider LS, von Schwarzenberg K, Lehr T, Ulrich M, Kubisch-Dohmen R, Liebl J, et al. Vacuolar-ATPase inhibition blocks iron metabolism to mediate therapeutic effects in breast cancer. *Cancer Res* 2015;75:2863–74.
- Schieder M, Rotzer K, Bruggemann A, Biel M, Wahl-Schott C. Planar patch clamp approach to characterize ionic currents from intact lysosomes. *Sci Signal* 2010;3:pl3.
- Wiedmann RM, von Schwarzenberg K, Palamidessi A, Schreiner L, Kubisch R, Liebl J, et al. The V-ATPase-inhibitor archazolid abrogates tumor metastasis via inhibition of endocytic activation of the Rho-GTPase Rac1. *Cancer Res* 2012;72:5976–87.
- Zengel P, Nguyen-Hoang A, Schildhammer C, Zantl R, Kahl V, Horn E. μ -Slide Chemotaxis: a new chamber for long-term chemotaxis studies. *BMC Cell Biol* 2011;12:21.
- Favia A, Desideri M, Gambarà G, D'Alessio A, Ruas M, Esposito B, et al. VEGF-induced neoangiogenesis is mediated by NAADP and two-pore channel-2-dependent Ca²⁺ signaling. *Proc Natl Acad Sci U S A* 2014;111:E4706–E15.
- Aslakson CJ, Miller FR. Selective events in the metastatic process defined by analysis of the sequential dissemination of subpopulations of a mouse mammary tumor. *Cancer Res* 1992;52:1399–405.

Nguyen et al.

25. Yang J, Mani SA, Donaher JL, Ramaswamy S, Itzykson RA, Come C, et al. Twist, a master regulator of morphogenesis, plays an essential role in tumor metastasis. *Cell* 2004;117:927–39.
26. Tao K, Fang M, Alroy J, Sahagian GG. Imagable 4T1 model for the study of late stage breast cancer. *BMC Cancer* 2008;8:228.
27. Forgac M. Vacuolar ATPases: rotary proton pumps in physiology and pathophysiology. *Nat Rev Mol Cell Biol* 2007;8:917–29.
28. Kobias F, Duchi S, DeFlorian G, Vaccari T. Pharmacologic inhibition of vacuolar H⁺ ATPase reduces physiologic and oncogenic Notch signaling. *Mol Oncol* 2014;8:207–20.
29. Kozik P, Hodson NA, Sahlender DA, Simecek N, Soromani C, Wu J, et al. A human genome-wide screen for regulators of clathrin-coated vesicle formation reveals an unexpected role for the V-ATPase. *Nat Cell Biol* 2012;15:50–60.
30. Lu Y, Hao BX, Graeff R, Wong CWM, Wu WT, Yue J. Two Pore Channel 2 (TPC2) inhibits autophagosomal-lysosomal fusion by alkalinizing lysosomal pH. *J Biol Chem* 2013;288:24247–63.
31. Cang C, Zhou Y, Navarro B, Seo Y-j, Aranda K, Shi L, et al. mTOR regulates lysosomal ATP-Sensitive Two-Pore Na⁺ channels to adapt to metabolic state. *Cell* 2013;152:778–90.
32. Pryor PR, Mullock BM, Bright NA, Gray SR, Luzio JP. The role of introrganellar Ca²⁺ in late endosome-lysosome heterotypic fusion and in the reformation of lysosomes from hybrid organelles. *J Cell Biol* 2000;149:1053–62.
33. Wong C-O, Li R, Montell C, Venkatachalam K. Drosophila TRPML is required for TORC1 activation. *Curr Biol* 2012;22:1616–21.
34. Bargal R, Avidan N, Ben-Asher E, Olender Z, Zeigler M, Frumkin A, et al. Identification of the gene causing mucopolipidosis type IV. *Nat Genet* 2000;26:118–23.
35. Slaugenhaupt SA, Acierno JS Jr, Helbling LA, Bove C, Goldin E, Bach G, et al. Mapping of the mucopolipidosis Type IV gene to chromosome 19p and definition of founder haplotypes. *Am J Hum Genet* 1999;65:773–78.
36. Chen C-C, Keller M, Hess M, Schiffmann R, Urban N, Wolfgardt A, et al. A small molecule restores function to TRPML1 mutant isoforms responsible for mucopolipidosis type IV. *Nat Commun* 2014;5:4681.
37. Huttenlocher A, Horwitz AR. Integrins in Cell Migration. *Cold Spring Harbor Perspect Biol* 2011;3:a005074–a74.
38. Heyder C, Gloria-Maercker E, Hatzmann W, Niggemann B, Zänker KS, Dittmar T. Role of the β 1-integrin subunit in the adhesion, extravasation and migration of T24 human bladder carcinoma cells. *Clin Exp Metastasis* 2005;22:99–106.
39. Shibue T, Weinberg RA. Integrin 1-focal adhesion kinase signaling directs the proliferation of metastatic cancer cells disseminated in the lungs. *Proc Natl Acad Sci U S A* 2009;106:10290–95.
40. Millard M, Odde S, Neamati N. Integrin targeted therapeutics. *Theranostics* 2011;1:154–88.
41. Almokadem S, Belani CP. Volociximab in cancer. *Expert Opin Biol Ther* 2012;12:251–57.

Cancer Research

The Journal of Cancer Research (1916–1930) | The American Journal of Cancer (1931–1940)

Two-Pore Channel Function Is Crucial for the Migration of Invasive Cancer Cells

Ong Nam Phuong Nguyen, Christian Grimm, Lina S. Schneider, et al.

Cancer Res 2017;77:1427-1438. Published OnlineFirst January 20, 2017.

Updated version Access the most recent version of this article at:
doi:[10.1158/0008-5472.CAN-16-0852](https://doi.org/10.1158/0008-5472.CAN-16-0852)

Cited articles This article cites 41 articles, 17 of which you can access for free at:
<http://cancerres.aacrjournals.org/content/77/6/1427.full.html#ref-list-1>

E-mail alerts [Sign up to receive free email-alerts](#) related to this article or journal.

Reprints and Subscriptions To order reprints of this article or to subscribe to the journal, contact the AACR Publications Department at pubs@aacr.org.

Permissions To request permission to re-use all or part of this article, contact the AACR Publications Department at permissions@aacr.org.



TPC2 polymorphisms associated with a hair pigmentation phenotype in humans result in gain of channel function by independent mechanisms

Yu-Kai Chao^{a,1}, Verena Schludi^{a,1}, Cheng-Chang Chen^a, Elisabeth Butz^a, O. N. Phuong Nguyen^a, Martin Müller^a, Jens Krüger^b, Claudia Kammerbauer^c, Manu Ben-Johny^d, Angelika M. Vollmar^a, Carola Berking^c, Martin Biel^a, Christian A. Wahl-Schott^{a,2}, and Christian Grimm^{a,2}

^aDepartment of Pharmacy, Center for Drug Research and Center for Integrated Protein Science Munich, Ludwig-Maximilians-Universität München, 81377 Munich, Germany; ^bHigh-Performance and Cloud Computing Group, Zentrum für Datenverarbeitung, Universität Tübingen, 72076 Tübingen, Germany; ^cDepartment of Dermatology, Medical Faculty, Ludwig-Maximilians-Universität München, 80337 Munich, Germany; and ^dCalcium Signals Laboratory, Department of Biomedical Engineering, The Johns Hopkins University School of Medicine, Baltimore, MD 21205

Edited by Dejian Ren, University of Pennsylvania, Philadelphia, PA, and accepted by Editorial Board Member David E. Clapham August 16, 2017 (received for review April 6, 2017)

Two-pore channels (TPCs) are endolysosomal cation channels. Two members exist in humans, TPC1 and TPC2. Functional roles associated with the ubiquitously expressed TPCs include VEGF-induced neoangiogenesis, LDL-cholesterol trafficking and degradation, physical endurance under fasting conditions, autophagy regulation, the acrosome reaction in sperm, cancer cell migration, and intracellular trafficking of pathogens such as Ebola virus or bacterial toxins (e.g., cholera toxin). In a genome-wide association study for variants associated with human pigmentation characteristics two coding variants of TPC2, rs35264875 (encoding M484L) and rs3829241 (encoding G734E), have been found to be associated with a shift from brown to blond hair color. In two recent follow-up studies a role for TPC2 in pigmentation has been further confirmed. However, these human polymorphic variants have not been functionally characterized until now. The development of endolysosomal patch-clamp techniques has made it possible to investigate directly ion channel activities and characteristics in isolated endolysosomal organelles. We applied this technique here to scrutinize channel characteristics of the polymorphic TPC2 variants in direct comparison with WT. We found that both polymorphisms lead to a gain of channel function by independent mechanisms. We next conducted a clinical study with more than 100 blond- and brown/black-haired individuals. We performed a genotype/phenotype analysis and subsequently isolated fibroblasts from WT and polymorphic variant carriers for endolysosomal patch-clamp experimentation to confirm key *in vitro* findings.

TPC | TPC2 | two-pore channel | polymorphism | pigmentation

Two-pore channels (TPCs) are endolysosomal cation channels which are distantly related to the endolysosomal TRP channels of the TRPML subfamily on the one hand and the voltage-gated calcium channels on the other hand. Two members exist in humans, TPC1 and TPC2. Functional roles associated with the ubiquitously expressed TPCs include VEGF-induced neoangiogenesis (1), endolysosomal LDL-cholesterol trafficking and degradation (2), physical endurance under fasting conditions (3), autophagy regulation (4, 5), the acrosome reaction in sperm (6), intracellular trafficking of certain pathogens such as filoviridae (e.g., Ebola or Marburg virus) (7), bacterial toxins (e.g., cholera toxin) (8), and a role in cancer cell migration (9). A few years ago, Sulem et al. (10) presented results from a genome-wide association study for variants associated with human pigmentation characteristics among 5,130 Icelanders, with follow-up analyses in 2,116 Icelanders and 1,214 Dutch individuals from which they claimed that two coding variants of hTPC2 (SNPs), rs35264875 (encoding M484L) and rs3829241 (encoding G734E), were associated with a shift from brown to blond hair color. Very recently, Ambrosio et al. (11) as well as Bellono et al. (12) confirmed a role

for TPC2 in pigmentation by showing that TPC2 regulates the pH and size of melanosomes, thus controlling the amount of melanin produced. Consequently, loss of TPC2 activity by knockout or knockdown leads to a strong increase of melanin production and melanosomal pH.

Hence, it seemed intriguing to functionally investigate these polymorphic TPC2 variants. We investigated the activity of WT hTPC2 side by side with hTPC2(G734E) and hTPC2(M484L) as well as the double-mutant isoform (M484L/G734E). First, we applied the endolysosomal patch-clamp technique in combination with small-molecule activators and blockers of TPC2 to directly assess channel activity. Second, we performed molecular dynamics simulations of TPC2 based on the recently published structures of TPC1 (13, 14) to investigate structural changes due to the SNPs. These results were corroborated by ion substitution experiments to assess pore sizes. Furthermore, we genotyped more than 100 blond- and brown/black-haired human individuals and isolated fibroblasts from selected donors to confirm key *in vitro* findings and the results of the genome-wide association study by Sulem et al. (10).

Significance

Polymorphisms in the endolysosomal cation channel TPC2 have been suggested to lead to a shift in human hair color from brown to blond. In two further studies a role for TPC2 in melanosomal pH regulation was postulated. Electrophysiological data on how these polymorphisms affect channel gating and activity are, however, missing. We show here that both polymorphisms lead to a gain of channel function by different mechanisms. In M484L sensitivity to its endogenous ligand $PI(3,5)P_2$ is strongly increased while in G734E channel inactivation by ATP is reduced. These findings are corroborated by molecular dynamics and ion substitution experiments. Furthermore, >100 blond- and brown/black-haired human individuals were genotyped and fibroblasts isolated from selected donors to confirm key *in vitro* findings.

Author contributions: Y.-K.C., V.S., C.-C.C., E.B., O.N.P.N., J.K., A.M.V., C.B., and C.G. designed research; Y.-K.C., V.S., C.-C.C., E.B., O.N.P.N., M.M., J.K., C.K., C.B., and C.G. performed research; Y.-K.C., V.S., C.-C.C., E.B., O.N.P.N., M.M., J.K., M.B.-J., and C.G. analyzed data; and M.B., C.A.W.-S., and C.G. wrote the paper.

The authors declare no conflict of interest.

This article is a PNAS Direct Submission. D.R. is a guest editor invited by the Editorial Board.

¹Y.-K.C. and V.S. contributed equally to this work.

²To whom correspondence may be addressed. Email: christian.wahl@cup.uni-muenchen.de or christian.grimm@cup.uni-muenchen.de.

This article contains supporting information online at www.pnas.org/lookup/suppl/doi:10.1073/pnas.1705739114/-DCSupplemental.

Results

Human TPC2 WT and Polymorphic Variants Show Comparable Subcellular Distribution but Differences in Basal Activity and Their Response to PI(3,5)P₂. WT hTPC2 and the polymorphic variants containing either M484L, G734E, or both M484L and G734E show similar subcellular distribution when overexpressed in HEK293 cells (*SI Appendix, Fig. S1A*). All variants localize to intracellular vesicular structures which are positively stained with LysoTracker (*SI Appendix, Fig. S1A*). A calculation of the Pearson correlation coefficients resulted in similar numbers for colocalization with LysoTracker for all variants (*SI Appendix, Fig. S1B*). Western blot analysis demonstrated that expression levels of the different variants in endolysosomal membranes are not significantly different (*SI Appendix, Fig. S1 C and D*). Treatment with vacuolin increased the size of endolysosomal vesicles to a similar extent in all variants (*SI Appendix, Fig. S1E*). Finally, dimerization efficiencies of TPC2 WT and the polymorphic variants were comparable as assessed by FRET experimentation (*SI Appendix, Fig. S2*).

The two polymorphisms are found in very different parts of the protein. While M484L resides in the second transmembrane domain of the second channel domain, G734E is found in the C terminus of the protein (Fig. 1A), suggesting different functional consequences.

We next performed endolysosomal patch-clamp experiments. Here, we found striking differences between the respective variants. The polymorphic variant M484L as well as the double-polymorphic variant showed, compared with WT, a significantly increased basal channel activity as well as a significantly increased channel activity after stimulation with PI(3,5)P₂ (3, 15). In contrast, G734E showed mean basal and stimulated activation levels similar to those of WT (Fig. 1B–F and *SI Appendix, Fig. S3A*). Average

capacitance values were comparable for all variants, indicating that differences in channel activity were not due to differences in the size of the patched vesicles (*SI Appendix, Fig. S3B*). Dose–response measurements revealed an EC₅₀ of 1,138 ± 376 nM for WT compared with 216 ± 55 nM for M484L, while G734E was not significantly different from WT with an EC₅₀ of 827 ± 183 nM (Fig. 1G; increased potency). In addition, the maximum response level was increased by two- to threefold, depending on the PI(3,5)P₂ concentration, in M484L compared with WT or G734E (Fig. 1G; increased efficacy).

Differences in ATP Inhibition Between TPC2 WT and Polymorphic Variants. We next assessed the inhibition of activated TPC2 WT and polymorphic variants by ATP. Block of TPC activity by ATP has been demonstrated before and was shown to be physiologically relevant during cell starvation (3). We confirm here that the channel activities of WT TPC2 and also the polymorphic variants M484L and G734E are efficiently blocked by applying high concentrations of ATP (1 mM). However, dose–response measurements revealed significant differences in the IC₅₀ values which were generated for each variant based on their individual PI(3,5)P₂ EC₅₀ values (Fig. 2). When we used the individual PI(3,5)P₂ EC₅₀ values to activate we obtained the following IC₅₀ values for the ATP block: WT (91 ± 19 μM), G734E (351 ± 37 μM), and M484L (102 ± 6 μM). These data demonstrate that significantly less ATP is necessary to block WT TPC2 or M484L variant activities compared with the G734E variant. Similar results were obtained when we used the individual PI(3,5)P₂ EC₈₀ values or a fixed concentration of 1 μM PI(3,5)P₂ to activate. The respective IC₅₀ values for the ATP block were as follows: WT (179 ± 15 μM) and G734E (384 ± 39 μM) for PI(3,5)P₂ EC₈₀ as

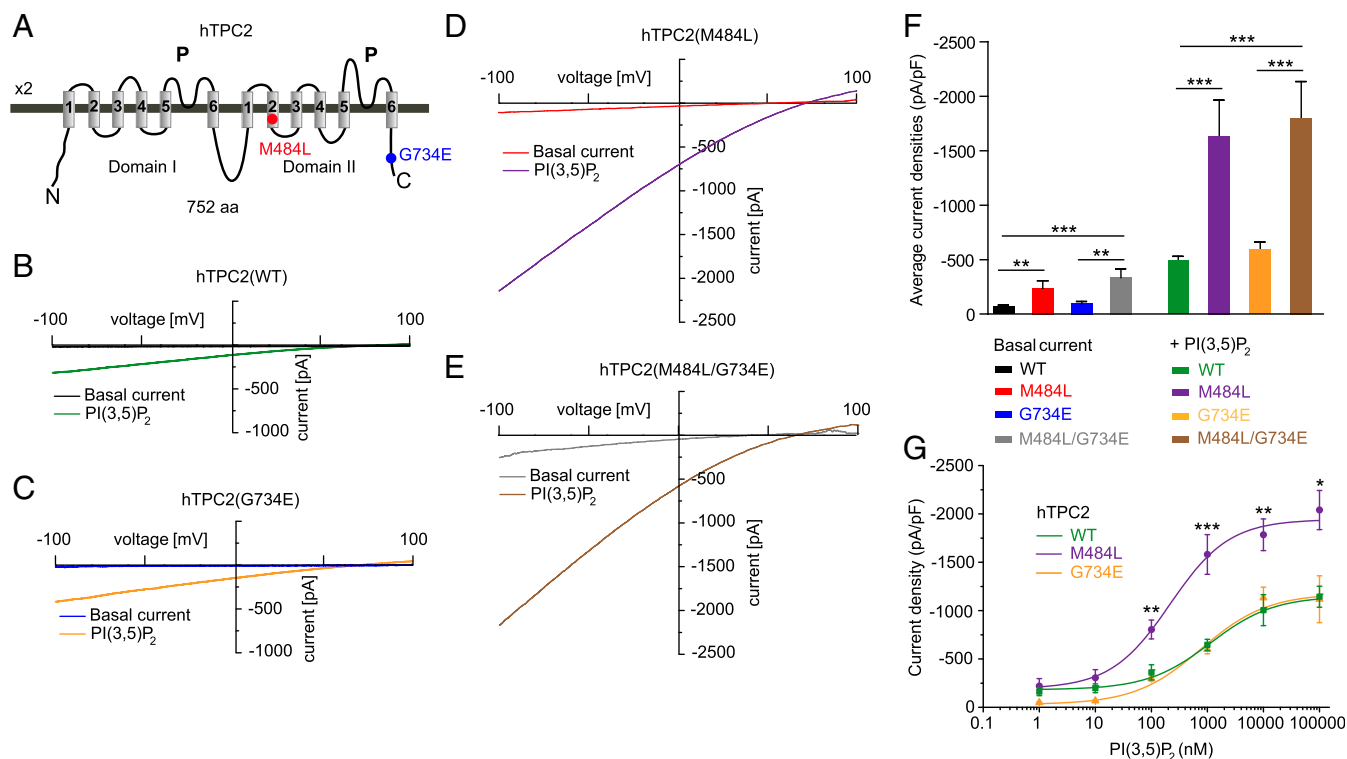


Fig. 1. Effect of PI(3,5)P₂ on endolysosomal vesicles expressing either human TPC2 WT or polymorphic variants. (A) Cartoon showing the estimated positions of the polymorphisms (SNPs) M484L and G734E. (B–E) Shown are representative basal and PI(3,5)P₂ (1 μM) activated currents in vacuolin-enlarged endolysosomal vesicles expressing either hTPC2 WT, hTPC2(M484L), hTPC2(G734E), or hTPC2(M484L/G734E) C-terminally fused to YFP. (F) Statistical summary of data as shown in B–E. Shown are average current densities at –100 mV. (G) PI(3,5)P₂ dose–response curves for hTPC2 WT and hTPC2(M484L) and hTPC2(G734E). In all experiments, currents were elicited by applying 500-ms voltage ramps from –100 to +100 mV every 5 s. In all statistical analyses mean values of at least 5–10 independent experiments are shown, each. To test for statistical significance the one-way ANOVA test followed by Tukey's posttest was applied. ****P* < 0.001, ***P* < 0.01.

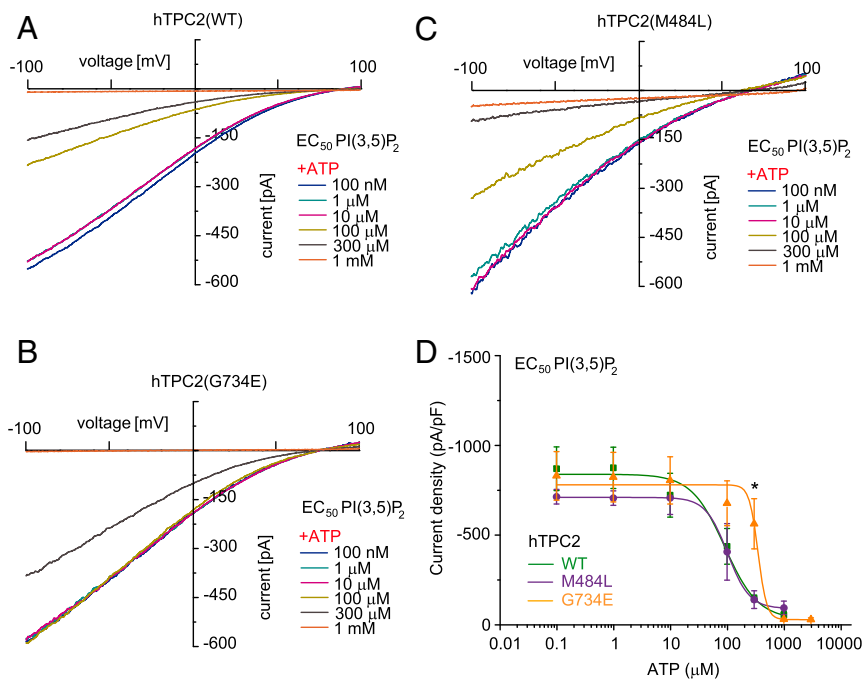


Fig. 2. Effect of ATP on human TPC2 WT and polymorphic variants using the respective EC_{50} values of $PI(3,5)P_2$ as activating concentrations. (A–C) Representative $PI(3,5)P_2$ (diC8) activated currents in vacuolin-enlarged hTPC2 WT and hTPC2 SNP expressing endolysosomal vesicles using the respective EC_{50} values as activating $PI(3,5)P_2$ concentrations and different concentrations of ATP as indicated to block the currents. (D) ATP dose–response curves from experiments as shown in A–C. In all experiments currents were elicited by applying 500-ms voltage ramps from -100 to $+100$ mV every 5 s. To test for statistical significance the Student's t test, unpaired was applied. $*P < 0.05$.

well as WT ($4 \pm 2 \mu M$) and G734E ($133 \pm 71 \mu M$) for the fixed concentration of $1 \mu M$ $PI(3,5)P_2$ (*SI Appendix, Fig. S4*).

In summary, these data suggest that both M484L and G734E variants are gain-of-function (GOF) polymorphisms.

Effect of mTOR Inhibitors. ATP is known to activate mTOR (mechanistic target of rapamycin) (16) and mTOR is the mediator that inhibits TPC2 by direct protein–protein interaction, as recently shown (3). To further investigate the cross-talk between channel activity and ATP inhibition, we tested the effect of mTOR inhibitors such as rapamycin and

torin-1 on TPC2 channel activity. Both compounds were found previously to enhance TPC2 channel activity by blocking the TPC2 inhibitor mTOR (3). We found that inhibition of mTOR increased TPC2(G734E) channel activity more efficiently than WT activity, suggesting a stronger effect of mTOR on WT compared with G734E. In contrast, the channel activity of the M484L isoform could not be further enhanced under the same conditions [for M484L a $PI(3,5)P_2$ concentration of $1 \mu M$ is a saturating concentration; $EC_{50} = 216 \pm 55$ nM] (Fig. 3 and *SI Appendix, Fig. S5 A and B*).

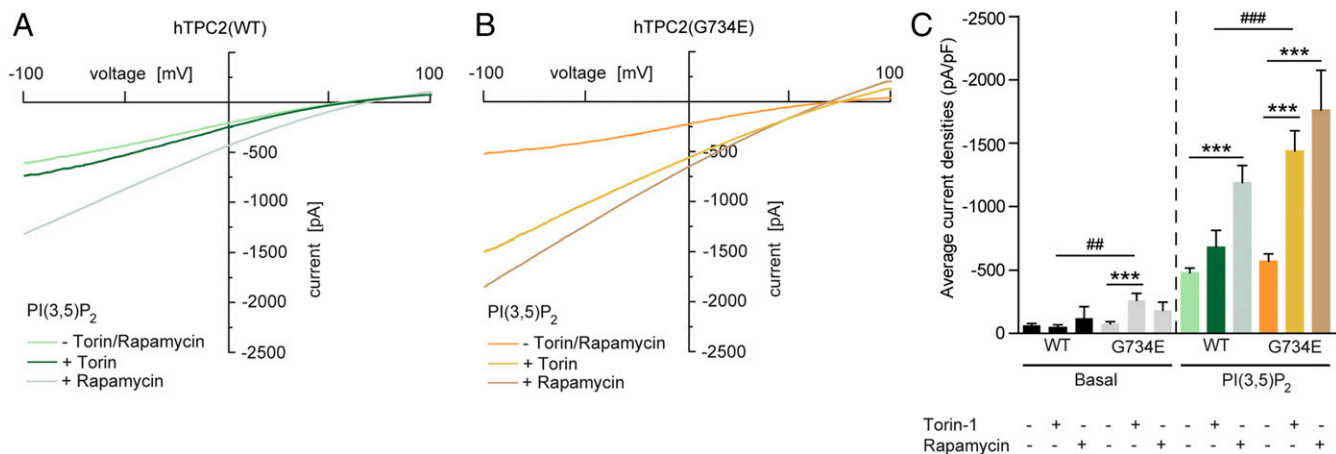


Fig. 3. Effect of rapamycin and torin-1 on human TPC2 WT and G734E. (A and B) Representative $PI(3,5)P_2$ ($1 \mu M$) activated currents in vacuolin-enlarged hTPC2 WT and hTPC2(G734E) expressing endolysosomal vesicles and the respective blocking effects of $2 \mu M$ torin-1 or $1 \mu M$ rapamycin. Cells were incubated with torin-1 for 12 h or with rapamycin for 10 min before experimentation. Currents were measured in the absence of ATP. (C) Statistical summary of data as shown in A and B including respective basal currents. Shown are average current densities at -100 mV. To test for statistical significance the one-way ANOVA test followed by Tukey's posttest was applied to basal and $PI(3,5)P_2$ conditions, respectively. $***$, $####P < 0.001$, $##P < 0.01$.

Ion Substitution Experiments. To further corroborate the findings obtained for the M484L variant we performed ion substitution experiments and molecular dynamics simulations based on the recently published structures of AtTPC1 (13, 14). In ion substitution experiments using the endolysosomal patch-clamp technique we found differences in the estimated pore diameters between WT and M484L, while there were no obvious differences between WT and G734E (Fig. 4 A–E and *SI Appendix, Fig. S5 C–E*). We used monovalent cations (sodium, lithium, rubidium, and cesium) in a concentration of 160 mM, each, to estimate the pore diameters of TPC2 WT and the M484L variant (Fig. 4 A–E). We determined permeability ratios relative to Na⁺ (P_X/P_{Na}) from the bionic reversal potentials, which resulted in estimations of 3.7 Å and 3.9 Å for the minimum pore diameter of TPC2 WT and the M484L variant, respectively. The estimation for the G734E variant diameter resulted in the same value as for WT (3.7 Å) (*SI Appendix, Fig. S5E*). These data suggest that M484L not only contributes to larger current amplitudes but also influences channel conformation and the narrowest part of the pore region.

Molecular Dynamics Simulations Confirm Dilated Pore in hTPC2(M484L) Variant. Multiple models of the TPC2 channel were submitted to prolonged molecular dynamics simulations of at least 100 ns, each. WT and M484L variant were simulated with PI(3,5)P₂ resembling the experimental layout. As each simulation system contained two channel models a total of over 800 ns was available for analysis. All models showed a high degree of stability preserving their overall structure and a continuous water column through the pore. For one of the two M484L models a dilation of the pore could be observed in the presence of PI(3,5)P₂ for ~10 ns around position A272. The pore radii of the dilated M484L pore were compared with the WT pore (Fig. 4 F–H). This finding suggests that the M484L mutation affects pore dynamics, further corroborating the data presented on the estimation of the pore sizes of TPC2 WT and M484L by ion substitution experimentation. Notably, Schieder et al. (17) had reported previously that TPC2 mutant isoform N273A (next to A272) shows a pore block, and Wang et al. (15) reported that the D276K mutation likewise leads to a pore block and loss of PI(3,5)P₂ response, emphasizing the importance of this region for channel activity.

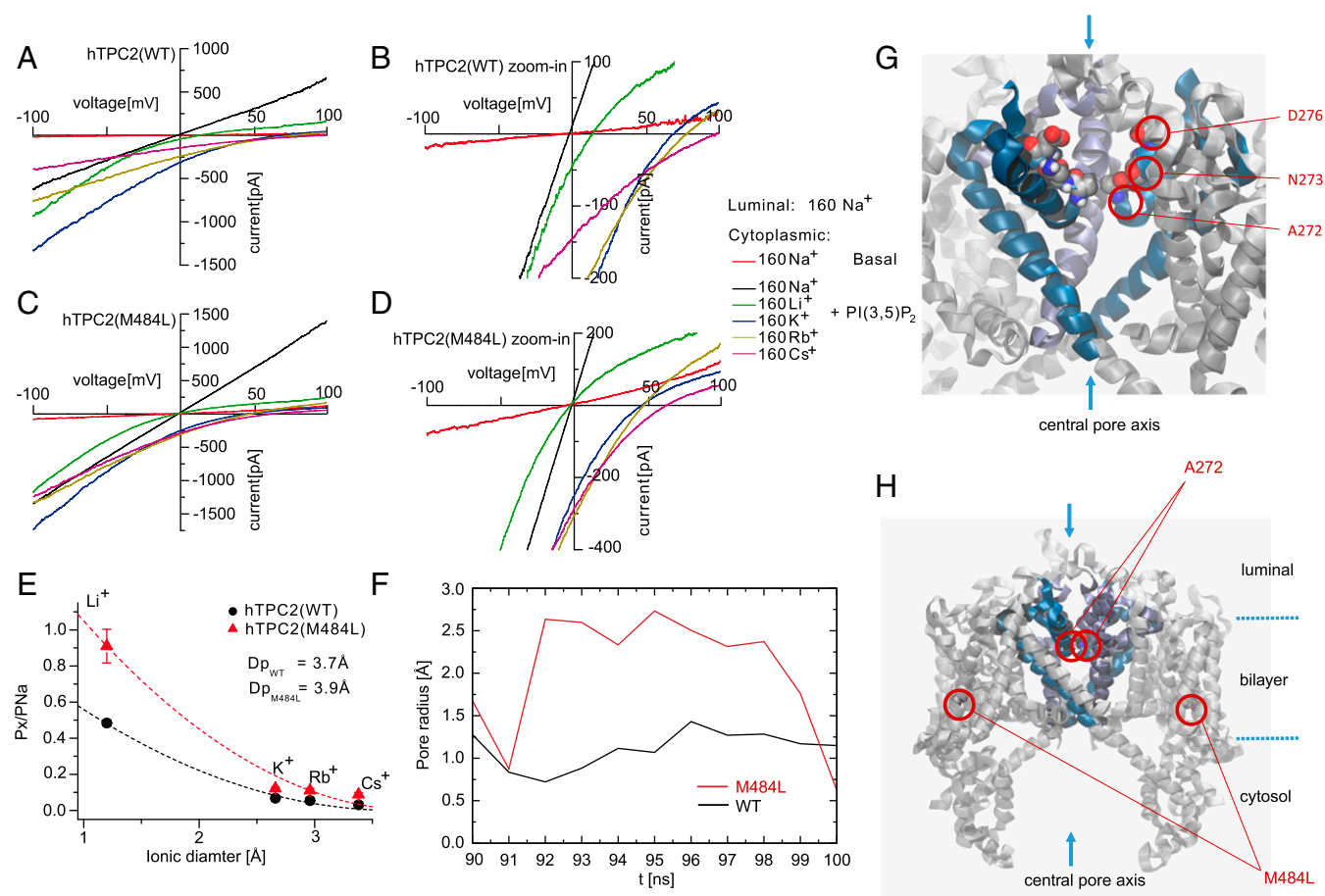


Fig. 4. Ion substitution experiments and molecular dynamics simulations. (A–D) Endolysosomal patch-clamp experiments showing PI(3,5)P₂-activated hTPC2 WT (A and B) or hTPC2(M484L) (C and D) currents under biionic conditions with luminal Na⁺ and bath solutions containing the following monovalent cations, respectively: Li⁺, K⁺, Rb⁺, and Cs⁺. (B and D) Expanded view of A and C, showing that the reversal potentials are shifted to negative voltage in M484L variant. (E) Summary of data as shown in A–D. Shown are the relative permeabilities (P_X/P_{Na}) of the different cations plotted against the diameter of cations. The dashed lines are fitted to Eq. 2 (see *Materials and Methods* for details). (F) Schematic representation of the TPC2 simulation system. The channel (gray) is embedded in a fully solvated POPC bilayer (transparent surfaces). As the channel has a conic shape the bilayer is bent locally. To cope with this effect always two channel models were embedded in antiparallel fashion into a larger bilayer patch. (G) Enlargement of the selectivity filter omitting part of the protein. D276, N273, and A272, which are present symmetrically on both subunits, are shown in VdW representation. (H) The pore radius of TPC2 is shown at the height of A272 for WT (blue) and the M484L variant (red) simulated in presence of PI(3,5)P₂. A representative window at the end of the independent simulations was chosen which presumably resembles an opening event. One of two M484L pores showed a dilation of more than 1 Å for almost 10 ns.

Endogenous TPC2 Channel Activity in Human Donor Fibroblasts. Next, we screened more than 100 blond- and brown/black-haired human donors for TPC2 polymorphisms and identified individuals which were either homozygous for WT, M484L, or G734E, or individuals which were heterozygous for the respective polymorphisms (Fig. 5 *A* and *B*). The obtained genotyping results were found to correlate well with the data published by Sulem et al. (10). Thus, the percentage of DNA samples isolated from blond-haired individuals which are homozygous for either M484L or G734E was 7.2% and 26.1% ($n = 69$), respectively, while DNA samples isolated from brown-, dark brown-, or black-haired individuals were in only 2.9% of the cases homozygous for M484L and in only 10.4% of the cases homozygous for G734E ($n = 67$). Among the blond-haired donors we found only 5.8% to be homozygous for WT. Among individuals with brown/black hair 23.9% were found to be homozygous for WT (Fig. 5*A*).

We subsequently isolated fibroblasts from selected individuals and analyzed them using the endolysosomal patch-clamp technique (Fig. 5 *C–F*). While we found only small endogenous PI(3,5)P₂ currents in WT or G734E fibroblast endolysosomes, significantly increased PI(3,5)P₂-mediated channel activity was detectable in endolysosomes isolated from donor fibroblasts homozygous for M484L, essentially confirming the *in vitro* findings. For ATP dose-

response measurements the PI(3,5)P₂-mediated currents in G734E endolysosomes were too small. As an activation control we used the TRPML-channel activator ML-SA1 (18). TRPML channel currents activated with ML-SA1 were not significantly different between M484L, G734E, and WT endolysosomes, suggesting that the differences in PI(3,5)P₂ response are not due to differences in TRPML channel activity (Fig. 5 *C–E*). In summary, these data confirm the strong GOF found for the M484L variant in overexpressing HEK293 cells and the data further confirm the increased association of the M484L and G734E variants with blond hair color compared with the WT TPC2 isoform.

Discussion

We show here that the TPC2 variants M484L and G734E reported previously to be associated with a shift in human hair color from brown to blond display distinct functional differences compared with WT. We used overexpressing HEK293 cells and endogenously expressing fibroblasts to functionally characterize the respective variants. In endolysosomal patch-clamp experiments we found that both variants show a gain of channel function compared with WT (*SI Appendix, Fig. S6*). While basal activity and activation with PI(3,5)P₂ was increased in M484L, affecting both efficacy and

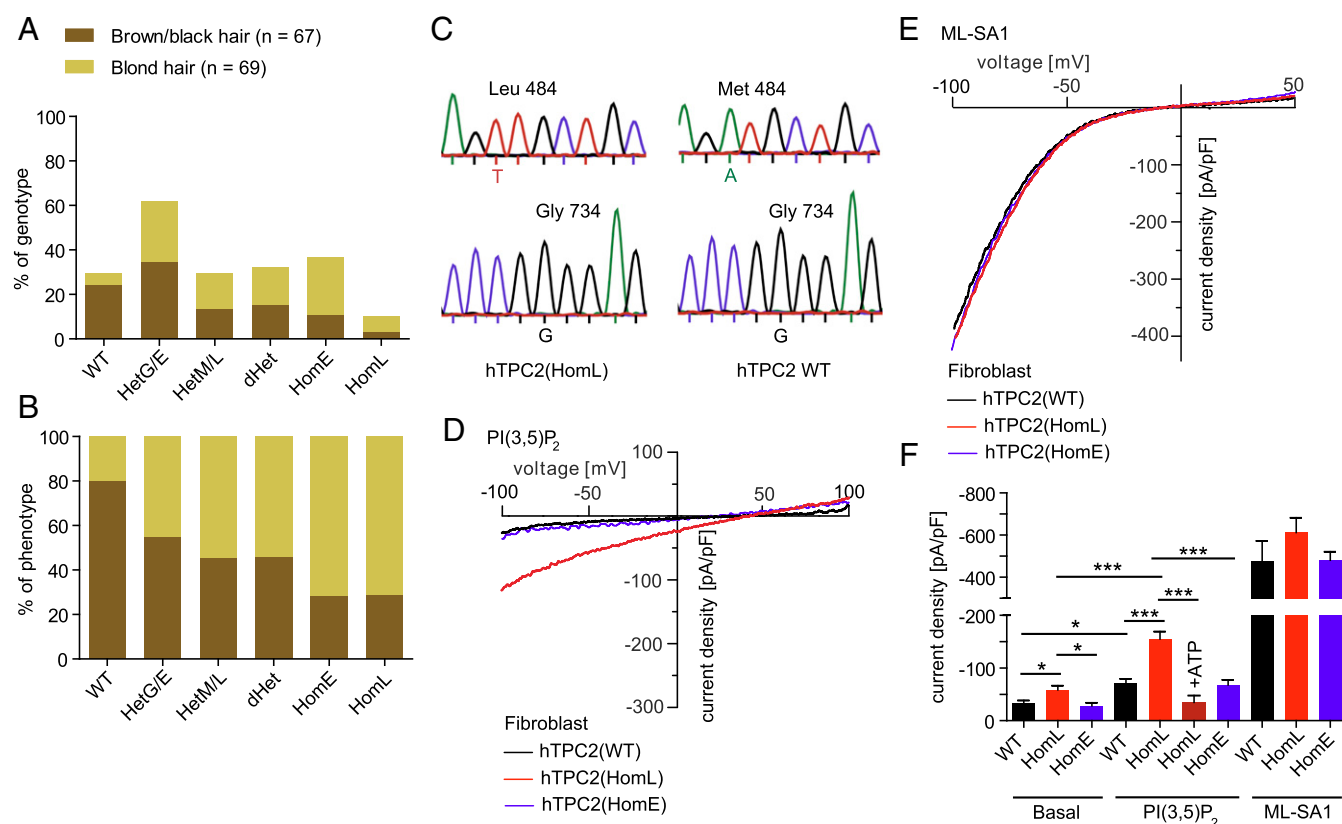


Fig. 5. Characterization of human fibroblasts isolated from TPC2 WT donors or donors carrying TPC2 polymorphisms. (*A* and *B*) Data summarizing sequencing results obtained from human genomic DNA samples. Shown in *A* is the genotype distribution (in percent) of individuals with either blond hair or brown/black hair (e.g., 23.9% of the brown/black hair donors but only 5.8% of the blond hair donors are genotype WT). In contrast, 26.1% of the blond hair donors are homozygous for E (homE) at position 734 while only 10.4% of the brown/black hair donors are homE. Shown in *B* is the phenotype distribution (in percent) of all genotyped individuals (e.g., 80% of all individuals with the genotype WT have brown/black hair while only 20% have blond hair). In contrast, 72% of all individuals with the genotype homE at position 734 and 71.4% of all individuals with the genotype L homozygous (homL) at position 484 are blond. The total numbers of donors were 67 (brown/black hair) and 69 (blond hair), respectively. (*C*) Examples of human donor genotyping results. Shown are respective sequences around position 484 (Leu/Met) and 734 (Gly). (*D* and *E*) Representative endolysosomal patch-clamp experiments showing PI(3,5)P₂ (10 μ M) activated currents in vacuolin-enlarged fibroblast endolysosomes isolated from donors homozygous for WT, M484L, and G734E. The TRPML channel activator ML-SA1 was used to demonstrate that TRPML currents were comparable in size in all fibroblast lines, in contrast to PI(3,5)P₂-mediated currents. (*F*) Statistical summary of data shown in *D* and *E*. Two independent donor fibroblast samples were used for each WT and M484L. One sample was used for G734E. Shown are the pooled average current densities at -100 mV of at least five independent experiments, each. To test for statistical significance one-way ANOVA test followed by Tukey's posttest was applied. *** $P < 0.001$, * $P < 0.05$.

potency of $\text{PI}(3,5)\text{P}_2$, inhibition of channel activity by ATP was less sensitive in G734E compared with WT (*SI Appendix, Fig. S6*). The M484L polymorphism leads to structural changes affecting the pore diameter of TPC2. Thus, M484L displays a significant pore dilation compared with WT as demonstrated by molecular dynamics simulations and ion substitution experiments. The G734E variant is less responsive to ATP and more sensitive to mTOR inhibitors than WT, the latter suggesting that the weaker ATP effect may be mediated by mTOR. While torin-1 is a selective ATP-competitive inhibitor of mTOR which effectively blocks phosphorylation of mTOR, rapamycin and related inhibitors form a complex with the intracellular immunophilin FKBP12; the resulting complex then interacts with and inhibits mTOR (19, 20). Despite these different mTOR inhibitory mechanisms, both torin-1 and rapamycin result in a stronger increase in G734E activity compared with WT, further emphasizing that the differences in ATP block may be directly mediated via mTOR and downstream effects. Nevertheless, we cannot fully exclude the possibility of mTOR-independent ATP effects.

Remarkably, human TPC2 cDNAs used for functional studies in past publications were often polymorphic variants. For example, Calcraft et al. (21) had used a TPC2 variant cloned from HEK293 cells containing both polymorphisms: M484L and G734E. Pitt et al. (22) had used a variant of human TPC2 containing the G734E polymorphism (GenBank accession no. AY029200) and Brailoiu et al. (23) had used the IMAGE clone 5214862 (GenBank accession no. BC063008) which also contains the polymorphism G734E. Thus, it seems that WT hTPC2, at least in its recombinant form, has not always been used as a reference in the existing publications.

In accordance with recent findings by Ambrosio et al. (11) as well as Bellono et al. (12), claiming that loss of TPC2 leads to increased melanin production, an increase in TPC2 channel activity as found here for the two SNPs would be expected to result in the opposite effect, a decrease in melanin production. Located in the basal epidermis and in hair follicles, melanocytes of the integument are responsible for hair coloration through production of melanin pigments in melanosomes (24). Two types of pigment are known to give hair its color: eumelanin and pheomelanin. Eumelanin has two subtypes, black and brown, which determine the darkness of the hair color. A low concentration of brown eumelanin results in blond hair, whereas a higher concentration of eumelanin will color the hair brown/black. Melanin production is strongly dependent on the activity of the enzyme tyrosinase (TYR). TYR activity is optimal at neutral pH (25–27). To achieve neutralization of melanosomal pH, the proper function of a cascade of ion transporters seems to be required (27). Consequently, polymorphisms in any of such transporters or ion channels rendering them dys- or malfunctioning may lead to changes in melanosome pH and thus to changes in melanin production, as suggested recently by Ito and Wakamatsu (27). For TPC2 this hypothesis has now been supported by works published by Ambrosio et al. (11) and Bellono et al. (12). Thus, loss of TPC2 leads to an increase in melanosomal pH and melanin production while overexpression of TPC2 leads to a decrease in melanin production. Like TPC2 overexpression, an increase in TPC2 activity would be expected to result in a decreased melanosomal pH and thus a decrease in melanin production. This would consequently explain the shift in hair color from brown to blond.

In addition to hair coloration, altered TPC2 channel activity may also impact human health, in particular under challenging conditions such as physical stress or infections. TPC2 knockout mice show an increased susceptibility to hypercholesterolemia and fatty liver hepatitis compared with WT when fed with a high-cholesterol diet (2), they show a decreased physical endurance under fasting conditions (3), and they are less susceptible to distinct viral infections (7). Migration of cancer cells and the formation of metastases was recently found to be reduced in TPC2 knockdown cells or after pharmacological inhibition of TPC2 (9). We therefore speculate

that humans carrying the GOF polymorphisms M484L or G734E, or both, may have, in particular under stress conditions, an altered susceptibility for diseases that are associated with the endolysosomal system. In addition, it may also be possible that changes in TPC2 activity affect melanosomes differently than lysosomes, for example due to differences in pH regulatory mechanisms with different consequences for human physiology and pathophysiology.

Materials and Methods

Molecular Biology. All human TPC2 variants were generated from hTPC2(M484L/G734E)-mCherry, a gift from Michael Zhu, University of Texas Medical School, Houston. Point mutations were removed from constructs by site-directed mutagenesis using QuikChange (Agilent) according to the procedures outlined in the manufacturer's manual or by overlap PCR experimentation. C-terminally fused YFP versions of WT and the polymorphic TPC2 variants were generated from the respective mCherry constructs and subcloned into pcDNA3.1 vector. Constructs used for FRET experiments are described in *Materials and Methods* and the figure legends in more detail.

Endolysosomal Membrane Preparations. To evaluate expression levels of TPC2 WT and variants in endolysosomal membranes, HEK293 cells were transfected with TPC2-constructs (YFP-tagged), respectively. Preparation of endolysosomes was performed as described previously (17, 28). For immunoblotting, antibodies were used in the following dilutions: rabbit anti-Rab7, 1:500 (20945; cell signaling); mouse anti-GFP, 1:2,000; mouse anti-HRP 1:2,000 (sc-2031; Santa Cruz); and rabbit anti HRP, 1:1,000 (NA934V; GE Healthcare).

Molecular Modeling. A model for TPC2 was constructed using Schrödinger Prime based on Protein Data Bank ID code 5E1J (14) with the UniProt sequence Q8NHX9 (21). Default settings were used using the multichain protocol modeling both subunits simultaneously. Always two of the resulting models were embedded into a 1-palmitoyl-2-oleoyl-*sn*-glycero-3-phosphocholine (POPC) bilayer in antiparallel orientation to reduce lateral stress following protocols described earlier (29, 30) and solvated with simple point charge water. CaCl_2 was added to balance the overall charge and to achieve nearly physiological ion concentrations. Using GROMACS-5.1 the periodic system was energy-minimized and constraints on the protein were gradually reduced (31–33). A total of 100 ns each were simulated with a time step of 2 fs for the WT, WT with $\text{PI}(3,5)\text{P}_2$, M484L, and M484L with $\text{PI}(3,5)\text{P}_2$. Two equivalents per pore were placed in the vicinity of M484L into the bilayer for the corresponding simulations. Neighbor searching was performed every 40 steps. The particle mesh Ewald algorithm was used for electrostatic interactions with a cutoff of 1.2 nm and Verlet cutoff scheme. A reciprocal grid of $192 \times 120 \times 120$ cells was used with fourth-order B-spline interpolation. A single cutoff of 1.2 was used for van der Waals interactions. Temperature coupling to 310 K was done with the V-rescale algorithm. Semiisotropic pressure coupling to 1 bar in the plane and perpendicular to it was done with the Berendsen algorithm. For all simulations the 53a6 force field was used with parameters for POPC adapted from ref. 29 and adapted for $\text{PI}(3,5)\text{P}_2$ from ref. 34. The analysis was performed using GROMACS tools, VMD, Schrödinger, and hole2 (31, 35–37).

FRET Experiments. Measurements of single-cell FRET based on aggregate (nonspatial) fluorescence recordings were performed and analyzed using the three-cube FRET method as described previously (38). For measurements, transiently transfected HEK293 cells were maintained in buffer solution composed of 140 mM NaCl, 5 mM KCl, 1 mM MgCl_2 , 2 mM CaCl_2 , 10 mM glucose, and 10 mM Na-Hepes, pH 7.4, at room temperature (RT). Fluorescence intensities of YFP or the GFP variants Citrine and Cerulean were recorded using a LEICA DMI6000B inverted epifluorescence microscope and a photomultiplier detection system (PTI). Excitation was done at $436 \text{ nm} \pm 2.5$ or $500 \text{ nm} \pm 2.5$ with a DeltaRam monochromator (Horiba). Epifluorescence emission was detected by a photomultiplier (PMT 914) and acquired on a personal computer using FelixGX software (Horiba). Three-cube FRET filter cubes were as follows (excitation; longpass beamsplitter; emission): CFP/Cerulean (ET436/20x; T455lp; ET480/40m), YFP/Citrine (ET500/20x; T515lp; ET535/30m), and FRET (ET436/20x; T455lp; ET535/30m) (Chrom Technology). The FRET ratio, which is defined as the fractional increase in YFP emission caused by FRET, was calculated using $\text{FR} = [\text{SFRET} - (R_D)(S_{\text{Cer}})] / [(R_A)(S_{\text{Citr}})]$. S_{FRET} , S_{Cer} , and S_{Citr} denote fluorescence intensities derived from measurements in individual cells coexpressing Citrine- or Cerulean-tagged proteins with the respective filter cube (excitation, emission): S_{FRET} ($436 \text{ nm} \pm 10$, $535 \text{ nm} \pm 15$), S_{CFP} ($436 \text{ nm} \pm 10$, $480 \text{ nm} \pm 20$), and S_{YFP} ($500 \text{ nm} \pm 10$, $535 \text{ nm} \pm 15$). R_D and R_A are experimentally predetermined constants from measurements applied to single cells expressing only Cerulean- or Citrine-tagged molecules that

correct for donor bleed through or acceptor cross-excitation. FRET efficiencies (E_A) can be calculated from FRs using the following equation (39):

$$E_A = [FR - 1] \cdot \frac{\varepsilon_{\text{citrine}}(436)}{\varepsilon_{\text{cerulean}}(436)} \quad [1]$$

$\varepsilon_{\text{citrine}}$ and $\varepsilon_{\text{cerulean}}$ are the setup specific average molar extinction coefficients for citrine and cerulean, respectively, over the precise bandwidth of the FRET cube excitation filter. In our setup, the calculated molecular extinction coefficient ratio is $\varepsilon_{\text{citrine}}(436)/\varepsilon_{\text{cerulean}}(436) = 0.0563$. Data were analyzed using FelixGX (Horiba PTL) and Microsoft Excel (Microsoft).

Whole-Endolysosomal Patch-Clamp Experiments. For whole-endolysosomal patch-clamp recordings, isolated intact endolysosomes from HEK293 cells were manually isolated after vacuolin treatment for at least 2 h. Human TPC2 WT and polymorphic TPC2 variants (C-terminally fused to YFP) were transiently transfected into HEK293 cells using TurboFect Transfection Reagent (ThermoFisher). Currents were recorded using an EPC-10 patch-clamp amplifier and PatchMaster acquisition software (HEKA). Data were digitized at 40 kHz and filtered at 2.8 kHz. Cytoplasmic solution contained 140 mM potassium methanesulfonate (KMSA), 5 mM KOH, 4 mM NaCl, 0.39 mM CaCl_2 , 1 mM EGTA, and 20 mM Hepes (pH adjusted with KOH to 7.2). Luminal solution was 140 mM NaMSA, 5 mM KMSA, 2 mM CaMSA, 1 mM CaCl_2 , 10 mM Hepes, and 10 mM MES (pH adjusted with MSA to 4.6). For the application of $\text{PI}(3,5)\text{P}_2$ (A.G. Scientific) and ATP-Mg (Sigma), cytoplasmic solution was completely exchanged by compound containing solution. Torin-1 and rapamycin were purchased from Tocris and LC Laboratories, respectively. All recordings were performed at 23–25 °C. For experiments using ATP and mTOR inhibitors, cell density was 50–60% and the time spent outside the incubator was 30 min.

To estimate the pore diameter of TPC2 WT and M484L, the relative permeability ratios of cations relative to Na^+ were plotted against the diameter of the respective monovalent cations as indicated in Fig. 4. The following equation was applied (40):

$$\frac{P_{X^+}}{P_{\text{Na}^+}} = k \left(1 - \frac{a}{d}\right)^2, \quad [2]$$

where a is the diameter of the permeating cation, k is a constant factor, and d is the pore diameter (41). The ionic radii of Li^+ , K^+ , Rb^+ , and Cs^+ are 0.6, 1.33, 1.48, and 1.69 Å, respectively (42). To calculate the permeability ratios the following equation was used:

$$\frac{P_{X^+}}{P_{\text{Na}^+}} = \frac{[Na]_i}{[X^+]_o} e^{\frac{VF}{RT}}, \quad [3]$$

where V is the reversal potential, R is the gas constant, F is the Faraday constant, and T is the temperature in Kelvin. To determine the relative Na^+ (P_{X^+}/P_{Na^+}) permeabilities of TPC2 WT and M484L, whole-endolysosome recordings were performed using ramp protocols (+100 to –100 mV with 500-ms increments). The bath solution contained 160 mM (pH 7.2, Hepes 5 mM) of the respective cations (Fig. 4 A–D) and the pipette solutions con-

tained 160 mM NaCl (pH 7.2, Hepes 5 mM). The recordings were started with symmetric Na^+ solutions. The cytoplasmic solution was then exchanged with the respective monovalent cation-containing solution.

Human Donor DNA Purification and Sequencing. Human genomic DNA was obtained from adult male and female individuals using the Gentra Puregene Buccal Cell Kit (Qiagen), according to manufacturer's instructions. Briefly, buccal cells were collected by scraping the inside of the mouth 10 times. For cell lysis, the collection brush was incubated in lysis solution at 65 °C for at least 15 min. Proteins were precipitated and centrifuged. To precipitate DNA, the supernatant was added to isopropanol and glycogen solution. The pellet was washed with 70% ethanol and air-dried before resuspension in DNA hydration solution. Samples were incubated at 65 °C for 1 h, followed by incubation at RT overnight to dissolve the DNA. Genomic DNA fragments were amplified using gene-specific primers [hTPC2(M484L) genomic DNA-forward: 5'-GGTGTCTCTGGTCTGGA-3'; hTPC2(M484L) genomic DNA-reverse: 5'-ACAGCCTTAGTCTCAGGG-3'; hTPC2(G734E) genomic DNA-forward: 5'-GGCCACCTACCAGATGACT-3'; hTPC2(G734E) genomic DNA-reverse: 5'-CGGACGTCACTGCACAG-3']. All DNA sequencing services were done by Eurofins MWG Operon.

Isolation of Human Fibroblasts. Human genomic DNA sampling and human fibroblast isolation were approved by the Ludwig-Maximilians-Universität Ethics Committee (headed by Prof. Dr. Eisenmenger; reference no. 254–16). Acquisition of human material was performed after obtaining written informed consent by the donors. Primary fibroblasts were isolated by Prof. Dr. Carola Berking and colleagues, Department of Dermatology, Ludwig-Maximilians-Universität München from the skin of healthy adult donors. Epidermis was separated from dermis using dispase II (10 mg/mL in PBS, pH 7.2–7.4, D4693; Sigma) and dermis was digested in collagenase (1 mg/mL in DMEM, C0130; Sigma) for 22 h at room temperature. Fibroblasts were cultured in DMEM with glutamine (Life Technologies, Inc.) and 10% FBS (FBS Superior, S0615; Biochrom). They were used for experiments at passages three to seven.

Statistical Analysis. Details of statistical analyses and n values are provided in the *Materials and Methods* or the figure legends. Statistical analyses were carried out using Origin 7.5 and GraphPad Prism 5. All error bars are depicted as mean \pm SEM. Significance is denoted on figures as outlined in the legends. Statistics were derived from at least three independent experiments.

ACKNOWLEDGMENTS. We thank Kerstin Skokann, Melanie Wallisch, and Berit Noack (Ludwig-Maximilians-Universität München) for technical support; Dr. Bernd Schröder (University of Kiel) for kindly providing the human TMEM192 cDNA; and Dr. Michael Zhu (University of Texas Medical School at Houston) for kindly providing the human TPC2(M484L/G734E)-mCherry cDNA. This work was supported, in part, by German Research Foundation Grants SFB/TRR152 TP04 (to C.G.), TP06 (to C.A.W.-S.), and TP12 (to M.B.) and by funding from the Neuronal Ceroid Lipofuscinosis Foundation, Hamburg, Germany.

- Favia A, et al. (2014) VEGF-induced neovascularization is mediated by NAADP and two-pore channel-2-dependent Ca^{2+} signaling. *Proc Natl Acad Sci USA* 111:E4706–E4715.
- Grimm C, et al. (2014) High susceptibility to fatty liver disease in two-pore channel 2-deficient mice. *Nat Commun* 5:4699.
- Cang C, et al. (2013) mTOR regulates lysosomal ATP-sensitive two-pore Na^+ channels to adapt to metabolic state. *Cell* 152:778–790.
- García-Rúa V, et al. (2016) Endolysosomal two-pore channels regulate autophagy in cardiomyocytes. *J Physiol* 594:3061–3077.
- Lin PH, et al. (2015) Lysosomal two-pore channel subtype 2 (TPC2) regulates skeletal muscle autophagic signaling. *J Biol Chem* 290:3377–3389.
- Arndt L, et al. (2014) NAADP and the two-pore channel protein 1 participate in the acrosome reaction in mammalian spermatozoa. *Mol Biol Cell* 25:948–964.
- Sakurai Y, et al. (2015) Ebola virus. Two-pore channels control Ebola virus host cell entry and are drug targets for disease treatment. *Science* 347:995–998.
- Ruas M, et al. (2010) Purified TPC isoforms form NAADP receptors with distinct roles for Ca^{2+} signaling and endolysosomal trafficking. *Curr Biol* 20:703–709.
- Nguyen ON, et al. (2017) Two-pore channel function is crucial for the migration of invasive cancer cells. *Cancer Res* 77:1427–1438.
- Sulem P, et al. (2008) Two newly identified genetic determinants of pigmentation in Europeans. *Nat Genet* 40:835–837.
- Ambrosio AL, Boyle JA, Aradi AE, Christian KA, Di Pietro SM (2016) TPC2 controls pigmentation by regulating melanosome pH and size. *Proc Natl Acad Sci USA* 113:5622–5627.
- Bellono NW, Escobar IE, Oancea E (2016) A melanosomal two-pore sodium channel regulates pigmentation. *Sci Rep* 6:26570.
- Kintzer AF, Stroud RM (2016) Structure, inhibition and regulation of two-pore channel TPC1 from *Arabidopsis thaliana*. *Nature* 531:258–262.
- Guo J, et al. (2016) Structure of the voltage-gated two-pore channel TPC1 from *Arabidopsis thaliana*. *Nature* 531:196–201.
- Wang X, et al. (2012) TPC proteins are phosphoinositide-activated sodium-selective ion channels in endosomes and lysosomes. *Cell* 151:372–383.
- Perl A (2015) mTOR activation is a biomarker and a central pathway to autoimmune disorders, cancer, obesity, and aging. *Ann N Y Acad Sci* 1346:33–44.
- Schieder M, Rötzer K, Brüggemann A, Biel M, Wahl-Schott C (2010) Planar patch clamp approach to characterize ionic currents from intact lysosomes. *Sci Signal* 3:pl3.
- Shen D, et al. (2012) Lipid storage disorders block lysosomal trafficking by inhibiting a TRP channel and lysosomal calcium release. *Nat Commun* 3:731.
- Faivre S, Kroemer G, Raymond E (2006) Current development of mTOR inhibitors as anticancer agents. *Nat Rev Drug Discov* 5:671–688.
- Hausch F, Kozany C, Theodoropoulou M, Fabian AK (2013) FKBP and the Akt/mTOR pathway. *Cell Cycle* 12:2366–2370.
- Calcraft PJ, et al. (2009) NAADP mobilizes calcium from acidic organelles through two-pore channels. *Nature* 459:596–600.
- Pitt SJ, et al. (2010) TPC2 is a novel NAADP-sensitive Ca^{2+} release channel, operating as a dual sensor of luminal pH and Ca^{2+} . *J Biol Chem* 285:35039–35046.
- Brailoiu E, et al. (2009) Essential requirement for two-pore channel 1 in NAADP-mediated calcium signaling. *J Cell Biol* 186:201–209.
- Borges CR, Roberts JC, Wilkins DG, Rollins DE (2001) Relationship of melanin degradation products to actual melanin content: Application to human hair. *Anal Biochem* 290:116–125.

